10-4-2016 12:00 AM

Modelling and Simulation of the Flexoelectric Effect on a Cantilevered Piezoelectric Nanoplate

Xining Wang, *The University of Western Ontario*

Supervisor: Liying Jiang, *The University of Western Ontario*

A thesis submitted in partial fulfillment of the requirements for the Master of Engineering Science degree in Mechanical and Materials Engineering

Abstract

Piezoelectric nanomaterials have attracted increasing attentions due to their distinct electromechanical features, especially the size-dependent properties, which differ greatly from their bulk counterparts.

Due to the large strain gradients presented in nanostructures, the flexoelectricity is believed to be responsible for such size-dependent properties. In this thesis, based on the Kirchhoff plate model and the extended linear piezoelectric theory, a modified continuum mechanics based model is developed to study the size-dependent flexoelectric effect upon the static bending behaviors of a cantilevered piezoelectric nanoplate (PNP). Finite difference method (DFM) is employed to obtain the approximate numerical solutions.

The numerical results indicate that the flexoelectric effect is more prominent with the decrease of the plate thickness, and it is also sensitive to the boundary conditions, the plate in-plane dimensions, and the applied mechanical and electrical loads.

The current work aims at providing an increased understanding of the size-dependent properties of the piezoelectric nanomaterials.

Keywords

Piezoelectric nanoplates; Size-dependent properties; Flexoelectricity; Electromechanical coupling

Acknowledgments

First and above all, I would like to express my sincere thanks to my supervisor Professor Liying Jiang, whose passion and dedication within the field of nanomaterials have inspired and motivated me. I would also like to thank Professor Jiang for her support, constructive feedbacks and guidance along the way.

I would also like to extend the thanks to my advisory committee members Professor Samuel Asokanthan, Professor Xueliang Sun and Professor Wenxing Zhou for their help.

Appreciation is also expressed to the faculty and staff members in the Department of Mechanical and Materials Engineering at Western University. As well, I am deeply indebted to the current and former members in Professor Liying Jiang's research group, especially Fengrui and Zhengrong.

Last but not least, I would like to express my gratitude to my friends and family for their encouragement and support throughout the journey, especially Zeena and my parents.

Table of Contents

List of Tables

List of Figures

Nomenclature

P_i	polarization tensor
u_i	displacement tensor
ε_{ij}	strain tensor
a_{kl}	reciprocal dielectric susceptibility tensor
c_{ijkl}	elastic constant tensor
d_{ijk}	piezoelectric constant tensor
b_{ijkl}	the higher order coupling between the polarization gradient and the polarization gradient
f_{ijkl}	direct flexocoupling coefficient
e_{ijkl}	reverse flexocoupling coefficient
σ_{ij}	stresses
E_i	electric field
σ_{ijm}	moment stress
E_{ij}	local electrical force
b	length of the plate
a	width of the plate
h	thickness of the plate
q	density of the uniformly distributed mechanical load
V	electrical voltage

$w(x,y)$	transverse out-plane displacement along the plate thickness direction
$u(x,y)$	in-plane displacements along the x direction
$v(x,y)$	in-plane displacements along the y direction
$u^0(x,y)$	in-plane displacements of the midplane along the x direction
$v^0(x,y)$	in-plane displacements of the midplane along the y direction
Φ	electric potential
E_{ij}	higher order electric field
k	background permittivity for ferroelectrics
k_0	permittivity of the vacuum
k_b	specific background permittivity
Ω	volume of the plate
W	work done by the external force
H	electric enthalpy density
U	internal energy density
α	angle between the outward normal of the boundary and the x axis

Chapter 1

1 General introduction

1.1 Introduction

Piezoelectric materials are smart materials that exhibit unique electromechanical coupling, which enables engineering designs to have more innovative features and functions. Such advanced materials have experienced growing interest in transduction technologies across all engineering platforms. Application examples include energy harvesters, sensors, transducers, actuators, medical imaging systems and structural health monitoring systems *etc*. As the dimension of various functional devices is reduced down to nanoscale, the need to develop piezoelectric nanomaterials as the building elements is becoming crucial. Attributing to the development of nanotechnology and synthesis techniques, various piezoelectric nanomaterials have been synthesized. The distinct mechanical and physical electrical properties of such nanomaterials make them appealing for a wide range of applications in nano-electromechanical systems (NEMS), such as piezoelectric nanogenerators, nanosensors, diodes and nanoresonators.

Better exploitation of these novel materials requires improved understanding of the underlying fundamentals governing the delicate multi-physics coupling behavior of the materials. Extensive efforts have been naturally devoted to experimental testing and atomistic simulations, from which it is found that the physical properties of piezoelectric nanomaterials are different from their corresponding bulk counterparts, i.e., the size-dependent properties. For example, size-dependent features are found in the Young's modulus, the fracture strain of ZnO nanowires, and piezoelectric coefficients of BaTiO3 (Chen *et al.*, 2006; Stan *et al.*, 2007; Desai and Haque, 2007; Zhang *et al.*, 2009; 2011).

The size dependent properties of piezoelectric nanomaterials may have a great impact on their potential applications, thus it is essential to have a better understanding of such size dependent features. Due to the extreme difficulty of performing experiments on nanostructures and the computational limitations of the atomistic simulations at both length and time scales, it is natural to resort to alternative efficient methods to study the

mechanical and physical properties of nanoscale materials, such as the continuum mechanics theories. However, the conventional models fail to capture the size effects since they neglect the variation of interatomic quantities. Thus, modified continuum models with the incorporation of the small scale features should be developed. Several modified continuum models have been proposed to investigate the properties of nanostructures, such as the linear surface elasticity model, the surface piezoelectricity model and the extended linear piezoelectricity theory. Their simulation results agree well with those from experiments and atomistic simulations.

Due to the large surface to volume ratio of structures at nanoscales, surface effects are believed to play an important role in the size-dependent properties of nanomaterials. Particularly for piezoelectric nanomaterials, flexoelectricity is also believed to contribute to their size-dependent properties, which refers to a spontaneous polarization in linear response to an inhomogeneous deformation or strain gradients. Unlike the piezoelectricity, the flexoelectricity is a universal effect for all dielectrics, even in centrosymmetric materials. It is found in the literature that the flexoelectricity can modify some physical characteristics of piezoelectric nanomaterials, such as the dielectric constant (Catalan *et al.*, 2004; 2005), shifts of domain configurations and modifications of the hysteresis loops (Lee *et al.*, 2011), the reduction of capacitance due to the dead layer effect (Majdoub *et al.*, 2009).

To better understand the flexoelectric effect, several theoretical frameworks have been established with the consideration of the nanoscale features, such as the theory proposed by Mindlin (1968) for dielectrics with the reverse flexoelectric effect, the theory developed by Maranganti *et al.* (2006) which includes the effects of the flexoelectricity, the reverse flexoelectricity and the strain gradients, and the model established by Hu and Shen (2010) with the consideration of the flexoelectricity, the electrostatic force and the surface effects. Based on these pioneering works, the flexoelectric effect on the physical and mechanical properties of piezoelectric nanostructures could be predicted quantitatively to some extent. However, the continuum modeling of the influence of the flexoelectricity on the physical properties of piezoelectric nanostructures is still limited in the literature, particularly for

comples configurations. Therefore, it is important to further uncover the flexoelectric effect on the mechanical and physical properties of these piezoelectric nanostructures.

1.2 Research objectives

To make better use of the nanoscale piezoelectricity for future design and applications, it is essential to have a thorough understanding on the characteristics of such nanoscale features. Since plates are one of the fundamental building blocks for piezoelectric nano-devices, current work will focus on such a configuration. The main objective of this thesis is to provide a fundamental understanding of the size-dependent electromechanical coupling properties of a cantilevered piezoelectric nanoplate (PNP) with the flexoelectric effect, based on a modified Kirchhoff plate model. Detailed works are listed as the following:

1) Developing a modified Kirchhoff model for cantilevered piezoelectric nanoplates considering the flexoelectric effect.
2) Obtaining approximate numerical solutions for the governing equations by finite difference method (FDM).
3) Studying the influence of the flexoelectric effect on the static bending and electromechanical coupling behaviors of cantilevered piezoelectric nanoplates.

1.3 Thesis outline

Chapter 1 introduces briefly the background of this study and states the research objectives and thesis outline.

Chapter 2 provides a detailed review of the history of piezoelectric materials and their nanoscale counterparts and potential applications, the flexoelectricity and surface effects that contributes to the size-dependent properties of piezoelectric nanostructures. Moreover, the flexoelectric effects and their size-dependent properties are reviewed in detail.

In Chapter 3, based on the extended linear theory of piezoelectricity and Kirchhoff plate model, a modified continuum mechanics based model that can capture the size features of

the cantilevered piezoelectric nanoplate is developed. In this model, the flexoelectric effect is incorporated in the governing equations and the boundary conditions.

In Chapter 4, finite difference method (FDM) is employed to obtain the numerical solutions to the problem. The discrete process of the governing equations and boundary conditions is presented in detail.

In Chapter 5, the size-dependent flexoelectric effect on the static bending behaviors and the electromechanical coupling of a cantilevered piezoelectric nanoplate is interpreted through the numerical results. The effects of different factors, such as the plate thickness, the plate in-plane dimensions, the applied voltages and the applied mechanical loads are investigated in detail.

Chapter 6 presents the conclusion based on the FEM result and provides recommendation for future research.

Chapter 2

2 Literature review

2.1 Piezoelectricity

The word *piezoelectricity* derives from Greek and means “electricity by pressure” (*piezo* comes from *piezein*, which means “to squeeze or press”; *electricity* comes from *elektron*, which means “shining light”). This term was suggested by Hankel (1881) to label the phenomenon first discovered by brothers Pierre and Jacques Curie (1880). Using certain crystals, the Curie brothers observed the production of positive and negative charges on several parts of the crystal surfaces when compressing the crystal in different directions. This phenomenon is known as the direct piezoelectric effect. By the end of the year after their discovery, the Curie brothers confirmed the existence of the reverse piezoelectric effect, which was first mathematically deducted by Lippmann (1881) using the fundamental thermodynamics theory. The reverse piezoelectric effect refers to the induction of mechanical deformations by the application of an electric field. The Curie brothers also found that the magnitude of the piezoelectric constant of quartz for the direct and reverse effects was the same.

It is found that the piezoelectric effect only exists in materials with non-centrosymmetric crystal structures. As illustrated in Figure 2-1, for non-centrosymmetric molecule, the centers of mass for the positive ions coincide with that for the negative ions without any applied force. Thus, the external effects of the positive and negative charges cancel out reciprocally, which results in an electrically neutral molecule. When an external force is applied to the material, the centers of mass for both the positive and negative ions experience relative displacement with respect to each other, producing a dipole moment. The dipole moment cancels out inside the material, and a distribution of charge appears in the material surface, thus a polarization develops and produces an internal electric field. On the contrary, in centrosymmetric materials, the center of masses of the positive and negative ions coincide at the center of symmetry even under mechanical strains, remaining zero net polarization, which indicates no piezoelectricity for such centrosymmetric materials. The piezoelectric effect is reversible, which means that materials possessing

direct piezoelectric effect also exhibit reverse piezoelectric effect. For the reverse piezoelectric effect under the applied electric field, the negative ions have a tendency to move towards the positive ions. This change results in the shift of negative and positive ions, which will change the dimension of the material and give rise to strains. The mechanisms of direct piezoelectricity and reverse piezoelectricity show that although those two phenomena are reversible, they are fundamentally different.

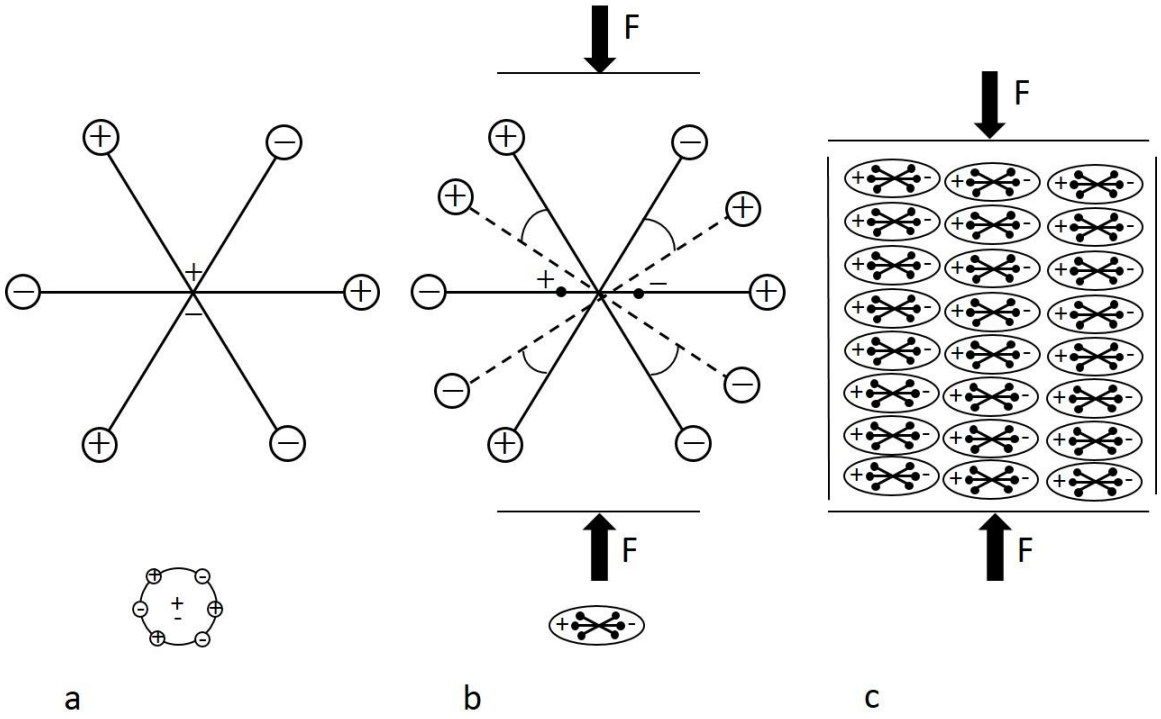

Figure 2-1 A molecular model for explaining the piezoelectricity: (a) unperturbed molecule; (b) molecule subjected to an external force, and (c) polarizing effect on the material surfaces (reproduced from Reference (Arnau, 2004))

Piezoelectricity is possessed by a group of natural materials such as quartz, zinc blende, sodium chlorate, calamine, topaz, tartaric acid, cane sugar, Rochelle salt and so on. However, due to the low electromechanical coupling effect, which limits the performance of those materials, the commercialization of piezoelectric materials was strongly inhibited in the early days. This situation was later changed when a major breakthrough came with the invention of piezoelectric ceramics, including barium titanate ($BaTiO_3$) in the 1940s

and the lead zirconate titanate (PZT) in the 1950s. Those materials exhibit high dielectric and piezoelectric properties, therefore their behaviors could be altered to desired responses and applications (Jordan and Ounaies, 2001). Piezoelectric ceramics comprise of small crystallites in large quantities. Below the Curie point (Shah, 2011; Yan, 2013), each elementary crystallite has a built-in electric dipole. Neighboring dipoles tend to align with each other to form regions known as domains, hence, resulting in a net dipole moment to the domain. Domains are distributed randomly throughout the material, and the polarization directions between domains differ from one to another. Thus, there is no overall polarization or piezoelectric effect. However, the ceramics may become piezoelectric by a poling process during which the material is subjected to a strong electric filed at a temperature slightly below the Curie point. As shown in Figure 2-2, during such a poling process, the electric field orients all the dipoles in the direction of the field. After the removal of the electric field, most dipoles remain locked in roughly the same direction, resulting in the appearance of permanent polarization. The poling process is usually the last step in manufacturing piezoelectric ceramics (Jordan and Ounaies, 2001).

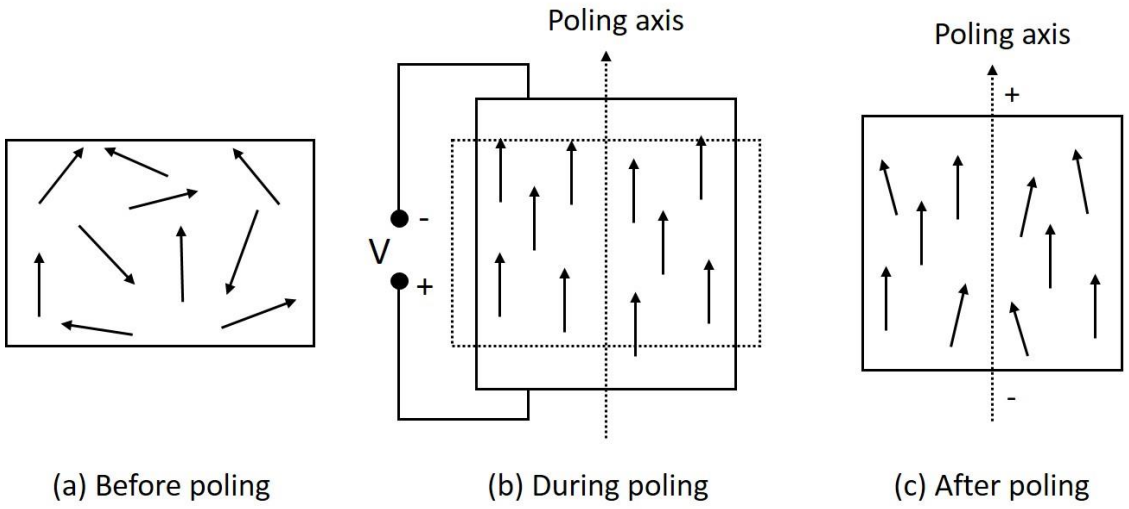

Figure 2-2 Effects of poling (reproduced from Reference (Morgan Matroc, Inc))

Due to the high electromechanical coupling effect and the development of modern technologies, the present-day needs and uses of piezoelectric materials are extended to various application areas, ranging from simple consumer products such as seat belt buzzer

to complex technological advancements, such as energy harvesting devices (Ottaman *et al*., 2002; Sodano *et al.*, 2004; Shu *et al.*, 2007), transformers (Flynn and Sanders, 2002; Ivensky *et al.*, 2002; Horsley *et al.*, 2007), sensors (Chee, 1998; Sirohi and Chopra, 2000, Steinem *et al.*, 2007), transducers (Krimholtz *et al.*, 1970a; 1970b; Leach, 1994; Dubois and Muralt, 1999), actuators (Crawley and De Luis, 1987; Ang *et al.*, 2007; Rakotondrabe, 2011), atomic force microscopy (Walters *et al.*, 1996; Christman *et al.*, 1998; Croft *et al.*, 2001), artificial muscles (Ashley, 2003), underwater sonars (Dahlstrom *et al.*, 1988; Ting, 1992; Tressler, 2008), medical imaging systems (Ritter *et al.*, 2002; Shuang *et al.*, 2007) and so on.

2.2 Piezoelectric nanomaterials and their size-dependent properties

Nanostructured materials are defined as materials with morphological features at nanoscale (Mishra and Sethy, 2013), which are smaller than $1\ \mu m$ in at least one dimension and potentially as small as atomic and molecular length scales ($\sim 0.2\ nm$) (Buzea *et al*., 2007). Compared with their bulk counterparts, nanomaterials exhibit unique properties such as larger fraction of surface atoms, large surface energy caused by high surface to volume ratio, spatial confinement, reduced imperfections and so on. With the development of synthesis techniques and nanotechnologies, diverse nanostructures can be achieved under specific growth conditions. Based on the dimension of the nanostructures, they are classified into three main categories (Fang *et al.*, 2013): zero-dimensional (0D) nanoparticles with all three dimensions at the nanoscales (Dodds *et al*., 2012) such as nanocluster material (Demishev *et al*., 2002), nanodispersions (Green, 2010) and quantum dots (Alivisators, 1996); one-dimensional (1D) nanostructures with nanoscale features in two dimensions such as nanotubes (Yin and Qu, 2014), nanowires (Wang and Song, 2006), nanobelts (Kulkarni, *et al.*, 2005), nanorods (Aydogdu, 2009), nanofibers (Zong *et al.*, 2002), nanorings (Wang and Duan, 2008) and *etc*.; two-dimensional (2D) nanostructures with nanoscale in one dimension such as nanofilms (Zhang and Wang, 2012), nanoribbons (Li *et al.*, 2008), graphene (Murmu and Pradhan, 2009) and quantum walls (Landi *et al.*, 2005).

"Small is different", such materials may have special mechanical and physical properties stemming from their nanoscale features. In mechanical property aspects, they have enhanced stiffness and strength compared to their macroscale counterparts, which make them potential applications as reinforcements in composites. Due to electron/phonon scattering at grain boundaries of nanoscale crystallization, the thermal and electrical conductivity of nanowires are noticeable reduced (Chen *et al.*, 2011).One of the most important features of nanowires is its considerable small thermal conductivity. Therefore, from manipulated materials to low-dimensional nanowires, it gives an innovative method to enhance the heat-electricity conversion efficiency for thermoelectric materials. The change in properties is not always preferable. For example, for ferroelectric materials smaller than 10 nm, the magnetisation direction can be switched using room temperature thermal energy, thus the materials will be useless for memory storage.

In recent years, the combination of nanotechnology and piezoelectric technology has resulted in a new class of piezoelectric nanostructures (Fang *et al.*, 2013).Those nanoscale piezoelectricity materials exhibit enhanced piezoelectric effect, excellent resilience, and semiconducting properties (Wang *et al,* 2007). Those unique features make them appealing for a wide range of applications in nanoelectromechanical systems (NEMS). One of the most promising applications is piezoelectric nanogenerators, first introduced by Wang and Song (2006). In their research, electricity was generated by deforming aligned piezoelectric nanowires with a conductive atomic force microscopy (AFM) tip, demonstrating a prototype of piezoelectric nanogenerators. Later, direct electricity generated from other one-dimensional and two-dimensional nanostructures has also been successfully demonstrated by researchers, including $BaTiO_3$ nanowirs (Wang *et al,* 2007), PVDF nanofibers (Chang *et al.*, 2010), $BaTiO_3$ nanofilms (Park *et al.*, 2010), and PZT nanoribbons (Qi *et al.*, 2010). The development of such piezoelectric nanogenerators opens up new ways for self-powering of wireless nanodevices and nanosystems. Apart from the piezoelectric nanogenerators, there are other applications using nanostructured piezoelectric materials such as nanosensors (Lao *et al*., 2007), diodes (Yang *et al.*, 2009) and nanoresonators (Asemi *et al.*, 2014). However, as these applications are still in the early stage of the development, there is still a long way to go to make them available commercially. Thus, in order to fulfill the potential application of piezoelectric

nanomaterials, it is essential to have a better understanding of the electromechanical coupling at the nanoscale.

For macroscale materials, their physical and mechanical properties can be well predicted by traditional technique. Extensive efforts have been made to investigate the properties of piezoelectric nanomaterials, including both experimental and atomistic studies. It is found that the physical properties of piezoelectric nanomaterials differ from their corresponding bulk counterparts, i.e., the size-dependent properties. By employing electric-field-induced resonance method, Chen *et al.* (2006) studied the Young's modulus of ZnO nanowires, and the experiment results showed that the Young's modulus increased dramatically with the decrease of the diameter. Using contact resonance atomic force microscopy (CR-AFM) and friction-type measurements, Stan *et al.* (2007) also found that the elastic property of ZnO nanowires showed size-dependence features. When the wire diameter was reduced to a certain small value, the radial elastic moduli and the shear modulus increased noticeably. Using a MEMS test-bed for quasi-static uniaxial tensile testing, Desai and Haque (2007) observed that the fracture strain of ZnO nanowires varied from 5% to 15% when decreasing the diameter from 500nm to 200nm. The study carried out by Wen *et al.* (2008) showed that the ultimate strength of ZnO nanowires could be up to 40 times of that of bulk material, in which the controlled lateral force atomic force microscopy (AFM) measurement was performed. Bühlmann *et al.* (2002) demonstrated a strong increase of the piezoelectric response of PZT films with lateral dimensions below 200nm based on piezoelectric sensitive scanning force microscopy in the contact mode. Zhao *et al.* (2004) measured the effective piezoelectric coefficient of ZnO nanobelt using piezoresponse force microscopy (PFM), and it was found that the effective piezoelectric coefficient of ZnO nanobelts depended on the frequency and was much larger than the corresponding values of the bulk ZnO. Zhu *et al.* (2008) investigated the piezoelectric property of a ZnO nanowire and found size dependence of the piezoelectric coefficient using a resonance shift method with a nano-electromechanical oscillator. Minary-Jolandan *et al.* (2012) directly measured three independent piezoelectric coefficients of d_{33}, d_{13} and d_{15} for GaN nanowires using an experimental approach based on scanning probe microscopy, and the result revealed that GaN nanowires displayed strong piezoelectricity in three dimensions, with up to six times of that for their bulk counterpart.

In addition to the experimental studies, atomistic simulations have also been employed to investigate the physical properties of nanoscale piezoelectric materials. For atomistic modeling, the atomic-level resolution is obtained by treating atoms as elementary units. Similar trends on the size-dependency have been observed. With molecular dynamical simulations, Komanduri *et al.* (2002) performed uniaxial tension on nanoscale silicon (Si) and germanium (Ge) using the multibody Tersoff potential, and they found that the extent of strain prior to failure was much higher than the one at the macroscale. Liang and Zhou (2003) analyzed the effects of size and strain rate on the tensile deformation of Cu nanowires using molecular dynamics simulations with an embedded atom method (EAM) potential. It was found that the yield stress decreased with the specimen size while ductility increased with the specimen size. Using molecular dynamics simulations, Kulkarni *et al.* (2005) studied the response of ZnO nanobelts to quasi-static tensile loading. It was demonstrated that the ultimate tensile strength and the Young's modulus of the belts were dependent on the size and the growth orientation. Agrawal *et al.* (2008) examined elasticity size effects in ZnO nanowires using a combined experimental (an in situ TEM tensile testing technique) and computational (large-scale atomic/molecular massively parallel simulator) approach, demonstrating the size-dependency of Young's modulus. Dai *et al* (2009) performed molecular dynamics simulation to study the tensile behavior of ZnO nanowires under tensile loading, and the relationship between the structural deformation and the size-dependent mechanical property was provided in detail. Using shell-model based molecular dynamics, Zhang *et al.* (2009; 2011) found that both the elastic modulus and piezoelectric coefficient of BaTiO3 nanowires are size dependent and their values differ from those of their bulk counterparts. Agrawal and Espinosa (2011) were the first to study the piezoelectric size effects of ZnO and GaN nanowires using principle-based density functional theory (DFT) calculation. They found a giant piezoelectric size effect, which was confirmed by Momeni *et al.* (2012) using a molecular dynamics approach.

From the literature, we can see that size dependency is a factor that significantly affects the properties of nanoscale piezoelectric materials. Thus, it is of great importance to have a better understanding of the underlying physics of such size dependent properties. However, the extremely small dimensions of nanostructures can raise serious challenges for experimental measurements. Meanwhile, atomistic simulations have computational

limitations at both length and time scales, since generally they can only model nanostructures within several nanometers. Therefore, continuum mechanics modelling could be an alternative and efficient way to investigate the properties of nanomaterials. The structure features of materials at nanoscale break the law of continuum mechanics. Conventional continuum models ignore the variation of interatomic quantities and fail to capture the size effects of materials at nanoscale. Therefore, modified continuum models are required to incorporate the size effects. Due to the large surface to volume ratio of structures at nanoscale, surface effects are believed to play a substantial role in the size-dependent properties of nanomaterials. Particularly for piezoelectric nanomaterials, flexoelectricity is also believed to contribute to their size-dependent properties. Therefore, these two features need to be incorporated in the continuum modeling.

2.3 Factors that contribute to size-dependent properties of piezoelectric nanomaterials: surface effects and flexoelectricity

2.3.1 Surface effects

The concept of surface effects originates from the surface tension of liquid. Surface tension is a contractive tendency of a liquid surface that allows it to resist an external force, which is caused by the cohesion. The surface tension is described by the Young-Laplace equation, which states that the difference between the hydrostatic pressures of a spherical surface is proportional to the surface tension and the mean curvature. Based on the solution of this equation, shapes governed by the surface tension can be determined, such as the shape of water drops, puddles and soap bubbles. The essence of surface tensions is explained by the fact that the environment for atoms in the vicinity of a surface is different from that for atoms in the bulk. Thus, the energy of surface atoms differs from that of the corresponding bulk atoms, which in turn results in excess free energy, *i.e.* the free surface energy in the solid (Streitz *et al.*, 1994). Different from liquids, the surface energy of solids is deformation dependent. The concept of surface stress in solids, introduced by Gibbs (1906), is defined through the change in excess free energy when the interface is deformed at a constant referential area. This surface stress is the work-conjugate to the surface strain with respect to surface energy. As the surface effect on the nearby atoms usually extends

to a few atomic layers, which are like a transition interphase, Gibbs idealized the surface energy and the surface stress as quantities in a continuum sense, belonging to a "mathematical surface" with a negligible thickness. Due to the large surface to volume ratio usually presented in nanomaterials, surface effects may be largely responsible for the size-dependent property of piezoelectric materials at nanoscale.

Due to the limitation of both atomistic simulations and experimental testing as discussed previously, modified continuum models have been extensively investigated by researchers to better understand the size-dependent properties of nanomaterials. In order to incorporate the surface effects in the continuum modeling, Gurtin and Murdoch (1975) did a pioneering work with the development of the linear surface elasticity theory. According to this theory, nanostruture could be decomposed into a bulk part and surface layers with negligible thickness adhered to the bulk part without slipping (Commarata, 1997; Shen and Hu, 2010). The properties and constitutive equations for the surface differ from those for the bulk part. The generalized Young-Laplace equations are employed to govern the equilibrium of the surface, while the material properties can be obtained from experiments or atomistic simulations. By employing such continuum theory, Miller and Shenoy (2000) studied the size-dependent elastic property of Al and Si nanowires and nanoplates considering the surface effects. Based on the continuum theory of mechanics, Dingreville and Cherkaoui (2005) developed a framework with the surface free energy incorporated, and the results showed the size-dependent property of the overall elastic behavior of structural elements. Through the augmented continuum theory with surface effects, the size dependence of torsional rigidities of nanosized bars was studied by Shenoy (2002), and the results agreed well with those calculated using direct atomistic calculations. By incorporating the Young-Laplace equation into the Euler Bernoulli beam theory, He and Lilley (2008) investigated the effect of surface stress and surface elasticity on the resonance frequencies of nanowires with different boundary conditions. Based on Gurtin's linear surface elastic theory, Wang *et al.* (2008) quantitatively investigated the twisting deformation of nanowires due to the effects of anisotropic surface stresses and surface elasticity, and they demonstrated that such effects might be a reason for the formation of some micro-/nanohelices. Wang and Feng (2009) investigated the size-dependent surface effect on the axial buckling and transverse vibration of nanowires using Timoshenko beam model. Assadi and Farshi

(2010) studied the size dependent free vibration of curved nanobeams and rings with the consideration of surface energies. Besides one-dimensional nanostructures, two-dimensional nanostructures have also been widely investigated with the consideration of the surface effects. He *et al.* (2003) analyzed the size-dependent deformation of elastic nanofilms with an arbitrary geometry and edge boundary conditions using the surface elasticity model. Wang and Zhao (2009) investigated the size-dependence of self-buckling and bending behaviors of nanoplates via incorporating surface effects. Lu *et al.* (2009) studied the elastic mechanical behavior of functionally graded nanomaterials taking into account surface effects by using modified Kirchhoff plate theory. Assadi *et al.* (2010) investigated the size dependent dynamic properties of nanoplates, in which the surface properties were considered, such as surface elasticity and residual stresses. Later, Assadi and Farshi (2011) also conducted a size dependent stability analysis of circular ultrathin films deposited on elastic medium considering surface energies.

In the surface elasticity model, the surface energy density is associated with the in-plane strain at the surface. In piezoelectric nanostructures, it is reasonable to assume that the surface energy density may also rely on the electric field at the surface. By extending the surface elasticity model, Huang and Yu (2006) proposed a surface piezoelectricity model, in which the effect of surface piezoelectricity is taken into consideration in addition to the residual surface stress and the surface elasticity. Their work observed a considerable influence of surface piezoelectricity on the stresses and electric fields of a piezoelectric ring when the ring scaled down to nanoscale. Extensive investigations have been conducted based on the piezoelectric surface model. Li *et al.* (2011) did research on the wrinkling of piezoelectric films on compliant substrates with surface effects included, and it was shown that the surface effects depended on the film thickness. By employing Huang and Yu's theory, Yan and Jiang (2011a; 2011b) studied the surfaces effects on the electromechanical coupling and bending behaviors of piezoelectric nanowires, as well as the vibrational and buckling behaviors of piezoelectric nanobeams with Euler-Bernoulli beam theory. Later, they applied the theory to curved piezoelectric nanobeams (Yan and Jiang, 2011c). Recently, Yan and Jiang (2012a; 2012b; 2012c) also systematically investigated surface effects on the static and dynamic behaviors of piezoelectric nanoplates using the modified Kirchhoff plate theory and the generalized Young-Laplace equations. Zhang *et al.* (2012)

examined the surface effects on the buckling of piezoelectric nanofilms due to an electrical voltage. Their results showed that the surface effects on the critical buckling voltage of a piezoelectric nanofilm relied sensitively on the thickness, the length-to-thickness ratio, and the residual surface stress. Zhang and Wang (2012) developed a sandwich-plate model to investigate the vibration of piezoelectric nanofilms, and it was found that the significant surface effect was originated primarily from the residual surface stress and the stress caused by an electrical voltage due to the surface piezoelectricity. Zhang *et al.* (2013) derived the governing equations of nanoscale piezoelectric plates considering surfaces effects, and found the size dependency of the effective properties and the natural frequencies. Later, Zhang *et al.* (2013) also presented a two-dimensional (2D) general equations for piezoelectric nanoshells considering the surface effects, and their results showed the size-dependent property of resonant frequencies of a piezoelectric cylindrical shell.

2.3.2 Flexoelectricity and its size-dependent property

The flexoelectric phenomenon was first predicted by Makevich and Tolpygo (1957). Currently, the flexoelectricity is applied in two areas of condensed matter physics: soft matter (liquid crystals and biological materials) and common solids (Yudin and Tagantsev, 2013). Unlike the piezoelectricity, which represents a conventional electromechanical coupling between the electric polarization and the uniform strain and is unique for noncentrosymmetric crystals, flexoelectricity is a universal effect for all dielectrics, even for centrosymmetric crystal structures. Flexoelectricity refers to a spontaneous polarization in linear response to an inhomogeneous deformation or strain gradients. Conversely, the reverse flexoelectricity refers to strain fields caused by polarization gradients. Tagantsev (1985) suggested four contributors to the flexoelectric effect: (1) the bulk dynamic flexoelectric effect, (2) the bulk static flexoelectric effect, (3) the surface flexoelectric effect, and (4) the surface piezoelectric effect. The first two contribute to the case of a propagating sound wave, and the last three contribute to the case of a strain gradient in a finite crystal medium.

In regards to the surface flexoelectric response, there are two contributing factors: surface piezoelectric effect and surface flexoelectric effect. The average piezoelectric constant for surface atoms is dependent on the surface and the crystallographic orientation (Tagantsev,

1986). According to Tagantsev and Yurkov (2012) and Yudlin and Tagantsev (2013), for surface piezoelectricity, the effect is expected to be comparable to that of the static bulk flexoelectricity and scales as the bulk dielectric constant in high-K material. For surface flexoelectricity, the effect is tangible for materials with moderate values of dielectric constants. However, it is of minor importance in high-K material, which makes it less appealing in terms of practical applications.

When an acoustic sound wave passes through a medium, it will generate a time-dependent strain gradient, which produces displacements of the ions. Accordingly, the acceleration of ions induces the flexoelectric response, which is called the dynamic flexoelectric effect. According to Tagantsev (1986) and Zubko *et al.* (2013), in a sound wave, both the static and the dynamic flexoelectric effects control the amplitude of the polarization, which differs considerably from the one for a static strain gradient condition. The result in the work of Tagantsev (1986) showed that the static and dynamic flexoelectric effects are of the same order in a sound wave. It is thus of great importance to account for the dynamic flexoelectric effect when investigating the properties of nanoscale dielectric materials in the dynamic electromechanical simulation (Kvasov and Tagantsev, 2015).

In this thesis, we are interested in the case of dielectric materials under static bending condition without considering surface effects. It means only bulk static flexoelectric effect is considered in this work. Bulk static flexoelectricity is related to a fourth-order flexoelectric tensor μ. Unlike the piezoelectric tensor, which vanishes for centrosymmetric material, the flexoelectric tensor is not zero for material of any symmetry; this difference was verified via lattice dynamics by Mindlin (1969) and Askar *et al.* (1970). According to Zubko *et al.* (2013), for centrosymmetric materials, under a homogenous deformation, the material will remain centrosymmetric since uniform strain does not break centrosymmetry. Thus, there is no polarization in such material under uniform deformation. In contrary, nonuniform deformation or strain gradients locally break the inverse symmetry of the material, rendering the formation of dipole moments and thus the induced polarization.

In a phenomenological way, the electric polarization P_i caused by the nonuniform strain ε_{jk} can be expressed by this equation,

$$P_i = \mu_{ijkl} \frac{\partial \varepsilon_{jk}}{\partial x_l} \qquad (2.1)$$

Obviously, the strength of the flexoelectric effect depends on the numerical values of the flexoelectric coefficient μ_{ijkl} or how large the strain gradients are. In general, the flexoelectric coefficients are rather insignificant relative to the piezoelectric coefficients in macro-scale piezoelectric materials. However, the strain gradients are closely linked with the feature scale of the structure. The essence of such a size-dependent flexoelectric effect is displayed in Figure 2-3. For two embedded triangular inclusions subject to a stress at two different length scales (μm vs. nm) but with the same aspect ratio, the strain field remains the same across both length scales, but the strain gradients scale as $1/a_i$. It is evident that for nanoscale materials, this flexoelectric effect becomes more significant. Thus, the size-dependent flexoelectricity may contribute significantly to the electromechanical coupling of piezoelectric materials at the nano-scale, which needs to be incorporated when modeling the electroelastic responses of piezoelectric nanostructures.

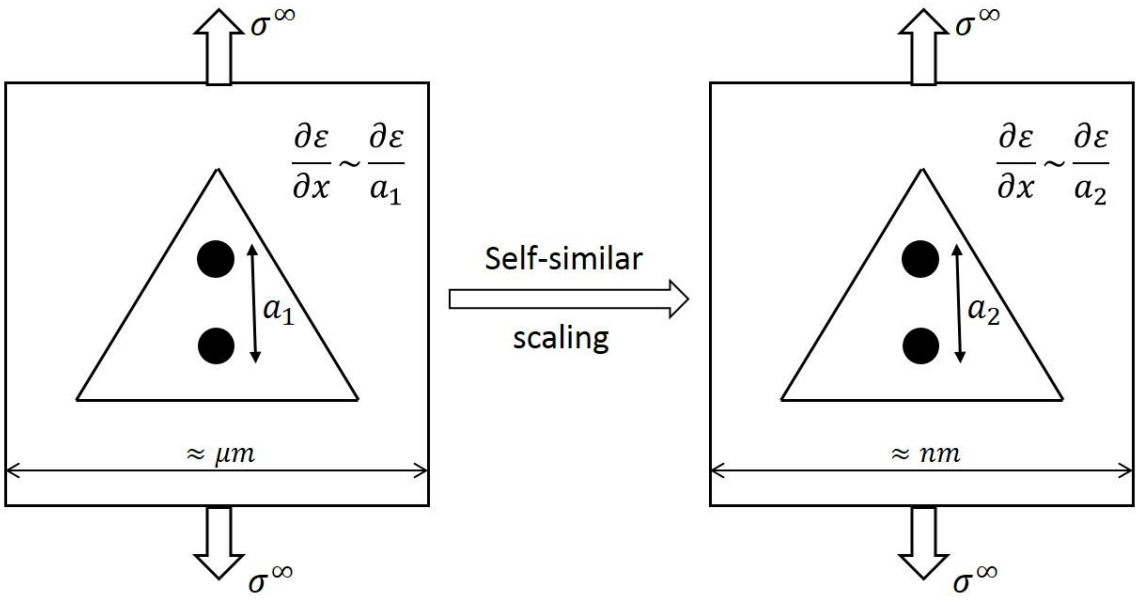

Figure 2-3 Illustration of size effects due to scaling of strain gradients (reproduced from Reference (Majdoub *et al.* (2008b))

2.3.3 Flexoelectricity characterization

Kogan (1964) proposed a phenomenological description of the flexoelectric effect, and the flexoelectric coefficient μ_{ij} was estimated to be the order of e/a (where e is the electron charge and a is the lattice parameters), which is usually as low as $10^{-10} - 10^{-11} C/m$. Later, Tagantsev (1985) investigated the flexoelectric phenomenon in details. For the flexoelectric effect, it was concluded that the flexoelectric coefficients μ_{ij} might be in proportion to the dielectric susceptibility χ_{ij} by the form of $\mu_{ij} = \gamma \chi_{ij} \frac{e}{a}$ (where γ is a constant whose value is close to unity). From this equation, it can be seen that the flexoelectric coefficient μ_{ij} is enhanced by the dielectrics with high dielectric susceptibility χ_{ij}. This theory was later proved by a series of beam bending experiments carried out by Ma and Cross using materials such as barium strontium titanate ($Ba_{0.67}Sr_{0.33}TiO_3$) (2002), lead zirconate tiatnate (PZT) ceramics (2005), and barium titanate ceramics (2006).

By applying uniaxial compression to a truncated triangle shaped sample, Cross (2006) measured some flexoelectric coefficients of $Pb(Mg_{1/3}Nb_{2/3})O_3$ and $Ba_{0.67}Sr_{0.33}TiO_3$, but individual longitudinal components were hard to obtain due to the inhomogeneous strain gradients distribution. Using the same method as Ma and Cross, Zubko *et al.* (2007; 2008) measured the flexoelectric coefficients of $SrTiO_3$ with different crystallographic orientations. It was found that it is impossible to obtain all components of the flexoelectric coefficients via this bending method. Using nanoindentation method, Gharbi *et al.* (2011) confirmed the order of flexoelectric coefficients of $BaTiO_3$ obtained by Ma and Cross's experiments. Zhou *et al.* (2012a) measured the flexoelectric coefficients of $BaTiO_3$ by applying a homogeneous electric field, instead of applying a mechanical load. In addition to experimental studies, atomistic simulations have also been employed to derive the flexoelectric coefficients. Askar *et al.* (1970) used a shell-type model to derive the polarization-gradient coefficients, while Tagantsev (1986) employed a rigid-ion model to calculate the flexoelectric coefficients. For a rigid-ion model, the ion is considered as a whole part; while for the shell-type model, the outmost electron shell can move with reference to the ionic core. Through a lattice dynamics based microscopic approach, Maranganti and Sharma (2009) provided estimates of the flexoelectric tensor for certain crystalline dielectrics. Another way to determine the flexoelectric coefficients is the use of

the first principle theory (also known as the *ab initio* princile). According to Hong *et al.* (2010), the first principle theory can generate the independent flexoelectric coefficients, and provide guidance for the order of the value one should expect from experiments. Hong *et al.* (2010) used a direct *ab initio* approach to calculate the longitudinal flexoelectric coefficient of $BaTiO_3$ and $SrTiO_3$, the hardest one to measure experimentally (Zubko *et al.*, 2007; 2008,). Using a first-principles-based effective Hamiltonian technique, Ponomareva *et al.* (2012) studied the magnitude and the sign of each flexoelectric tensors in $(Ba_{0.5}Sr_{0.5})TiO_3$ thin films, and they found that the flexoelectric coefficients depended strongly on the film's thickness and temperature. Hong and Vanderbilt (2013) studied the flexoelectric coefficients using the first principle calculation, and it was found that the flexoelectric response could be divided into "longitudinal" and "transverse" components. Xu *et al.* (2013) determined the transverse and shear flexoelectric coefficients of $BaTiO_3$ and $SrTiO_3$ via direct atomistic methods based on the first principle calculation. In addition to the methods mentioned above, with the techniques of harmonic decompositions and Cartan decompositions, Le Quang and He (2011) solved the basic problem of determining the number of independent components contained in a flexoelectric tensor for a given symmetry class. Based on the fundamental tensor relationship of the flexoelectricity, Shu *et al.* (2011) studied the symmetry of flexoelectric coefficients in matrix form for crystalline medium, and the non-zero and independent elements in the matrices were also calculated for 32 point groups and 7 Ci groups.

2.3.4 Flexoelectric effects on the properties of nanoscale dielectrics

In the literature, it was found that the flexoelectricity has a great impact on the properties of piezoelectric nanomaterials. Using the flexoelectric effect, Fousek *et al*. (1999) proposed a theory that by shaping the composite constituents properly, it is possible to create piezoelectric components without using piezoelectric materials. This concept was realized experimentally by Zhu *et al.* (2006), who fabricated a piezoelectric composite from $Ba_{0.67}Sr_{0.33}TiO_3$ (BST) composition. Kityk *et al.* (2000) examined the elastic behavior of $SrTiO_3$ using a three-point-bending method. They found nonlinear elastic anomalies in the real and imaginary parts of the complex Young's modulus, which could be explained by assuming the ferroelectric order was induced by the applied strain gradient due to

flexoelectric coupling. Research carried out by Catalan *et al.* (2004; 2005) showed the important role played by flexoelectricity in decreasing the dielectric constant of ferroelectric thin films. Majdoub *et al.* (2009) explained that the flexoelectricity might be the dominant contributor to the dead layer effect in nanocapacitors, which rendered the magnitude of capacitance of such film lower than expected. Due to the flexoelectricity, Lee *et al.* (2011) showed that the domain configuration of $HoMnO_3$ ferroelectric thin film changed from poly-domain to mono-domain, leading to a large systematic modification of the hysteresis loops. Catalan *et al*. (2011) found that in certain domain walls in $PbTiO_3$, the flexoelectricity could induce polarization rotation, which is a characteristic of the morphotropic phase boundaries (MPB) with high piezoelectricity. By investigating the morphotropic phase boundaries (MPB) in ferroics, Borisevich *et al.* (2012) demonstrated that the flexoelectricity could render the effective domain wall energy negative, thus, making modulated phases near MPB stable. Lee *et al.* (2012) showed that the flexoelectricity could generate a rectifying diode effect and could also govern the local transport characteristics. The experiment carried out by Lu *et al.* (2012) suggested that due to the flexoelectric effect, the stress gradient induced by the tip of an atomic force microscope (AFM) could switch the polarization mechanically in the nanoscale ferroelectric film.

To describe the flexoelectric effect phenomenologically, the Landau-Ginsburg-Devonshire (LGD) theory has been widely adopted by researchers. Based on such theory, Eliseev *et al.* (2009) pointed out that the flexoelectric effect on nano-rods and thin pills could change the uni-cell symmetry, leading to the shift of the phase transition temperature, the change of the spatial distribution of the order parameter, the distortion of the nanoparticle shape and the renormalization of extrapolation length of the boundary conditions. Zhou *et al.* (2012b) demonstrated that the flexoelectricity could result in the increase of the theoretical critical thickness in epitaxial $BaTiO_3$ thin films, especially in the tension stressed films. Yudin *et al.* (2012) also adopted such theory to study the flexoelectric influence on the internal structure of neutral domain walls, and it was found that the flexoelectricity had an effect on the symmetry of domain walls, resulting in additional anisotropy and a domain wall structure different from the classical Bloch-wall structure. Chen and Soh (2012) phenomenologically studied the flexoelectric effect on the nanocomposite thin bilayer

films. The results showed that with the decrease of the film thickness, the polarization caused by flexoelectricity became more and more dominant, and it could even surpass the polarization caused by electrostricition and change the polarization value from negative to positive. Tagantsev and Yurkov (2012) phenomenologically suggested that the incorporation of the flexoelectric coupling could modify the mechanical boundary conditions of the nanostructures. This suggestion was later justified by Yan and Jiang (2013). They found that when considering the flexoelectric effect, the boundary condition of a cantilevered beam was more complicated than that of the conventional one.

To better understand the flexoelectric effect, it is of importance to establish the theoretical framework taking into consideration the nanoscale feature. Based on Toupin's (1956) linear piezoelectricity theory, Mindlin (1968) proposed a continuum field theory for the dielectrics with the reverse flexoelectric effect, which does not incorporate the direct flexoelectricity. Later, Maranganti *et al.* (2006) developed a complete theoretical framework for isotropic non-piezoelectric continuum materials considering the flexoelectric effect, its converse flexoelectric effect and the strain gradient effects. In this work, the fundamental solutions (Green's functions) for the governing equations were derived, which provided explicit results for the strain-mismatched embedded inclusion problem. Recently, Hu and Shen (2010) established a more comprehensive theoretical model with the consideration of the flexoelectricity, the electrostatic force and the surface effects for nanosized dielectrics.

Relying on these theoretical frameworks, many efforts have been devoted to investigating the flexoelectric effect on the physical and mechanical properties of the piezoelectric nanostructure. Based on the framework of Maranganti *et al.* (2006), Sharma *et al.* (2007) quantitatively demonstrated the possibility to create piezoelectric composite materials without using piezoelectric constituents. This theory was later verified by experiments carried out by Sharma *et al.* (2010), who created piezoelectric thin-film superlattices from non-piezoelectric materials. Using atomistic and theoretical approaches, Majdoub *et al.* (2008b) showed that the size-dependent piezoelectric coefficients of piezoelectric nanostructures were enhanced strongly by flexoelectricity. Later, by employing an atomically dynamical continuum model in which nanobeams were under dynamical

mechanical excitations, Majdoub *et al.* (2008a) found that the flexoelectricity could dramatically enhance the energy-harvesting ability in nanostructure. Using a continuum model considering the piezoelectric and flexoelectric effects, Liu *et al.* (2012) studied the flexoelectric effect on the electric potential distribution of bent ZnO nanowire cantilevers. The results showed that the flexoelectricity might fill the gap between the experimental and classical piezoelectric theoretical results. Based on the extended linear piezoelectric theory (Hu and Shen, 2010), Yan and Jiang (2013) proposed modified Bernoulli and Timoshenko beam models to investigate the influence of flexoelectricity on the bending and vibration behaviors of piezoelectric nanobeams. The results indicated that the size-dependent flexoelectric effect was sensitive to the boundary conditions, and the applied electrical load might reverse the deflection direction under certain loading conditions. Using the conventional Kirchhoff plate theory and the extended linear piezoelectric theory, Zhang and Jiang (2014) studied the electroelastic responses and the free vibrational behaviors of a clamped piezoelectric nanoplate considering flexoelectric effect. It was found that the flexoelectricity was more noticeable for thinner plates with smaller thickness, and the effect was dependent on the in-plane dimensions and the applied electric voltage. Based on the Kirchhoff plate theory, Liang *et al.* (2016) investigated the buckling and vibration of flexoelectric nanofilms, and the results indicated that the critical buckling loads and the natural frequency were influenced by the size-dependent flexoelectricity.

2.4 Summary

From the literature review stated above, it has demonstrated the importance of understanding the size dependent properties of piezoelectric nanomaterials in order to make better use of such nanostructures for future design and applications. For piezoelectric nanomaterials, the flexoelectricity is believed to contribute to its size dependent properties. Although efforts have been put into investigating the flexoelectric effect on the physical and electrical properties of piezoelectric nanostructures, the continuum modeling of such effect is still limited in the literature, especially for complex configurations. Thus, it is essential to further uncover the flexoelectric effect on the mechanical and physical properties of these piezoelectric nanomaterials.

Chapter 3

3 Modeling of cantilevered piezoelectric nanoplates (PNPs)

In this chapter, a mathematical model for a cantilevered piezoelectric nanoplate (PNP) accounting for the flexoelectricity is derived to study the size-dependent electromechanical behavior of the PNP.

3.1 Extended linear piezoelectric theory

Flexoelectricity represents an instantaneous polarization induced by non-uniform deformations or strain gradients. In order to take into account the effect induced by the strain gradients and some other coupling effects induced by polarization gradients (Hu and Shen, 2010), we adopt the extended linear theory of piezoelectricity to build the mathematical model in the current work. Under this theory, the most general form of the internal energy density function U can be expressed as,

$$\begin{aligned} U = {} & \frac{1}{2}a_{kl}P_kP_l + \frac{1}{2}c_{ijkl}\varepsilon_{ij}\varepsilon_{kl} + d_{ijk}\varepsilon_{ij}P_k + \frac{1}{2}b_{ijkl}P_{i,j}P_{k,l} + e_{ijkl}\varepsilon_{ij}P_{k,l} \\ & + f_{ijkl}u_{i,jk}P_l + \frac{1}{2}g_{ijklmn}u_{i,jk}u_{l,mn} + h_{ijk}P_iP_{j,k} \\ & + r_{ijklm}\varepsilon_{ij}u_{k,lm} + \eta_{ijkmn}P_{i,j}u_{k,mn} \end{aligned} \tag{3.1}$$

where P_i stands for the component for the polarization tensor, u_i is the component for the displacement tensor, and ε_{ij} is the component for the strain tensor defined as $\varepsilon_{ij} = \frac{1}{2}(u_{i,j} + u_{j,i})$. a_{kl}, c_{ijkl} and d_{ijk} are the elements of the reciprocal dielectric susceptibility, elastic constant, and piezoelectric constant tensors, respectively. These three terms stand for the conventional electromechanical couplings the same as those in the linear piezoelectric theory. The other terms are the higher order couplings between the electric polarization and the strain fields. b_{ijkl} represents the higher order coupling between the polarization gradient and the polarization gradient; f_{ijkl} is the component for direct flexocoupling coefficients, dictating the coupling between the strain gradient and the polarization; while e_{ijkl} is the component for the reverse flexocoupling coefficients, representing the coupling

between the polarization gradient and the strain. In accordance with References (Sharma *et al.*, 2010; Shen and Hu, 2010), it was justified that these two flexocoupling coefficient tensors satisfy $f_{ijkl} = -e_{ijkl}$. For simplicity purpose and to make the problem more mathematically tractable, the higher order couplings between the strain and the strain gradient ($r_{ijklm}\varepsilon_{ij}u_{k,lm}$), the strain gradient and the strain gradient ($g_{ijklmn}u_{i,jk}u_{l,mn}$), and the strain gradient and the polarization gradient ($\eta_{ijkmn}P_{i,j}u_{k,mn}$) are ignored in the current work as in the existing studies (Majdoub *et al.*, 2008b; Sharma *et al.*, 2010; Yan and Jiang, 2013; Zubko *et al.*, 2013; Zhang, Yan and Jiang, 2014; Zhang and Jiang, 2014). Thus, the expression of U can be reduced to

$$U = \frac{1}{2}a_{kl}P_kP_l + \frac{1}{2}c_{ijkl}\varepsilon_{ij}\varepsilon_{kl} + d_{ijk}\varepsilon_{ij}P_k + \frac{1}{2}b_{ijkl}P_{i,j}P_{k,l} + f_{ijkl}u_{i,jk}P_l + e_{ijkl}\varepsilon_{ij}P_{k,l} \tag{3.2}$$

Accordingly, the constitutive equations for the piezoelectric medium can be derived from the internal energy density function U as (Zhang, Yan and Jiang, 2014; Hu and Shen, 2014),

$$\sigma_{ij} = \frac{\partial U}{\partial \varepsilon_{ij}} = c_{ijkl}\varepsilon_{kl} + d_{ijk}P_k + e_{ijkl}P_{k,l} \tag{3.3}$$

$$\sigma_{ijm} = \frac{\partial U}{\partial u_{i,jm}} = f_{ijmk}P_k \tag{3.4}$$

$$E_i = \frac{\partial U}{\partial P_i} = a_{ij}P_j + d_{jki}\varepsilon_{jk} + f_{jkli}u_{j,kl} \tag{3.5}$$

$$E_{ij} = \frac{\partial U}{\partial P_{i,j}} = b_{ijkl}P_{k,l} + e_{klij}\varepsilon_{kl} \tag{3.6}$$

where σ_{ij} and E_i are the stresses and the electric fields, respectively, and they have the same meaning as those traditional ones in the linear piezoelectric theory. It is clear that the flexoelectricity induces some effects upon these traditional quantities. For example, the extra term in the electric field E_i is induced by the direct flexoelectricity while the extra term in the stress fields σ_{ij} is caused by the reverse flexoelectricity. The flexoelectric effect also induces higher order stresses and higher order electric fields, i.e., σ_{ijm} (also called

moment stress) and E_{ij} (also called local electrical force). These two quantities are not involved in the classical linear piezoelectricity.

For convenience purpose, the contracted index notation is adopted here for the conventional material constant tensors, for example, $c_{11} = c_{1111}, d_{31} = d_{311}$ and$f_{13} = f_{1133}$. Extensive efforts have been made to interpret and determine the flexocoupling coefficient tensor f_{ijkl} (Maranganti and Sharma, 2009; Sharma *et al.*, 2010). It is found that the flexocoupling coefficient tensor f_{ijkl} has the same number of independent components as the flexoelectric coefficient tensor μ_{ijkl} by following a relation $f_{ijkl} = a_{im}(\mu_{mjkl} + \mu_{mjlk} - \mu_{mklj})$. For a given symmetry class of materials, Le Quang and He (2011) explained explicitly how to determine the number and types of all possible rotational symmetries for flexoelectric tensors. Shu *et al.* (2011) has calculated the non-zero and independent elements of the direct flexoelectric coefficients in the matrix form. In the current work, the tetragonal barium titanate $BaTiO_3$ (point group 4 mm) is used as the example material, with its flexoelectric coefficient tensors given by Shu *et al.* (2011).

3.2 Derivation of the governing equations and the boundary conditions

In the current work, the focus of the investigation is on the electroelastic response of a cantilevered PNP with length b, width a, and thickness h as shown in Figure 3-1. A Cartesian coordinate system (x, y, z) is used to describe the plate with xy plane being the midplane of the undeformed plate and z axis along the plate thickness direction. For the plate, the edge $y = 0$ is clamped while the other three edges are free to move. The piezoelectric plate is polarized along the z direction and is coated with electrodes on the upper surface ($z = h/2$) and the lower surface ($z = -h/2$). The plate is subjected to both mechanical and electrical loads, i.e., a uniformly distributed mechanical load with density q and a constant electric voltage V across the plate thickness. In order to perform the bending analysis of the piezoelectric plate, the Kirchhoff plate theory is adopted here with the displacement fields being defined as:

$$u(x,y,z) = u^0(x,y) - z\frac{\partial w(x,y,z)}{\partial x} \quad (3.7)$$

$$v(x,y,z) = v^0(x,y) - z\frac{\partial w(x,y,z)}{\partial y} \quad (3.8)$$

$$w(x,y,z) = w(x,y) \quad (3.9)$$

where $w(x,y)$ is the transverse out-plane displacement along the plate thickness direction; $u(x,y,z)$ and $v(x,y,z)$ are the in-plane displacements along the x and y directions, respectively; $u^0(x,y)$ and $v^0(x,y)$ are the in-plane displacements of the midplane along the x and y directions, respectively. As discussed in the literature (Yan and Jiang, 2012a; Yan and Jiang, 2013), such in-plane displacements of the midplane is caused by the applied electrical load due to the electromechanical coupling under the current loading condition. Obviously, such in-plane displacements are also influenced by the flexoelectric effect. Based on the displacement fields, the non-zero strains for the plate can thus be obtained as,

$$\varepsilon_{xx} = \frac{\partial u}{\partial x} = \frac{\partial u^0}{\partial x} - z\frac{\partial^2 w}{\partial x^2} \quad (3.10)$$

$$\varepsilon_{yy} = \frac{\partial v}{\partial y} = \frac{\partial v^0}{\partial y} - z\frac{\partial^2 w}{\partial y^2} \quad (3.11)$$

$$\varepsilon_{xy} = \frac{1}{2}\left(\frac{\partial u}{\partial y} + \frac{\partial v}{\partial x}\right) = \frac{1}{2}\left(\frac{\partial u^0}{\partial y} + \frac{\partial v^0}{\partial x}\right) - z\frac{\partial^2 w}{\partial x \partial y} \quad (3.12)$$

Accordingly, the strain gradients along the plate thickness direction are derived as,

$$\varepsilon_{xx,z} = -\frac{\partial^2 w}{\partial x^2} \quad (3.13)$$

$$\varepsilon_{yy,z} = -\frac{\partial^2 w}{\partial y^2} \quad (3.14)$$

$$\varepsilon_{xy,z} = -\frac{\partial^2 w}{\partial x \partial y} \quad (3.15)$$

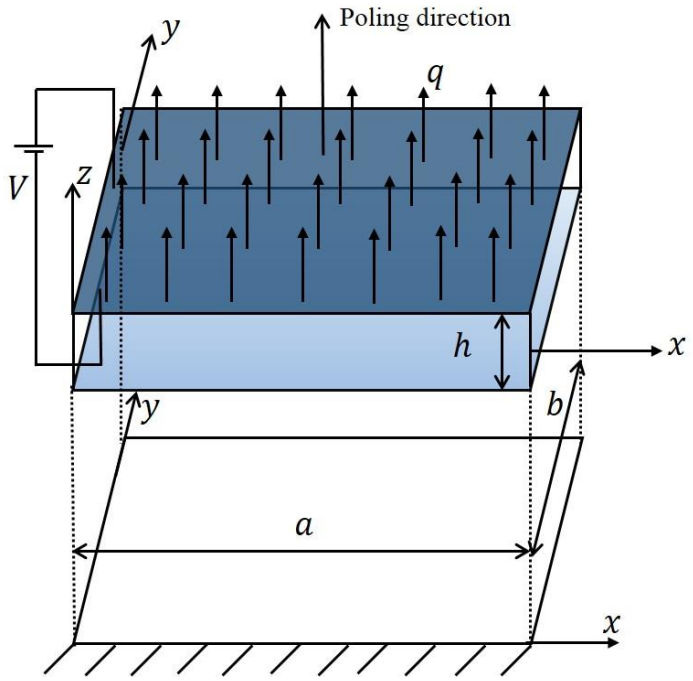

Figure 3-1 Schematic of a cantilevered piezoelectric nanoplate under applied mechanical and electrical loads

It should be mentioned that the strain gradients along the x and y directions (for example, $\varepsilon_{xx,x} = \frac{\partial^2 u^0}{\partial x^2} - z\frac{\partial^3 w}{\partial x^3}$ and $\varepsilon_{yy,y} = \frac{\partial^2 v^0}{\partial y^2} - z\frac{\partial^3 w}{\partial y^3}$) are neglected in comparison with the strain gradients along the thickness direction as defined in Eqs. (3.13) - (3.15). This assumption has also been adopted in the literature (Yan and Jiang, 2013; Zhang, Yan and Jiang, 2014) for Euler nanobeams and a Kirchhoff nanoplate, respectively, since the thickness of the objects is much smaller than the in-plane dimensions, i.e., $h \ll a, b$. Thus, in the following analysis, we will only take into account the flexoelectricity induced by the strain gradients along the thickness direction, i.e., $\varepsilon_{xx,z}$, $\varepsilon_{yy,z}$ and $\varepsilon_{xy,z}$.

For a piezoelectric nanobeam subjected to an electric potential Φ across its thickness direction, Wang and Feng (2010) stated that the electric field in the length direction was insignificant compared with that in the thickness direction, which was supported by the available numerical simulation results (Gao and Wang, 2007). In the same way, for a thin piezoelectric nanoplate with large in-plane dimension to thickness ratio, it is reasonable to only consider the electric field along the thickness direction when the plate is under an

electric potential Φ across its thickness direction (Zhao *et al.*, 2007; Yan and Jiang, 2012; Zhang, Yan and Jiang, 2014; Zhang and Jiang, 2014). Thus, the electric field in z direction E_z and the higher order electric field E_{ij}, $(i = z, j = x, y, \text{and } z)$ for a piezoelectric nanoplate can be expressed as

$$E_z = a_{33}P_z + d_{31}(\varepsilon_{xx} + \varepsilon_{yy}) + f_{13}(\varepsilon_{xx,z} + \varepsilon_{yy,z}) \quad (3.16)$$

$$E_{zx} = b_{31}P_{z,z} \quad (3.17)$$

$$E_{zy} = b_{32}P_{z,z} \quad (3.18)$$

$$E_{zz} = b_{33}P_z + e_{13}(\varepsilon_{xx} + \varepsilon_{yy}) \quad (3.19)$$

The electric field E_z can also be expressed with regards to the electric potential Φ and the higher order local electrical field E_{ij} as,

$$E_z = -\frac{\partial \Phi}{\partial z} + E_{zx,x} + E_{zy,y} + E_{zz,z} \quad (3.20)$$

Without the presence of free body charges, the Gauss's law can be expressed as,

$$-k\Phi_{zz} + P_{z,z} = 0 \quad (3.21)$$

where $k = k_0 k_b$is the so-called background permittivity for ferroelectrics (Hlinka and Marton, 2006; Tagantsev and Gerra, 2006), while $k_0 = 8.85 \times 10^{-12}\ C\ V^{-1}m^{-1}$ is the permittivity of the vacuum (or the air), and $k_b = 6.62$ is the specific background permittivity for $BaTiO_3$ when the electric field is in the same direction as the polarization.

Since the voltage is applied along the plate thickness direction, the electric boundary conditions for the plate are defined as,

$$E_{ij}n_j = 0 \quad (3.22)$$

$$\Phi\left(-\frac{h}{2}\right) = 0 \quad (3.23)$$

$$\Phi\left(\frac{h}{2}\right) = V \tag{3.24}$$

Manipulating Eqs. (3.16)-(3.21) and considering the electric boundary conditions stated above, the electric potential Φ, the electric field E_z, and the polarization P_z can be expressed in terms of the plate transverse displacement w, the in-plane displacements u^0 and v^0, and the applied voltage V as

$$\begin{aligned}\Phi = {} & \frac{b_{33}\lambda^2 - a_{33}}{\lambda} C_1 e^{\lambda z} - \frac{b_{33}\lambda^2 - a_{33}}{\lambda} C_2 e^{-\lambda z} \\ & + (f_{13} - e_{13})\left(\frac{\partial^2 w}{\partial x^2} + \frac{\partial^2 w}{\partial y^2}\right) z + \frac{d_{31}}{2} z^2 \left(\frac{\partial^2 w}{\partial x^2} + \frac{\partial^2 w}{\partial y^2}\right) \\ & - d_{31} z \left(\frac{\partial u^0}{\partial x} + \frac{\partial v^0}{\partial y}\right) - \frac{a_{33}}{2} C_3 z^2 - a_{33} C_4 z + C_5\end{aligned} \tag{3.25}$$

$$\begin{aligned}E_z = {} & a_{33} C_1 e^{\lambda z} + a_{33} C_2 e^{-\lambda z} - \frac{d_{31}}{1 + k a_{33}} z \left(\frac{\partial^2 w}{\partial x^2} + \frac{\partial^2 w}{\partial y^2}\right) \\ & + d_{31}\left(\frac{\partial u^0}{\partial x} + \frac{\partial v^0}{\partial y}\right) + a_{33} C_4 - f_{13}\left(\frac{\partial^2 w}{\partial x^2} + \frac{\partial^2 w}{\partial y^2}\right)\end{aligned} \tag{3.26}$$

$$P_z = C_1 e^{\lambda z} + C_2 e^{-\lambda z} + C_3 z + C_4 \tag{3.27}$$

With

$$\lambda = \sqrt{\frac{1 + k a_{33}}{k b_{33}}} \tag{3.28}$$

$$C_1 = \frac{e_{13} h \left(\frac{\partial^2 w}{\partial x^2} + \frac{\partial^2 w}{\partial y^2}\right) - 2 e_{13}\left(\frac{\partial u^0}{\partial x} + \frac{\partial v^0}{\partial y}\right)}{2 b_{33} \lambda \left(e^{\frac{\lambda h}{2}} - e^{\frac{-\lambda h}{2}}\right)} \tag{3.29}$$

$$C_2 = \frac{e_{13} h \left(\frac{\partial^2 w}{\partial x^2} + \frac{\partial^2 w}{\partial y^2}\right) + 2 e_{13}\left(\frac{\partial u^0}{\partial x} + \frac{\partial v^0}{\partial y}\right)}{2 b_{33} \lambda \left(e^{\frac{\lambda h}{2}} - e^{\frac{-\lambda h}{2}}\right)} \tag{3.30}$$

$$C_3 = \frac{kd_{31}}{1+ka_{33}}\left(\frac{\partial^2 w}{\partial x^2}+\frac{\partial^2 w}{\partial y^2}\right) \tag{3.31}$$

$$C_4 = \left(\frac{f_{13}}{a_{33}}+\frac{f_{13}}{b_{33}\lambda^2}\right)\left(\frac{\partial^2 w}{\partial x^2}+\frac{\partial^2 w}{\partial y^2}\right)-\frac{d_{31}}{a_{33}}\left(\frac{\partial u^0}{\partial x}+\frac{\partial v^0}{\partial y}\right)-\frac{V}{a_{33}h} \tag{3.32}$$

$$\begin{aligned} C_5 = {} & \frac{b_{33}\lambda^2-a_{33}}{b_{33}\lambda}e_{13}\left(\frac{\partial u^0}{\partial x}+\frac{\partial v^0}{\partial y}\right) \\ & +\left(k\frac{b_{33}\lambda^2-a_{33}}{\lambda}-\frac{h^2}{8}\right)\frac{d_{31}}{1+ka_{33}}\left(\frac{\partial^2 w}{\partial x^2}+\frac{\partial^2 w}{\partial y^2}\right)+\frac{V}{2} \end{aligned} \tag{3.33}$$

It is worth to mention that when the impacts of the strain gradients and the polarization gradients are ruled out, we can get the same expressions of the electric fields as the ones for the classical piezoelectric plate.

After the derivation of the electric fields, both the traditional stresses and the higher order stresses can be determined by substituting Eq. (3.27) into Eqs. (3.3) and (3.4). These stresses can also be expressed in terms of the plate transverse displacement w, the in-plane displacements u^0 and v^0, and the applied voltage V, i.e.,

$$\begin{aligned} \sigma_{xx} = {} & c_{11}\left(\frac{\partial u^0}{\partial x}-z\frac{\partial^2 w}{\partial x^2}\right)+c_{12}\left(\frac{\partial v^0}{\partial y}-z\frac{\partial^2 w}{\partial y^2}\right)+(d_{31}+e_{13}\lambda)C_1e^{\lambda z} \\ & +(d_{31}-e_{13}\lambda)C_2e^{-\lambda z}+d_{31}C_3z+d_{31}C_4+e_{13}C_3 \end{aligned} \tag{3.34}$$

$$\begin{aligned} \sigma_{yy} = {} & c_{21}\left(\frac{\partial u^0}{\partial x}-z\frac{\partial^2 w}{\partial x^2}\right)+c_{22}\left(\frac{\partial v^0}{\partial y}-z\frac{\partial^2 w}{\partial y^2}\right)+(d_{32}+e_{23}\lambda)C_1e^{\lambda z} \\ & +(d_{32}-e_{23}\lambda)C_2e^{-\lambda z}+d_{32}C_3z+d_{32}C_4+e_{23}C_3 \end{aligned} \tag{3.35}$$

$$\sigma_{xy} = c_{66}\left(\frac{\partial u^0}{\partial y}+\frac{\partial v^0}{\partial x}-2z\frac{\partial^2 w}{\partial x\partial y}\right) \tag{3.36}$$

$$\sigma_{xxz} = f_{13}C_1e^{\lambda z}+f_{13}C_2e^{\lambda z}+f_{13}C_3z+f_{13}C_4 \tag{3.37}$$

$$\sigma_{yyz} = f_{23}C_1e^{\lambda z}+f_{23}C_2e^{\lambda z}+f_{23}C_3z+f_{23}C_4 \tag{3.38}$$

Based on the above Eqs. (3.34)-(3.36), it can be seen that resultant in-plane forces could be defined as,

$$N_{xx} = \int_{-\frac{h}{2}}^{\frac{h}{2}} \sigma_{xx} dz$$
$$= h\left(c_{11}\frac{\partial u^0}{\partial x} + c_{12}\frac{\partial v^0}{\partial y}\right) + \frac{d_{31}f_{13}h}{a_{33}(1+ka_{33})}\left(\frac{\partial^2 w}{\partial x^2} + \frac{\partial^2 w}{\partial y^2}\right) \quad (3.39)$$
$$-\left(\frac{2f_{13}^2}{b_{33}\lambda} + \frac{d_{31}^2 h}{a_{33}}\right)\left(\frac{\partial u^0}{\partial x} + \frac{\partial v^0}{\partial y}\right) - \frac{d_{31}V}{a_{33}}$$

$$N_{yy} = \int_{-\frac{h}{2}}^{\frac{h}{2}} \sigma_{yy} dz$$
$$= h\left(c_{12}\frac{\partial u^0}{\partial x} + c_{11}\frac{\partial v^0}{\partial y}\right) + \frac{d_{31}f_{13}h}{a_{33}(1+ka_{33})}\left(\frac{\partial^2 w}{\partial x^2} + \frac{\partial^2 w}{\partial y^2}\right) \quad (3.40)$$
$$-\left(\frac{2f_{13}^2}{b_{33}\lambda} + \frac{d_{31}^2 h}{a_{33}}\right)\left(\frac{\partial u^0}{\partial x} + \frac{\partial v^0}{\partial y}\right) - \frac{d_{31}V}{a_{33}}$$

$$N_{xy} = \int_{-\frac{h}{2}}^{\frac{h}{2}} \sigma_{xy} dz = hc_{66}\left(\frac{\partial u^0}{\partial y} + \frac{\partial v^0}{\partial x}\right) \quad (3.41)$$

It is clear that these forces are induced by the strain and the applied electrical load due to the electromechanical coupling, which is influenced by the flexoelectric effect. Apparently, for a cantilevered nanoplate with forces applied only in the thickness direction, those in-plane forces are 0 due to the traction free conditions in the axial directions. As a result, there will be relaxation strains developed in the plate as discussed in Reference (Yan and Jiang, 2013), and it will have an influence on the electroelastic performance of the plate. The relaxation strain ε_0 is deduced from the traction free boundary condition as,

$$\varepsilon_0 = \frac{\frac{d_{31}V}{a_{33}} - \frac{d_{31}f_{13}h}{a_{33}(1+ka_{33})}\left(\frac{\partial^2 w}{\partial x^2} + \frac{\partial^2 w}{\partial y^2}\right)}{h(C_{11}+C_{12}) - 2\left(\frac{2f_{13}^2}{b_{33}\lambda} + \frac{d_{31}^2 h}{a_{33}}\right)} \quad (3.42)$$

In order to determine the governing equations and the mechanical boundary conditions of the cantilevered piezoelectric nanoplate, the energy method is adopted in the current work. In the entire volume Ω of the piezoelectric nanoplate, without the consideration of the kinetic energy, Hamilton's principle takes the form of (Yan and Jiang, 2013; Hu and Shen, 2014),

$$-\delta \int_{\Omega} H d\Omega + \delta W = 0 \qquad (3.43)$$

where W is the work done by the external force. For a cantilevered nanoplate, $W = \iint q w dx dy$. $H = U - \frac{1}{2} k \Phi_{,z} \Phi_{,z} + \Phi_{,z} P_z$ (Toupin, 1956; Hu and Shen, 2014) is the electric enthalpy density, in which U is the internal energy density defined by Eq. (3.2). By combining Eqs (3.2)-(3.6), the internal energy density U of the plate can be expressed as $U = \frac{1}{2}(\sigma_{xx}\varepsilon_{xx} + \sigma_{yy}\varepsilon_{yy} + 2\sigma_{xy}\varepsilon_{xy} + \sigma_{xxz}\varepsilon_{xx,z} + \sigma_{yyz}\varepsilon_{yy,z} + E_z P_z + E_{zz} P_{z,z})$. Therefore, in our case, the expression of $\int_{\Omega} H d\Omega$ can be determined in terms of the displacements and the electric potential as:

$$\begin{aligned}
\int_{\Omega} H d\Omega = \iint \Bigg\{ & \left(c_{11}\frac{h^3}{24} + D_{11}\right)\left[\left(\frac{\partial^2 w}{\partial x^2}\right)^2 + \left(\frac{\partial^2 w}{\partial y^2}\right)^2\right] \\
& + \left(c_{12}\frac{h^3}{12} + 2D_{11}\right)\frac{\partial^2 w}{\partial x^2}\frac{\partial^2 w}{\partial y^2} + \frac{f_{13}V}{a_{33}}\left(\frac{\partial^2 w}{\partial x^2} + \frac{\partial^2 w}{\partial y^2}\right) \\
& + \left(\frac{c_{11}h}{2} + D_{22}\right)\left[\left(\frac{\partial u}{\partial x}\right)^2 + \left(\frac{\partial v}{\partial y}\right)^2\right] + (c_{11}h + 2D_{22})\frac{\partial u}{\partial x}\frac{\partial v}{\partial y} \\
& - \frac{d_{31}V}{a_{33}}\left(\frac{\partial u}{\partial x} + \frac{\partial v}{\partial y}\right) + D_{12}\left(\frac{\partial^2 w}{\partial x^2} + \frac{\partial^2 w}{\partial y^2}\right)\left(\frac{\partial u}{\partial x} + \frac{\partial v}{\partial y}\right) \\
& + \frac{c_{66}h}{2}\left(\frac{\partial u}{\partial y} + \frac{\partial v}{\partial x}\right)^2 + c_{66}\frac{h^3}{6}\left(\frac{\partial^2 w}{\partial x \partial y}\right)^2 - \left(\frac{kV^2}{2h}\right. \\
& \left. + \frac{V^2}{2a_{33}h}\right)\Bigg\} dx dy
\end{aligned} \qquad (3.44)$$

Applying the variation, the Hamilton's principle can be expressed as,

$$
\begin{aligned}
-\delta \iint \Bigg\{ & \left(c_{11}\frac{h^3}{24} + D_{11}\right)\left[\left(\frac{\partial^2 w}{\partial x^2}\right)^2 + \left(\frac{\partial^2 w}{\partial y^2}\right)^2\right] \\
& + \left(c_{12}\frac{h^3}{12} + 2D_{11}\right)\frac{\partial^2 w}{\partial x^2}\frac{\partial^2 w}{\partial y^2} + \frac{f_{13}V}{a_{33}}\left(\frac{\partial^2 w}{\partial x^2} + \frac{\partial^2 w}{\partial y^2}\right) \\
& + \left(\frac{c_{11}h}{2} + D_{22}\right)\left[\left(\frac{\partial u}{\partial x}\right)^2 + \left(\frac{\partial v}{\partial y}\right)^2\right] + (c_{11}h + 2D_{22})\frac{\partial u}{\partial x}\frac{\partial v}{\partial y} \\
& - \frac{d_{31}V}{a_{33}}\left(\frac{\partial u}{\partial x} + \frac{\partial v}{\partial y}\right) + D_{12}\left(\frac{\partial^2 w}{\partial x^2} + \frac{\partial^2 w}{\partial y^2}\right)\left(\frac{\partial u}{\partial x} + \frac{\partial v}{\partial y}\right) \\
& + \frac{c_{66}h}{2}\left(\frac{\partial u}{\partial y} + \frac{\partial v}{\partial x}\right)^2 + c_{66}\frac{h^3}{6}\left(\frac{\partial^2 w}{\partial x \partial y}\right)^2 - (\frac{kV^2}{2h} \\
& + \frac{V^2}{2a_{33}h})\Bigg\} dxdy + \delta W = 0
\end{aligned}
\tag{3.45}
$$

with

$$
\begin{aligned}
& \delta \iint (\frac{\partial^2 w}{\partial x^2})^2 \, dxdy \\
& \qquad = 2\iint \frac{\partial^4 w}{\partial x^4}\delta w dxdy + 2\int \frac{\partial^2 w}{\partial x^2}\frac{\partial \delta w}{\partial n}\cos^2\alpha \, ds \\
& \qquad - 2\int \frac{\partial^3 w}{\partial x^3}\cos\alpha \, \delta w ds
\end{aligned}
\tag{3.46}
$$

$$
\begin{aligned}
& \delta \iint (\frac{\partial^2 w}{\partial y^2})^2 \, dxdy \\
& \qquad = 2\iint \frac{\partial^4 w}{\partial y^4}\delta w dxdy + 2\int \frac{\partial^2 w}{\partial y^2}\frac{\partial \delta w}{\partial n}\sin^2\alpha \, ds \\
& \qquad - 2\int \frac{\partial^3 w}{\partial y^3}\sin\alpha \, \delta w ds
\end{aligned}
\tag{3.47}
$$

$$\delta \iint \frac{\partial^2 w}{\partial x^2}\frac{\partial^2 w}{\partial y^2}\,dxdy$$
$$= 2\iint \frac{\partial^2 w}{\partial x^2}\frac{\partial^2 w}{\partial y^2}\,\delta w dxdy$$
$$+ \int \left(\frac{\partial^2 w}{\partial x^2}\sin^2\alpha + \frac{\partial^2 w}{\partial y^2}\cos^2\alpha\right)\frac{\partial \delta w}{\partial n}\,ds \qquad (3.48)$$
$$+ \int \left(-\frac{\partial^3 w}{\partial x^2 \partial y}\sin\alpha - \frac{\partial^3 w}{\partial x \partial y^2}\cos\alpha\right)\delta w ds$$

$$\delta \iint \left(\frac{\partial^2 w}{\partial x \partial y}\right)^2 dxdy$$
$$= 2\iint \frac{\partial^2 w}{\partial x^2}\frac{\partial^2 w}{\partial y^2}\,\delta w dxdy$$
$$+ \int \left\{\frac{\partial}{\partial s}\left[\frac{\partial^2 w}{\partial x \partial y}(\sin^2\alpha - \cos^2\alpha)\right] - -\frac{\partial^3 w}{\partial x^2 \partial y}\sin\alpha \right. \qquad (3.49)$$
$$\left. - \frac{\partial^3 w}{\partial x \partial y^2}\cos\alpha\right\}\delta w ds$$

$$\delta \iint \frac{\partial^2 w}{\partial x^2}\,dxdy = \int \frac{\partial \delta w}{\partial n}\cos^2\alpha\,ds \qquad (3.50)$$

$$\delta \iint \frac{\partial^2 w}{\partial y^2}\,dxdy = \int \frac{\partial \delta w}{\partial n}\sin^2\alpha\,ds \qquad (3.51)$$

$$\delta \iint \left(\frac{\partial w}{\partial x}\right)^2 dxdy = -2\iint \frac{\partial^2 w}{\partial x^2}\delta w dxdy + 2\int \frac{\partial w}{\partial x}\delta w \cos\alpha\,ds \qquad (3.52)$$

$$\delta \iint \left(\frac{\partial w}{\partial y}\right)^2 dxdy = -2\iint \frac{\partial^2 w}{\partial y^2}\delta w dxdy + 2\int \frac{\partial w}{\partial y}\delta w \sin\alpha\,ds \qquad (3.53)$$

$$\delta \iint \frac{\partial^2 w}{\partial x^2}\frac{\partial u}{\partial x}dxdy$$
$$= -\iint \frac{\partial^3 w}{\partial x^3}\delta u dxdy + \iint \frac{\partial^3 u}{\partial x^3}\delta w dxdy$$
$$+ \int \frac{\partial^2 w}{\partial x^2}\delta u \cos\alpha\, ds - \int \frac{\partial^2 u}{\partial x^2}\delta w \cos\alpha\, ds$$
$$+ \int \frac{\partial u}{\partial x}\frac{\partial \delta w}{\partial n}\cos^2\alpha\, ds \qquad (3.54)$$

$$\delta \iint \frac{\partial^2 w}{\partial x^2}\frac{\partial v}{\partial y}dxdy$$
$$= -\iint \frac{\partial^3 w}{\partial x^2 \partial y}\delta v dxdy + \iint \frac{\partial^3 v}{\partial x^2 \partial y}\delta w dxdy$$
$$+ \int \frac{\partial^2 w}{\partial x^2}\delta v \sin\alpha\, ds - \int \frac{\partial^2 v}{\partial x \partial y}\delta w \cos\alpha\, ds$$
$$+ \int \frac{\partial v}{\partial y}\frac{\partial \delta w}{\partial n}\cos^2\alpha\, ds \qquad (3.55)$$

$$\delta \iint \frac{\partial^2 w}{\partial y^2}\frac{\partial u}{\partial x}dxdy$$
$$= -\iint \frac{\partial^3 w}{\partial x \partial y^2}\delta u dxdy + \iint \frac{\partial^3 u}{\partial x \partial y^2}\delta w dxdy$$
$$+ \int \frac{\partial^2 w}{\partial y^2}\delta u \cos\alpha\, ds - \int \frac{\partial^2 u}{\partial x \partial y}\delta w \sin\alpha\, ds$$
$$+ \int \frac{\partial u}{\partial x}\frac{\partial \delta w}{\partial n}\sin^2\alpha\, ds \qquad (3.56)$$

$$\delta \iint \frac{\partial u}{\partial x}\frac{\partial v}{\partial y}dxdy$$
$$= -\iint \frac{\partial^2 u}{\partial x \partial y}\delta v dxdy - \iint \frac{\partial^2 v}{\partial x \partial y}\delta u dxdy$$
$$+ \int \frac{\partial u}{\partial x}\delta v \sin\alpha\, ds + \int \frac{\partial v}{\partial y}\delta u \cos\alpha\, ds \qquad (3.57)$$

$$\delta \iint \frac{\partial u}{\partial y}\frac{\partial v}{\partial x}dxdy = -\iint \frac{\partial^2 u}{\partial x \partial y}\delta v dxdy - \iint \frac{\partial^2 v}{\partial x \partial y}\delta u dxdy + \int \frac{\partial u}{\partial y}\delta v \cos\alpha \, ds + \int \frac{\partial v}{\partial x}\delta u \sin\alpha \, ds \quad (3.58)$$

$$\delta \iint \frac{\partial u}{\partial x}dxdy = \int \delta u \cos\alpha \, ds \quad (3.59)$$

$$\delta \iint \frac{\partial v}{\partial y}dxdy = \int \delta v dxdy \quad (3.60)$$

Where α stands for the angle between the outward normal of the boundary and the x axis as demonstrated by Figure 3-2(a). The particular values of this angle for each boundary of the plate are shown in Figure 3-2(b).

Thus, the Hamilton's principle can be further expanded as,

$$\begin{aligned}&\iint \left\{\delta w\left(2\left(c_{11}\frac{h^3}{24}+D_{11}\right)\left(\frac{\partial^4 w}{\partial x^4}+\frac{\partial^4 w}{\partial y^4}\right)+2\left(c_{12}\frac{h^3}{12}+2D_{11}+c_{66}\frac{h^3}{6}\right)\frac{\partial^4 w}{\partial x^2 \partial y^2}+D_{12}\left(\frac{\partial^3 u}{\partial x^3}+\frac{\partial^3 u}{\partial x \partial y^2}+\frac{\partial^3 v}{\partial y^3}+\frac{\partial^3 v}{\partial y \partial x^2}\right)-q\right)+\delta u\left((C_{12}h+2D_{22}+c_{66}h)\frac{\partial^2 v}{\partial x \partial y}+(c_{11}h+2D_{22})\frac{\partial^2 u}{\partial x^2}+c_{66}h\frac{\partial^2 u}{\partial y^2}+D_{12}\left(\frac{\partial^3 w}{\partial x^3}+\frac{\partial^3 w}{\partial x \partial y^2}\right)\right)+\delta v\left((c_{12}h+2D_{22}+c_{66}h)\frac{\partial^2 u}{\partial x \partial y}+(c_{11}h+2D_{22})\frac{\partial^2 v}{\partial y^2}+c_{66}h\frac{\partial^2 v}{\partial x^2}+D_{12}\left(\frac{\partial^3 w}{\partial y^3}+\frac{\partial^3 w}{\partial y \partial x^2}\right)\right)\right\}dxdy\\&+\int_\Omega \left\{\delta w\left(2\left(c_{11}\frac{h^3}{24}+D_{11}\right)\left(\frac{\partial^3 w}{\partial x^3}\cos\alpha+\frac{\partial^3 w}{\partial y^3}\sin\alpha\right)+\left(c_{12}\frac{h^3}{12}+2D_{11}\right)\left(\frac{\partial^3 w}{\partial y \partial x^2}\sin\alpha+\frac{\partial^3 w}{\partial x \partial y^2}\cos\alpha\right)+D_{12}\left(\frac{\partial^2 u}{\partial x^2}\cos\alpha+\frac{\partial^2 u}{\partial x \partial y}\sin\alpha+\frac{\partial^2 v}{\partial y^2}\sin\alpha+\frac{\partial^2 v}{\partial x \partial y}\cos\alpha\right)-c_{66}\frac{h^3}{6}\left(\frac{\partial}{\partial s}\left[\frac{\partial^2 w}{\partial x \partial y}(\sin^2\alpha-\cos^2\alpha)\right]-\right.\right.\end{aligned} \quad (3.61)$$

$$\frac{\partial^3 w}{\partial x \partial y^2}\cos\alpha - \frac{\partial^3 w}{\partial y \partial x^2}\sin\alpha\Big)\Big) + \frac{\partial \delta w}{\partial n}\Big(2\Big(c_{11}\frac{h^3}{24} + D_{11}\Big)\Big(\frac{\partial^2 w}{\partial x^2}\cos^2\alpha + \frac{\partial^2 w}{\partial y^2}\sin^2\alpha\Big) + \Big(c_{12}\frac{h^3}{12} + 2D_{11}\Big)\Big(\frac{\partial^2 w}{\partial x^2}\sin^2\alpha + \frac{\partial^2 w}{\partial y^2}\cos^2\alpha\Big) + D_{12}\Big(\frac{\partial u}{\partial x} + \frac{\partial v}{\partial y}\Big) + \frac{f_{13}V}{a_{33}}\Big) + \delta u\Bigg((c_{11}h + 2D_{22})\frac{\partial u}{\partial x}\cos\alpha + (c_{12}h + 2D_{22})\frac{\partial v}{\partial y}\cos\alpha + D_{12}\Big(\frac{\partial^2 w}{\partial x^2} + \frac{\partial^2 w}{\partial y^2}\Big)\cos\alpha + c_{66}h\Big(\frac{\partial u}{\partial y} + \frac{\partial v}{\partial x}\Big)\sin\alpha - \frac{d_{31}V}{a_{33}}\cos\alpha\Bigg) + \delta v\Bigg((c_{12}h + 2D_{22})\frac{\partial u}{\partial x}\sin\alpha + (c_{11}h + 2D_{22})\frac{\partial v}{\partial y}\sin\alpha + D_{12}\Big(\frac{\partial^2 w}{\partial x^2} + \frac{\partial^2 w}{\partial y^2}\Big)\sin\alpha + c_{66}h\Big(\frac{\partial u}{\partial y} + \frac{\partial v}{\partial x}\Big)\cos\alpha - \frac{d_{31}V}{a_{33}}\sin\alpha\Bigg)\Bigg\} ds = 0$$

It can be seen that the left-hand side of the Equation (3.61) is composed of two parts: the volume integration and the surface integration. To guarantee the left-hand side of the Equation (3.61) equals to 0, those two integration parts should be independent of each other and take 0 at the same time. Thus, the volume integration will give the governing equations, while the surface integration will give the boundary conditions for the cantilevered piezoelectric nanoplate. Since the virtual displacements are arbitrary in the body, i.e., the values of δw, δu and δv are uncertain, their coefficients must take the value of 0, which, therefore, yield the governing equations as:

$$2\Big(c_{11}\frac{h^3}{24} + D_{11}\Big)\Big(\frac{\partial^4 w}{\partial x^4} + \frac{\partial^4 w}{\partial y^4}\Big) + 2\Big(c_{12}\frac{h^3}{12} + 2D_{11} + c_{66}\frac{h^3}{6}\Big)\frac{\partial^4 w}{\partial x^2 \partial y^2} + D_{12}\Big(\frac{\partial^3 u}{\partial x^3} + \frac{\partial^3 u}{\partial x \partial y^2} + \frac{\partial^3 v}{\partial y^3} + \frac{\partial^3 v}{\partial y \partial x^2}\Big) - q = 0 \qquad (3.62)$$

$$(c_{12}h + 2D_{22} + c_{66}h)\frac{\partial^2 v}{\partial x \partial y} + (c_{11}h + 2D_{22})\frac{\partial^2 u}{\partial x^2} + c_{66}h\frac{\partial^2 u}{\partial y^2} + D_{12}\Big(\frac{\partial^3 w}{\partial x^3} + \frac{\partial^3 w}{\partial x \partial y^2}\Big) = 0 \qquad (3.63)$$

$$(c_{12}h + 2D_{22} + c_{66}h)\frac{\partial^2 u}{\partial x \partial y} + (c_{11}h + 2D_{22})\frac{\partial^2 v}{\partial y^2} + c_{66}h\frac{\partial^2 v}{\partial x^2} + D_{12}\left(\frac{\partial^3 w}{\partial y^3} + \frac{\partial^3 w}{\partial y \partial x^2}\right) = 0 \quad (3.64)$$

with

$$D_{11} = -\frac{f_{13}^2 h^2}{4b_{33}\lambda}\frac{e^{\frac{\lambda h}{2}} + e^{\frac{-\lambda h}{2}}}{e^{\frac{\lambda h}{2}} - e^{\frac{-\lambda h}{2}}} - \frac{k d_{31}^2 h^3}{24(1 + k a_{33})} + \frac{b_{33} h k^2 d_{31}^2}{2(1 + k a_{33})^2} - \frac{f_{13}^2 h}{2a_{33}(1 + k a_{33})} \quad (3.65)$$

$$D_{12} = \frac{2f_{13}d_{31}}{b_{33}\lambda^3} + \frac{h f_{13} d_{31}}{a_{33}} - \frac{k h f_{13} d_{31}}{1 + k a_{33}} \quad (3.66)$$

$$D_{22} = \frac{f_{13}^2 h^2}{b_{33}\lambda}\frac{e^{\frac{\lambda h}{2}} + e^{\frac{-\lambda h}{2}}}{e^{\frac{\lambda h}{2}} - e^{\frac{-\lambda h}{2}}} - \frac{2f_{13}^2}{b_{33}\lambda} - \frac{h d_{31}^2}{2a_{33}} \quad (3.67)$$

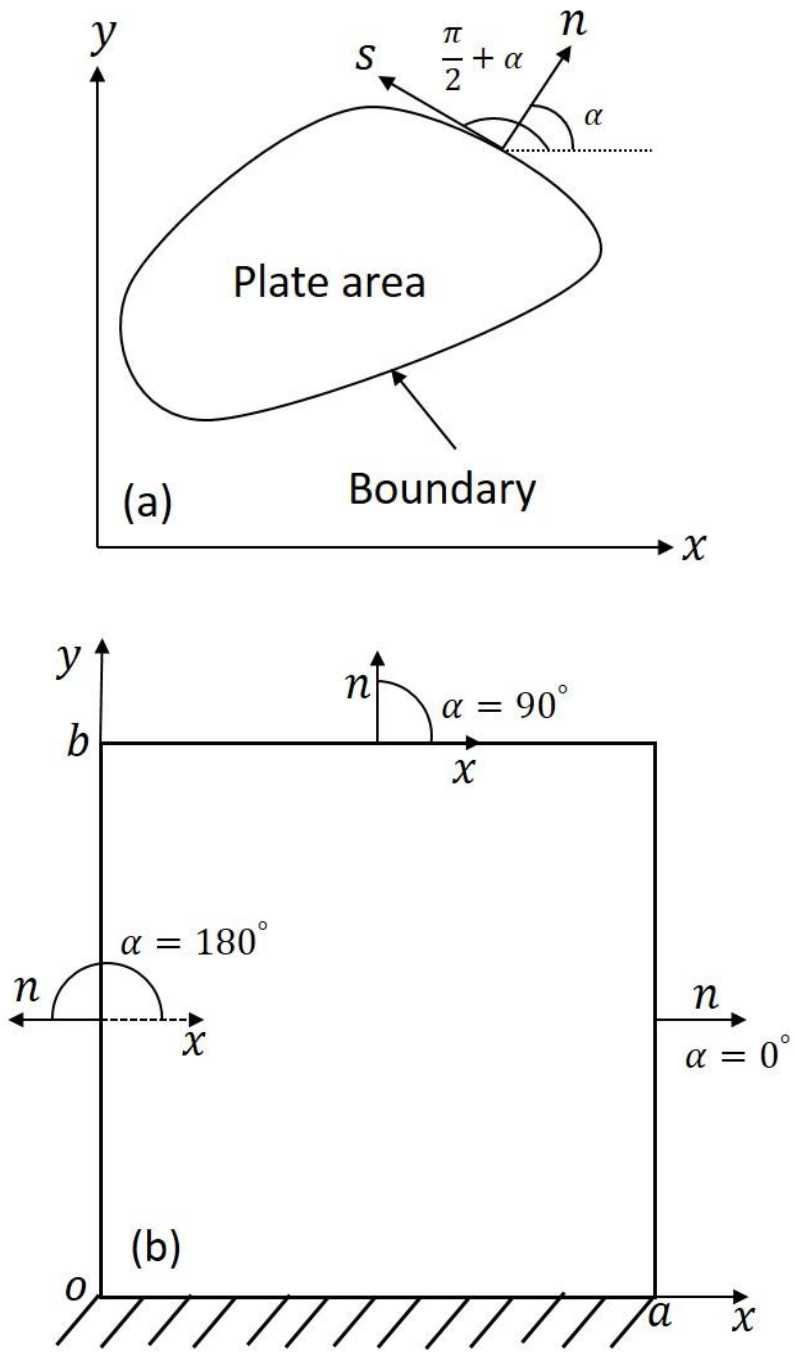

Figure 3-2 (a) demonstration of α angle, and (b) α angle for each boundary

As discussed in the previous paragraph, the boundary conditions can be derived via the surface integration of the left-hand side of the Equation (3.61). For the clamped edge ($y =$

0), the virtual displacements are 0, i.e., $\delta w = \delta u = \delta v = 0$, so the boundary conditions along the clamped edge can be expressed as:

$$u = v = w = 0 \tag{3.68}$$

$$\frac{\partial u}{\partial y} = \frac{\partial v}{\partial y} = \frac{\partial w}{\partial y} = 0 \tag{3.69}$$

For the two free edges ($x = 0$, and $x = a$), which are perpendicular to the clamped edge, the angles α are π and 0, respectively. Therefore, the boundary conditions can be derived as,

$$2\left(c_{11}\frac{h^3}{24} + D_{11}\right)\frac{\partial^2 w}{\partial x^2} + \left(c_{12}\frac{h^3}{12} + 2D_{11}\right)\frac{\partial^2 w}{\partial y^2} + D_{12}\left(\frac{\partial u}{\partial x} + \frac{\partial v}{\partial y}\right) + \frac{f_{13}V}{a_{33}} = 0 \tag{3.70}$$

$$2\left(c_{11}\frac{h^3}{24} + D_{11}\right)\frac{\partial^3 w}{\partial x^3} + \left(c_{12}\frac{h^3}{12} + 2D_{11} + c_{66}\frac{h^3}{6}\right)\frac{\partial^3 w}{\partial x \partial y^2} + D_{12}\left(\frac{\partial^2 u}{\partial x^2} + \frac{\partial^2 v}{\partial x \partial y}\right) = 0 \tag{3.71}$$

$$(c_{11}h + 2D_{22})\frac{\partial u}{\partial x} + (c_{12}h + 2D_{22})\frac{\partial v}{\partial y} + D_{12}\left(\frac{\partial^2 w}{\partial x^2} + \frac{\partial^2 w}{\partial y^2}\right) - \frac{d_{31}V}{a_{33}} = 0 \tag{3.72}$$

$$c_{66}h\left(\frac{\partial u}{\partial y} + \frac{\partial v}{\partial x}\right) = 0 \tag{3.73}$$

Similarly, for the free edge ($y = b$), which is parallel to the clamped edge with $\alpha = \frac{\pi}{2}$, the boundary conditions are determined as,

$$2\left(c_{11}\frac{h^3}{24} + D_{11}\right)\frac{\partial^2 w}{\partial y^2} + \left(c_{12}\frac{h^3}{12} + 2D_{11}\right)\frac{\partial^2 w}{\partial x^2} + D_{12}\left(\frac{\partial u}{\partial x} + \frac{\partial v}{\partial y}\right) + \frac{f_{13}V}{a_{33}} = 0 \tag{3.74}$$

$$2\left(c_{11}\frac{h^3}{24}+D_{11}\right)\frac{\partial^3 w}{\partial y^3}+\left(c_{12}\frac{h^3}{12}+2D_{11}+c_{66}\frac{h^3}{6}\right)\frac{\partial^3 w}{\partial y\partial x^2} + D_{12}\left(\frac{\partial^2 v}{\partial y^2}+\frac{\partial^2 u}{\partial x\partial y}\right)=0 \quad (3.75)$$

$$(c_{11}h+2D_{22})\frac{\partial u}{\partial x}+(c_{12}h+2D_{22})\frac{\partial v}{\partial y}+D_{12}\left(\frac{\partial^2 w}{\partial x^2}+\frac{\partial^2 w}{\partial y^2}\right)-\frac{d_{31}V}{a_{33}}=0 \quad (3.76)$$

$$c_{66}h\left(\frac{\partial u}{\partial y}+\frac{\partial v}{\partial x}\right)=0 \quad (3.77)$$

Thus, by solving the governing equations with the displacements satisfying the boundary conditions, we will get the solution for the static bending response of the cantilevered piezoelectric nanoplate.

Chapter 4

4 Finite difference method (FDM)

From the previous chapter, it is seen that for the cantilevered PNP with combined bending and in-plane deformations, the governing equations and the boundary conditions are more complicated than the conventional cantilevered PNP. Thus, it is very difficult, if not impossible, to obtain the analytical solutions. Hence, finite difference method (FDM) is pursued here to find the numerical solutions for characterizing the electroelastic responses of the plate. Using FDM, all of the governing equations and the boundary conditions are discretized, and the problem is reduced to solving a number of algebraic equations.

Following the standard procedure of the FDM, the plate is discretized into (Smith, 1985) a system of rectangular meshes (elements) formed by two sets of lines with equal space as shown in Figure 4-1. One set of lines is parallel to the x direction while the other is parallel to the y direction. The lines are separated by $(M+1)$ nodes along the x direction and $(N+1)$ nodes along the y direction, which means there are $(M+1)\times(N+1)$ mesh points in total. In the current work, square meshes are used, so the step size Δx along the x direction and the step size Δy along the y direction satisfy $\Delta x = \Delta y = \frac{a}{M} = \frac{b}{N}$. Algebraic equations are found for these mesh points. Obviously, the accuracy can be improved by increasing the number of mesh points to reduce the mesh size. In the course of numerical calculation, we will ensure the accurate results by using sufficiently small meshes.

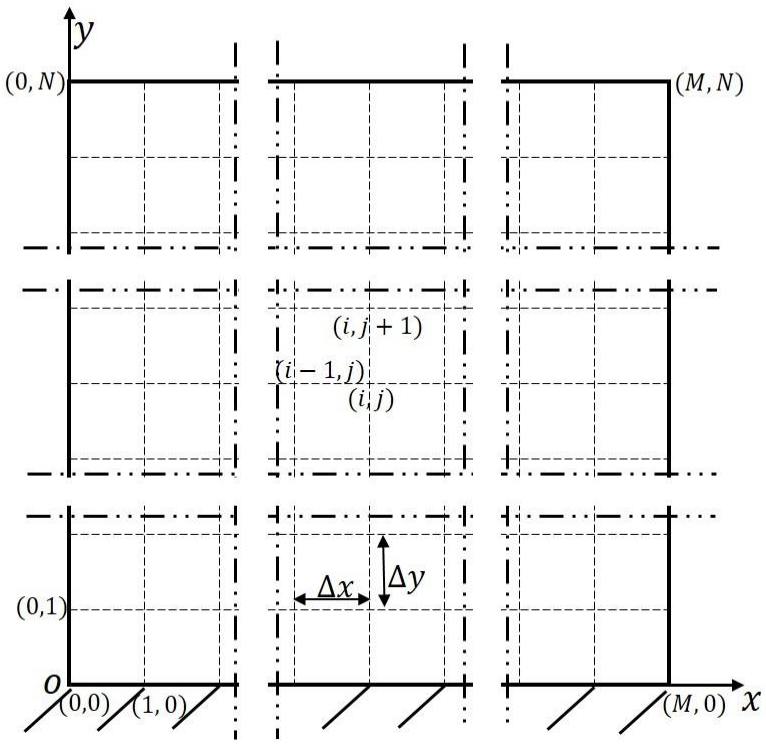

Figure 4-1 Finite difference grid of a cantilevered PNP

4.1 Finite difference approximation of derivatives

In order to discretize the functions and their derivatives in the governing equations and the boundary conditions, we start with the Taylor series for a function $f(x, y)$ which is single-valued, finite, and continuous with variables x and y. By neglecting the higher order terms, we have,

$$f(x + \Delta x, y) \approx f(x, y) + \Delta x \frac{\partial f(x, y)}{\partial x} + \frac{\Delta x^2}{2} \frac{\partial^2 f(x, y)}{\partial x^2} \quad (4.1)$$

$$f(x - \Delta x, y) \approx f(x, y) - \Delta x \frac{\partial f(x, y)}{\partial x} + \frac{\Delta x^2}{2} \frac{\partial^2 f(x, y)}{\partial x^2} \quad (4.2)$$

$$f(x, y + \Delta y) \approx f(x, y) + \Delta y \frac{\partial f(x, y)}{\partial y} + \frac{\Delta y^2}{2} \frac{\partial^2 f(x, y)}{\partial y^2} \quad (4.3)$$

$$f(x, y - \Delta y) \approx f(x, y) - \Delta y \frac{\partial f(x, y)}{\partial y} + \frac{\Delta y^2}{2} \frac{\partial^2 f(x, y)}{\partial y^2} \quad (4.4)$$

From Eqs. (4.1)-(4.4), the approximations for the function $f(x,y)$ and its first and second derivatives with respect to x and y are derived as,

$$f(x,y) \approx \frac{f(x+\Delta x,y)-f(x-\Delta x,y)+f(x,y+\Delta y)-f(x,y-\Delta y)}{4} \quad (4.5)$$

$$\frac{\partial f(x,y)}{\partial x} \approx \frac{f(x+\Delta x,y)-f(x-\Delta x,y)}{2\Delta x} \quad (4.6)$$

$$\frac{\partial f(x,y)}{\partial y} \approx \frac{f(x,y+\Delta y)-f(x,y-\Delta y)}{2\Delta y} \quad (4.7)$$

$$\frac{\partial^2 f(x,y)}{\partial x^2} \approx \frac{f(x-\Delta x,y)-2f(x,y)+f(x+\Delta x,y)}{\Delta x^2} \quad (4.8)$$

$$\frac{\partial^2 f(x,y)}{\partial y^2} \approx \frac{f(x,y-\Delta y)-2f(x,y)+f(x,y+\Delta y)}{\Delta y^2} \quad (4.9)$$

If we take the third and the fourth order terms into consideration, the function $f(x,y)$ can be expressed by Taylor series as:

$$f(x+\Delta x,y) \approx f(x,y)+\Delta x\frac{\partial f(x,y)}{\partial x}+\frac{\Delta x^2}{2}\frac{\partial^2 f(x,y)}{\partial x^2}+\frac{\Delta x^3}{6}\frac{\partial^3 f(x,y)}{\partial x^3}+\frac{\Delta x^4}{24}\frac{\partial^4 f(x,y)}{\partial x^4} \quad (4.10)$$

$$f(x-\Delta x,y) \approx f(x,y)-\Delta x\frac{\partial f(x,y)}{\partial x}+\frac{\Delta x^2}{2}\frac{\partial^2 f(x,y)}{\partial x^2}-\frac{\Delta x^3}{6}\frac{\partial^3 f(x,y)}{\partial x^3}+\frac{\Delta x^4}{24}\frac{\partial^4 f(x,y)}{\partial x^4} \quad (4.11)$$

$$f(x+2\Delta x,y) \approx f(x,y)+2\Delta x\frac{\partial f(x,y)}{\partial x}+2\Delta x^2\frac{\partial^2 f(x,y)}{\partial x^2}+\frac{8\Delta x^3}{6}\frac{\partial^3 f(x,y)}{\partial x^3}+\frac{16\Delta x^4}{24}\frac{\partial^4 f(x,y)}{\partial x^4} \quad (4.12)$$

$$f(x-2\Delta x,y)\approx f(x,y)-2\Delta x\frac{\partial f(x,y)}{\partial x}+2\Delta x^2\frac{\partial^2 f(x,y)}{\partial x^2} -\frac{8\Delta x^3}{6}\frac{\partial^3 f(x,y)}{\partial x^3}+\frac{16\Delta x^4}{24}\frac{\partial^4 f(x,y)}{\partial x^4} \quad (4.13)$$

Manipulating Eqs. (4.10)-(4.13) leads to the approximations for the third and the fourth order derivatives of the function $f(x,y)$ with respect to x, as,

$$\frac{\partial^3 f(x,y)}{\partial x^3} \approx \frac{-f(x-2\Delta x,y)+2f(x-\Delta x,y)-2f(x+\Delta x,y)+f(x+2\Delta x,y)}{2\Delta x^3} \quad (4.14)$$

$$\frac{\partial^4 f(x,y)}{\partial x^4} \approx \frac{f(x-2\Delta x,y)-4(x-\Delta x,y)+6f(x,y)-4f(x+\Delta x,y)+f(x+2\Delta x,y)}{\Delta x^4} \quad (4.15)$$

Similarly, the approximations for the third and fourth order derivatives of the function $f(x,y)$ with respect to y are expressed as,

$$\frac{\partial^3 f(x,y)}{\partial y^3} \approx \frac{-f(x,y-2\Delta y)+2f(x,y-\Delta y)-2f(x,y+\Delta y)+f(x,y+2\Delta y)}{2\Delta y^3} \quad (4.16)$$

$$\frac{\partial^4 f(x,y)}{\partial y^4} \approx \frac{f(x,y-2\Delta y)-4(x,y-\Delta y)+6f(x,y)-4f(x,y+\Delta y)+f(x,y+2\Delta y)}{\Delta y^4} \quad (4.17)$$

For the first order derivative of $f(x,y)$ with respect x, Taylor's series can be expressed as,

$$\frac{\partial f(x,y+\Delta y)}{\partial x}\approx\frac{\partial f(x,y)}{\partial x}+\Delta y\frac{\partial^2 f(x,y)}{\partial x\partial y} \quad (4.18)$$

$$\frac{\partial f(x,y-\Delta y)}{\partial x} \approx \frac{\partial f(x,y)}{\partial x} - \Delta y \frac{\partial^2 f(x,y)}{\partial x \partial y} \tag{4.19}$$

By deducting Eqs. (4.18) and (4.19), we can get the second order mixed partial derivative of the function f with respect to x and y as,

$$\begin{aligned}\frac{\partial^2 f(x,y)}{\partial x \partial y} \approx \frac{1}{4\Delta x \Delta y}\{&f(x-\Delta x, y-\Delta y) - f(x+\Delta x, y-\Delta y) \\ &- f(x-\Delta x, y+\Delta y) + f(x+\Delta x, y+\Delta y)\}\end{aligned} \tag{4.20}$$

For the second order derivative of $f(x,y)$ with respect to x, Taylor's series can be expressed as,

$$\frac{\partial^2 f(x,y+\Delta y)}{\partial x^2} \approx \frac{\partial^2 f(x,y)}{\partial x^2} + \Delta y \frac{\partial^3 f(x,y)}{\partial x^2 \partial y} + \frac{\Delta y^2}{2}\frac{\partial^4 f(x,y)}{\partial x^2 \partial y^2} \tag{4.21}$$

$$\frac{\partial^2 f(x,y-\Delta y)}{\partial x^2} \approx \frac{\partial^2 f(x,y)}{\partial x^2} - \Delta y \frac{\partial^3 f(x,y)}{\partial x^2 \partial y} + \frac{\Delta y^2}{2}\frac{\partial^4 f(x,y)}{\partial x^2 \partial y^2} \tag{4.22}$$

By manipulating Eqs. (4.21) and (4.22), it gives the third order mixed partial derivative of the function f, which differentiates twice with respect to x and once with respect to y, and the fourth order mixed partial derivative of the function $f(x,y)$ with respect to x and y as,

$$\begin{aligned}\frac{\partial^3 f(x,y)}{\partial x^2 \partial y} \approx \frac{1}{2\Delta x^2 \Delta y}\{&-f(x-\Delta x, y-\Delta y) + 2f(x, y-\Delta y) - f(x \\ &+ \Delta x, y-\Delta y)\} + f(x-\Delta x, y+\Delta y) - 2f(x, y+\Delta y) \\ &+ f(x+\Delta x, y+\Delta y)\end{aligned} \tag{4.23}$$

$$\begin{aligned}\frac{\partial^4 f(x,y)}{\partial x^2 \partial y^2} \approx \frac{1}{\Delta x^2 \Delta y^2}\{&f(x-\Delta x, y-\Delta y) - 2f(x, y-\Delta y) \\ &+ f(x+\Delta x, y-\Delta y) - 2f(x-\Delta x, y) + 4f(x,y) \\ &- 2f(x+\Delta x, y) + f(x-\Delta x, y+\Delta y) - 2f(x, y+\Delta y) \\ &+ f(x+\Delta x, y+\Delta y)\}\end{aligned} \tag{4.24}$$

Similarly, we can also get the third order mixed partial derivative of function $f(x,y)$, which differentiates once with respect to x and twice with respect to y, as,

$$\begin{aligned}\frac{\partial^3 f(x,y)}{\partial x \partial y^2} \approx \frac{1}{2\Delta x \Delta y^2}\{&-f(x-\Delta x, y-\Delta y)+2f(x-\Delta x, y)\\&-f(x-\Delta x, y+\Delta y)+f(x+\Delta x, y-\Delta y)\\&-2f(x+\Delta x, y)+f(x+\Delta x, y+\Delta y)\}\end{aligned} \quad (4.25)$$

4.2 Finite difference scheme of the governing equations and the boundary conditions

For the purpose of making deduction process easier, we use (i,j) to represent the position of the mesh point, which is the $(i+1)$th element in the x direction and the $(j+1)$th element in the y direction.

4.2.1 Finite difference scheme of the governing equations

By applying the finite difference approximations for the derivatives of function $f(x,y)$ to the displacements u, v and w, the standard finite difference scheme of the governing equations (3.62)-(3.64) can be formulated in terms of the nodal displacements as,

$$\begin{aligned}&\frac{A}{\Delta x^4}\{w(i-2,j)-4w(i-1,j)+6w(i,j)-4w(i+1,j)+w(i+\\&2,j)\}+\frac{A}{\Delta y^4}\{w(i,j-2)-4w(i,j-1)+6w(i,j)-4w(i,j+1)+\\&w(i,j+2)\}+\frac{B}{\Delta x^2 \Delta y^2}\{w(i-1,j-1)-2w(i,j-1)+w(i+1,j-\\&1)-2w(i-1,j)+4w(i,j)-2w(i+1,j)+w(i-1,j+1)-\\&2w(i,j+1)+w(i+1,j+1)\}-\frac{D_{12}}{2h^3}\{u(i-2,j)-2u(i-1,j)+\\&2u(i+1,j)-u(i+2,j)\}-\frac{D_{12}}{2\Delta x \Delta y^2}\{u(i-1,j-1)-2u(i-1,j)+\\&u(i-1,j+1)-u(i+1,j-1)+2u(i+1,j)-u(i+1,j+1)\}-\\&\frac{D_{12}}{2\Delta x^2 \Delta y}\{v(i-1,j-1)-2v(i,j-1)+v(i+1,j-1)-v(i-1,j+\\&1)+2v(i,j+1)-v(i+1,j+1)\}-\frac{D_{12}}{2\Delta y^3}\{v(i,j-2)-2v(i,j-1)+\\&2v(i,j+1)-v(i,j+2)\}-q_{i,j}=0\end{aligned} \quad (4.26)$$

$$\frac{D}{4\Delta x\Delta y}\{v(i-1,j-1)-v(i+1,j-1)-v(i-1,j+1)+v(i+1,j+1)\}+\frac{E}{\Delta x^2}\{u(i-1,j)-2u(i,j)+u(i+1,j)\}+\frac{G}{\Delta y^2}\{u(i,j-1)-2u(i,j)+u(i,j+1)\}+\frac{D_{12}}{2\Delta x^3}\{-w(i-2,j)+2w(i-1,j)-2w(i+1,j)+w(i+2,j)\}+\frac{D_{12}}{2\Delta x\Delta y^2}\{-w(i-1,j-k)+2w(i-1,j)-w(i-1,j+1)+w(i+1,j-1)-2w(i+1,j)+w(i+1,j+1)\}=0 \quad (4.27)$$

$$\frac{D}{4\Delta x\Delta y}\{u(i-1,j-1)-u(i+1,j-1)-u(i-1,j+1)+u(i+1,j+1)\}+\frac{F}{\Delta y^2}\{v(i,j-1)-2v(i,j)+v(i,j+1)\}+\frac{G}{\Delta x^2}\{v(i-1,j)-2v(i,j)+v(i+1,j)\}+\frac{D_{12}}{2\Delta x^3}\{-w(i,j-2)+2w(i,j-1)-2w(i,j+1)+w(i,j+2)\}+\frac{D_{12}}{2\Delta x\Delta y^2}\{-w(i-1,j-1)+2w(i-1,j)-w(i-1,j+1)+w(i+1,j-1)-2w(i+1,j)+w(i+1,j+1)\}=0 \quad (4.28)$$

where

$$A = c_{11}\frac{h^3}{12}+2D_{11} \quad (4.29)$$

$$B = 2(c_{12}\frac{h^3}{12}+2D_{11}+c_{66}\frac{h^3}{6}) \quad (4.30)$$

$$D = hc_{12}+2D_{22}+hc_{66} \quad (4.31)$$

$$E = F = hc_{11}+2D_{22} \quad (4.32)$$

$$G = hc_{66} \quad (4.33)$$

Applying Eqs. (4.26)-(4.28) to all mesh points will form a system of $(M+1)\times(N+1)$ algebraic equations, with all the internal and out-of-the-plate mesh points shown in Figure 4-2.

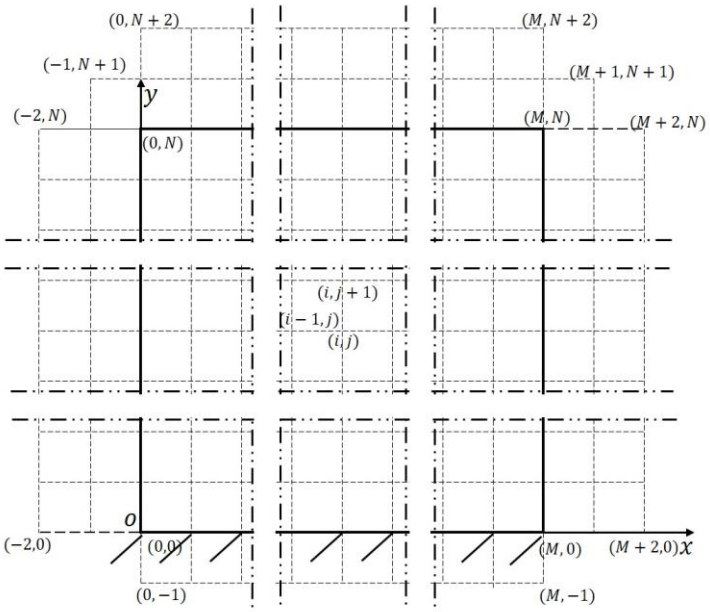

Figure 4-2 Internal and out-of-the-plate mesh points of the cantilevered PNP

4.2.2 Finite difference scheme of the boundary conditions

Following the same procedure as shown above, the finite difference approximations for the boundary conditions of Eqs. (3.68)-(3.77) can be derived.

(1) Finite difference approximation of the boundary conditions for points along the clamped edge $y = 0$, $(0 \le i \le M, j = 0)$

$$u(i,0) = v(i,0) = w(i,0) = 0 \tag{4.34}$$

$$\frac{\partial u(i,0)}{\partial y} = \frac{u(i,1) - u(i,-1)}{2\Delta y} = 0 \tag{4.35}$$

$$\frac{\partial v(i,0)}{\partial y} = \frac{v(i,1) - v(i,-1)}{2\Delta y} = 0 \tag{4.36}$$

$$\frac{\partial w(i,0)}{\partial y} = \frac{w(i,1) - w(i,-1)}{2\Delta y} = 0 \tag{4.37}$$

(2) Finite difference approximation of the boundary conditions for points along the free edge $x = 0$, $(i = 0, 0 \le j \le N)$

$$D_1\{w(-1,j)-2w(0,j)+w(1,j)\}+D_2\{w(0,j-1)-2w(0,j)+ w(0,j+1)\}+\frac{D_3\Delta x}{2}\{-u(-1,j)+u(1,j)\}+\frac{D_3\Delta x}{2}\{-v(0,j-1)+ v(0,j+1)\}+\frac{f_{13}V}{a_{33}}\Delta x^2=0 \quad (4.38)$$

$$\frac{D_1}{2}\{-w(-2,j)+2w(-1,j)-2w(1,j)+w(2,j)\}+\frac{D_4}{2}\{-2(-1,j-1)+2w(-1,j)-w(-1,j+1)+w(1,j-1)-2w(1,j)+w(1,j+1)\}+D_3\Delta x\{u(-1,j)-2w(0,j)+u(1,j)\}+\frac{D_3\Delta x}{4}\{v(-1,j-1)- v(1,j-1)-v(-1,j+1)+v(1,j+1)\}=0 \quad (4.39)$$

$$D_3\{w(-1,j)-2w(0,j)+w(1,j)\}+D_3\{w(0,j-1)-2w(0,j)+ w(0,j+1)\}+\frac{D_5\Delta x}{2}\{-u(-1,j)+u(1,j)\}+\frac{D_6\Delta x}{2}\{-v(0,j-1)+ v(0,j+1)\}-\frac{d_{31}V}{a_{33}}\Delta x^2=0 \quad (4.40)$$

$$\{-v(-1,j)+v(1,j)\}+\{-u(0,j-1)+u(0,j+1)\}=0 \quad (4.41)$$

(3) Finite difference approximation of the boundary conditions for points along the free edge $x=a$, $(i=M, 0\le j\le N)$

$$D_1\{w(M-1,j)-2w(M,j)+w(M+1,j)\}+D_2\{w(M,j-1)- 2w(M,j)+w(M,j+1)\}+\frac{D_3\Delta x}{2}\{-u(M-1,j)+u(M+1,j)\}+ \frac{D_3\Delta x}{2}\{-v(M,j-1)+u(M,j+1)\}+\frac{f_{13}V}{a_{33}}\Delta x^2=0 \quad (4.42)$$

$$\frac{D_1}{2}\{-w(M-2,j)+2w(M-1,j)-2w(M+1,j)+w(M+2,j)\}+ \frac{D_4}{2}\{-w(M-1,j-1)+2w(M-1,j)-2w(M-1,j+1)+w(M+ 1,j-1)-2w(M+1,j)+w(M+1,j+1)\}+D_3h\{u(M-1,j)- 2u(M,j)+u(M+1,j)\}+\frac{D_3\Delta x}{4}\{v(M-1,j-1)-v(M+1,j-1)- v(M-1,j+1)+v(M+1,j+1)\}=0 \quad (4.43)$$

$$D_3\{w(M-1,j)-2w(M,j)+w(M+1,j)\}+D_3\{w(M,j-1)-2w(M,j)+w(M,j+1)\}+\frac{D_5\Delta x}{2}\{-u(M-1,j)+u(M+1,j)\}+\frac{D_6\Delta x}{2}\{-v(M,j-1)+V(M,j+1)\}-\frac{d_{31}V}{a_{33}}\Delta x^2=0 \quad (4.44)$$

$$\{-v(M-1,j)+v(M+1,j)\}+\{-u(M,j-1)+u(M,j+1)\}=0 \quad (4.45)$$

(4) Finite difference approximation of the boundary conditions for points along the free edge $y=b$, $(0\le i\le M, j=N)$

$$D_1\{w(i,N-1)-2w(i,N)+w(i,N+1)\}+D_2\{w(i-1,N)-2w(i,N)+w(i+1,N)\}+\frac{D_3\Delta x}{2}\{-u(i-1,N)+u(i+1,N)\}+\frac{D_3\Delta x}{2}\{-v(i,N-1)+v(i,N+1)\}+\frac{f_{13}V}{a_{33}}\Delta x^2=0 \quad (4.46)$$

$$\frac{D_1}{2}\{-w(i,N-1)+2w(i,N-1)-2w(i,N+1)+w(i,N+2)\}+\frac{D_4}{2}\{-w(i-1,N-1)+2w(i,N-1)-w(i+1,N-1)+w(i-1,N+1)-2w(i,N+1)+w(i+1,N+1)\}+D_3\Delta x\{v(i,N-1)-2v(i,N)+v(i,N+1)\}+\frac{D_3\Delta x}{4}\{u(i-1,N-1)-u(i+1,N-1)-u(i-1,N+1)+u(i+1,N+1)\}=0 \quad (4.47)$$

$$D_3\{w(i-1,N)-2w(i,N)+w(i+1,N)\}+D_3\{w(i,N-1)-2w(i,N)+w(i,N+1)\}+\frac{D_5\Delta x}{2}\{-u(i-1,N)+u(i+1,N)\}+\frac{D_6\Delta x}{2}\{-v(i,N-1)+v(i,N+1)\}-\frac{d_{31}V}{a_{33}}\Delta x^2=0 \quad (4.48)$$

$$\{-v(i-1,N)+v(i+1,N)\}+\{-u(i,N-1)+u(i,N+1)\}=0 \quad (4.49)$$

where

$$D_1=c_{11}\frac{h^3}{12}+2D_{11} \quad (4.50)$$

$$D_2 = c_{12}\frac{h^3}{12} + 2D_{11} \quad (4.51)$$

$$D_3 = D_{12} \quad (4.52)$$

$$D_4 = c_{12}\frac{h^3}{12} + 2D_{11} + 2c_{66}\frac{h^3}{6} \quad (4.53)$$

$$D_5 = hc_{12} + 2D_{22} \quad (4.54)$$

$$D_6 = hC_{11} + 2D_{22} \quad (4.55)$$

From the finite difference scheme of the governing equations, it can be seen that there are mesh points outside the plate boundary. These out-of-the-plate mesh points are used to derive the finite difference approximations of the internal points near the edges. In order to solve the algebraic equations, the displacements of these out-of-the-plate points must be determined in terms of the internal points by enforcing the boundary conditions.

4.3 Displacements of out-of-the-plate mesh points

(1) Out-of-the-plate mesh points relating to the boundary conditions of the points along the clamped edge $y = 0$, $(j = 0)$

From Eqs. (4.35)-(4.37), the displacements of the out-of-plate mesh points $(i, -1)$, $(0 \leq i \leq M)$ can be expressed in terms of the internal points as,

$$u(i,-1) = u(i,1) \quad (4.56)$$

$$v(i,-1) = v(i,1) \quad (4.57)$$

$$w(i,-1) = w(i,1) \quad (4.58)$$

(2) Out-of-the-plate mesh points relating to the boundary conditions of the points along the free edge $x = 0$, $(i = 0)$

In order to determine the displacements for the mesh points outside the free edge ($x = 0$), we manipulate the boundary conditions of Eqs. (4.38)-(4.41) for points along the free edge, i.e., points $(0, j)$, $(2 \leq j \leq (N-1)$, and conclude that,

$$u(-1,j) = \Big\{(D_2D_3 - D_1D_3)w(0,j-1) + (2D_1D_3 - 2D_2D_3)w(0,j) + (D_2D_3 - D_1D_3)w(0,j+1) + \Big(\frac{D_3^2\Delta x}{2} - \frac{D_1D_5\Delta x}{2}\Big)u(1,j) + \Big(\frac{D_1D_6\Delta x}{2} - \frac{D_3^2\Delta x}{2}\Big)v(0,j-1) + \Big(\frac{D_3^2\Delta x}{2} - \frac{D_1D_6\Delta x}{2}\Big)v(0,j+1) + D_1\frac{d_{31}V\Delta x^2}{a_{33}} + D_3\frac{f_{13}V\Delta x^2}{a_{33}}\Big\}\frac{1}{\Big\{\frac{D_3^2\Delta x}{2} - \frac{D_1D_5\Delta x}{2}\Big\}} \quad (4.59)$$

$$v(-1,j) = v(1,j) - u(0,j-1) + u(0,j+1) \quad (4.60)$$

$$w(-1,j) = \Big\{(D_2D_5 - D_3^2)w(0,j-1) + (4D_3^2 - 2D_1D_5 - 2D_2D_5)w(0,j) + (D_1D_5 - D_3^2)w(1,j) + (D_2D_5 - D_3^2)w(0,j+1) + \Big(\frac{D_3D_6\Delta x}{2} - \frac{D_3D_5\Delta x}{2}\Big)v(0,j-1) + \Big(\frac{D_3D_5\Delta x}{2} - \frac{D_3D_6\Delta x}{2}\Big)v(0,j+1) + D_3\frac{d_{31}V\Delta x^2}{a_{33}} + D_5\frac{f_{13}V\Delta x^2}{a_{33}}\Big\}\frac{1}{D_3^2 - D_1D_5} \quad (4.61)$$

$$w(-2,j) = \Big\{\Big(-\frac{D_4}{2}\Big)w(-1,j-1) + (D_1 + D_4)w(-1,j) + \Big(-\frac{D_4}{2}\Big)w(-1,j+1) + \frac{D_4}{2}w(1,j-1) + (-D_1 - D_4)w(1,j) + \frac{D_1}{2}w(2,j) + \frac{D_4}{2}w(1,j+1) + D_3h\Delta x(-1,j) + (-2D_3\Delta x)u(0,j) + D_3h\Delta x(1,j) + \frac{D_3\Delta x}{4}v(-1,j-1) + \Big(-\frac{D_3\Delta x}{4}\Big)v(1,j-1) + \Big(-\frac{D_3\Delta x}{4}\Big)v(-1,j+1) + \frac{D_3\Delta x}{4}v(1,j+1)\Big\}\frac{2}{D_1} \quad (4.62)$$

(3) Out-of-the-plate mesh points relating to the boundary conditions of the points along the free edge $x = a$, $(i = M)$

From the boundary conditions for points (M, j), $(2 \leq j \leq (N-1))$, along the free edge $x = a$, the displacements of the mesh points outside the free edge ($x = a$) are determined as,

$$u(M+1,j)=\Big\{(D_2D_3-D_1D_3)w(M,j-1)+(2D_1D_3-2D_2D_3)w(M,j)+(D_2D_3-D_1D_3)w(M,j+1)-\Big(\frac{D_3^2\Delta x}{2}-\frac{D_1D_5\Delta x}{2}\Big)u(M-1,j)+\Big(\frac{D_1D_6\Delta x}{2}-\frac{D_3^2\Delta x}{2}\Big)v(M,j-1)+\Big(\frac{D_3^2\Delta x}{2}-\frac{D_1D_6\Delta x}{2}\Big)v(M,j+1)+D_1\frac{d_{31}V\Delta x^2}{a_{33}}+D_3\frac{f_{13}V\Delta x^2}{a_{33}}\Big\}\frac{-1}{\Big\{\frac{D_3^2\Delta x}{2}-\frac{D_1D_5\Delta x}{2}\Big\}} \quad (4.63)$$

$$v(M+1,j)=v(M-1,j)+u(M,j-1)-u(M,j+1) \quad (4.64)$$

$$w(M+1,j)=\Big\{(D_2D_5-D_3^2)w(w(M,j-1))+(4D_3^2-2D_1D_5-2D_2D_5)w(M,j)+(D_1D_5-D_3^2)w(M-1,j)+(D_2D_5-D_3^2)w(M,j+1)+\Big(\frac{D_3D_6\Delta x}{2}-\frac{D_3D_5\Delta x}{2}\Big)v(M,j-1)+\Big(\frac{D_3D_5\Delta x}{2}-\frac{D_3D_6\Delta x}{2}\Big)v(M,j+1)+D_3\frac{d_{31}V\Delta x^2}{a_{33}}+D_5\frac{f_{13}V\Delta x^2}{a_{33}}\Big\}\frac{1}{D_3^2-D_1D_5} \quad (4.65)$$

$$w(M+2,j)=\Big\{\Big(-\frac{D_4}{2}\Big)w(M-1,j-1)+(D_1+D_4)w(M-1,j)+\Big(-\frac{D_4}{2}\Big)w(M-1,j+1)+\frac{D_4}{2}w(M+1,j-1)+(-D_1-D_4)w(M+1,j)-\frac{D_1}{2}w(M-2,j)+\frac{D_4}{2}w(M+1,j+1)+D_3\Delta xu(M-1,j)+(-2D_3\Delta x)u(M,j)+D_3\Delta xu(M+1,j)+\frac{D_3\Delta x}{4}v(M-1,j-1)+\Big(-\frac{D_3\Delta x}{4}\Big)v(M+1,j-1)+\Big(-\frac{D_3\Delta x}{4}\Big)v(M-1,j+1)+\frac{D_3\Delta x}{4}v(M+1,j+1)\Big\} \quad (4.66)$$

(4) Out-of-the-plate mesh points relating to the boundary conditions of the points along the free edge $y=b$, $(j=N)$

From the boundary conditions for the mesh points (i,N), $(2\le i\le(M-1))$, the expressions for the displacements of the mesh points outside the free edge $(y=b)$ are determined as,

$$u(i,N+1)=u(i,N-1)+v(i-1,N)-v(i+1,N) \quad (4.67)$$

$$v(i,N+1)=\Big\{(2D_1D_3-2D_2D_3)w(i,N)+(D_2D_3-D_1D_3)w(i-1,N)+(D_2D_3-D_1D_3)w(i+1,N)+\left(\frac{D_1D_5\Delta x}{2}-\frac{D_3^2\Delta x}{2}\right)v(i,N-1)+\left(\frac{D_1D_6\Delta x}{2}-\frac{D_3^2\Delta x}{2}\right)u(i-1,N)+\left(\frac{D_3^2\Delta x}{2}-\frac{D_1D_6\Delta x}{2}\right)v(i+1,N)+D_1\frac{d_{31}V\Delta x^2}{a_{33}}+D_3\frac{f_{13}V\Delta x^2}{a_{33}}\Big\}\frac{1}{\left(\frac{D_1D_5\Delta x}{2}-\frac{D_3^2\Delta x}{2}\right)} \quad (4.68)$$

$$w(i,N+1)=\Big\{(D_1D_5-D_3^2)w(i,N-1)+(4D_3^2-2D_1D_5-2D_2D_5)w(i,N)+(D_2D_5-D_3^2)w(i-1,N)+(D_2D_5-D_3^2)w(i+1,N)+\left(\frac{D_3D_6\Delta x}{2}-\frac{D_3D_5\Delta x}{2}\right)u(i-1,N)+\left(\frac{D_3D_5\Delta x}{2}-\frac{D_3D_6}{2}\right)u(i+1,N)+D_3\frac{d_{31}V\Delta x^2}{a_{33}}+D_5\frac{f_{13}V\Delta x^2}{a_{33}}\Big\}\frac{1}{D_3^2-D_1D_5} \quad (4.69)$$

$$w(i,N+2)=\Big\{(-D_1-D_4)w(i,N+1)+\frac{D_4}{2}w(i-1,N+1)+\frac{D_4}{2}w(i+1,N+1)+\left(-\frac{D_1}{2}\right)w(i,N-2)+(D_1+D_4)w(i,N-1)+\left(-\frac{D_4}{2}\right)w(i-1,N-1)+\left(-\frac{D_4}{2}\right)w(i+1,N-1)+\left(-\frac{D_3\Delta x}{4}\right)u(i-1,N+1)+\frac{D_3\Delta x}{4}u(i+1,N+1)+\frac{D_3\Delta x}{4}u(i-1,N-1)+\left(-\frac{D_3\Delta x}{4}\right)u(i+1,N-1)+D_3\Delta x v(i,N+1)+D_3\Delta x v(i,N-1)+(-2D_3\Delta x)v(i,N)\Big\}\frac{-2}{D_1} \quad (4.70)$$

(5) The other remaining out-of-the-plate mesh points

There are out-of-the-plate mesh points involved in the governing equation scheme, whose displacements have not been determined yet. Those mesh points can be divided into two types: one whose displacements are related to the boundary conditions, and the other one whose displacements are not related to the boundary conditions. Thus, in this section, efforts will be put into determining the displacements of the remaining out-of-the-plate mesh points with regards to the internal points.

(5.1) Out-of-the-plate mesh points relating to the boundary conditions of the corner points $(0,0)$ and $(M,0)$

For the point $(0,0)$ intersecting the clamped edge $y=0$ and the free edge $x=0$, and the point $(M,0)$ intersecting the clamped edge $y=0$ and the free edge $x=a$, $w(0,0)$ and $w(M,0)$ can be expressed by the central-difference method as,

$$w(0,0)=\frac{w(-1,0)+w(1,0)+w(0,-1)+w(0,1)}{4}=0 \qquad (4.71)$$

$$w(M,0)=\frac{w(M-1,0)+w(M+1,0)+w(M,-1)+w(M,1)}{4}=0 \qquad (4.72)$$

Manipulating Eqs.(4.71)-(4.72) leads to the expressions of $w(-1,0)$ and $w(M+1,0)$ with respect to internal points as,

$$w(-1,0)=-2w(1,1) \qquad (4.73)$$

$$w(M+1,0)=-2w(M,1) \qquad (4.74)$$

Similarly, we can get the expressions of $u(-1,0)$, $v(-1,0)$, $u(M+1,0)$ and $v(M+1,0)$ with regards to internal points as,

$$u(-1,0)=-2u(1,1) \qquad (4.75)$$

$$v(-1,0)=-2v(1,1) \qquad (4.76)$$

$$u(M+1,0)=-2u(M,1) \qquad (4.77)$$

$$v(M+1,0)=-2v(M,1) \qquad (4.78)$$

(5.2) Out-of-the-plate mesh points relating to the boundary conditions of the corner points $(0,N)$

For the corner point $(0,N)$, it satisfies both the boundary conditions for the free edge $x=0$ and for the free edge $y=b$. Manipulating Eqs. (3.70), (3.72), (3.74) and (3.76) leads to,

$$u(-1,N) = u(1,N) - 2\Delta x \frac{(D_1 + D_2)\frac{d_{31}V}{a_{33}} + 2D_3\frac{f_{13}V}{a_{33}}}{(D_1 + D_2)(D_5 + D_6) - 4D_3^2} \quad (4.79)$$

$$v(0,N+1) = v(0,N-1) + 2\Delta x \frac{(D_1 + D_2)\frac{d_{31}V}{a_{33}} + 2D_3\frac{f_{13}V}{a_{33}}}{(D_1 + D_2)(D_5 + D_6) - 4D_3^2} \quad (4.80)$$

$$w(0,N+1) = 2w(0,N) - w(0,N-1) + \Delta x^2 \frac{(D_5+D_6)\frac{f_{13}V}{a_{33}} + 2D_3\frac{d_{31}V}{a_{33}}}{4D_3^2 - (D_1+D_2)(D_5+D_6)} \quad (4.81)$$

$$\begin{aligned} w(-2,N) &= 2w(-1,N) - 2w(1,N) + w(2,N) + \{-w(-1,N-1) + \\ &2w(-1,N) - w(-1,N+1) + w(1,N-1) - 2w(1,N) + w(1,N+ \\ &1)\}\frac{D_4}{D_1} + \{u(-1,N) - 2u(0,N) + u(1,N)\}\frac{2\Delta x D_{12}}{D_1} + \{v(-1,N-1) - \\ &v(1,N-1) - v(-1,N+1) + v(1,N+1)\}\frac{\Delta x D_{12}}{2D_1} \end{aligned} \quad (4.82)$$

$$\begin{aligned} w(0,N+2) &= w(0,N-2) - 2w(0,N-1) + 2w(0,N+1) + \\ &\{w(-1,N-1) - 2w(0,N-1) + w(1,N-1) - w(-1,N+1) + \\ &2w(0,N+1) - w(1,N+1)\}\frac{D_4}{D_1} + \{-v(0,N-1) + 2v(0,N) - \\ &v(0,N+1)\}\frac{2\Delta x D_{12}}{D_1} + \{-u(-1,N-1) + u(0,N-1) + u(-1,N+1) - \\ &u(0,N+1)\}\frac{\Delta x D_{12}}{2D_1} \end{aligned} \quad (4.83)$$

Combining the boundary conditions of Eq. (4.41) and $u(0,N) = \frac{u(0,N+1)+u(0,N-1)}{2}$ results in,

$$u(0,N+1) = 2u(0,N) - u(0,N-1) \quad (4.84)$$

$$v(-1,N) = 2u(0,N) - 2u(0,N-1) + v(1,N) \quad (4.85)$$

With the central-difference method, when governing equations (4.26)-(4.28) are applied to the corner point $(0,N)$, it can be seen that five out-of-the-plate points ($(-2,N)$, $(-1,N)$, $(0,N+1)$, $(0,N+2)$ and $(-1,N+1)$) are involved. So far, we have determined the expressions of $w(-2,N)$, $w(-1,N)$, $w(0,N+1)$ and $w(0,N+2)$ in terms of the internal

points. In order to determine the expression of $w(-1, N+1)$, one more boundary equation is needed. Shimpi and Sivakumar (1994) solved this problem and derived an additional equation by employing the corner reaction condition or the twisting moment 'M_{xy}'. According to Timoshenko and Woinowsky-Krieger (1959), Fo-van (1980) and Lin and Yuan (1985), the twisting moment M_{xy} is defined as,

$$M_{xy} = D(1-\gamma)\frac{\partial^2 w}{\partial x \partial y} \qquad (4.86)$$

where D is the flexural rigidity of the plate. Applying finite difference method to Eq. (4.86), we can get the expression of $w(-1, N+1)$ as,

$$w(-1, N+1) = w(-1, N-1) + w(0, N+1) - w(0, N-1) \qquad (4.87)$$

(5.3) Out-of-the-plate points relating to the boundary conditions of the corner point (M, N)

Following the same procedure for determining the displacements for the mesh points outside the corner point $(0, N)$, we can determine the displacement expressions for the mesh points outside the corner point (M, N) as,

$$u(M, N+1) = 2u(M, N) - u(M, N-1) \qquad (4.88)$$

$$v(M+1, N) = -2u(M, N) + 2u(M, N-1) + v(M-1, N) \qquad (4.89)$$

$$u(M+1, N) = u(M-1, N) + 2\Delta x \frac{(D_1+D_2)\frac{d_{31}V}{a_{33}} + 2D_3\frac{f_{13}V}{a_{33}}}{(D_1+D_2)(D_5+D_6) - 4D_3^2} \qquad (4.90)$$

$$v(M, N+1) = v(M, N-1) + 2\Delta x \frac{(D_1+D_2)\frac{d_{31}V}{a_{33}} + 2D_3\frac{f_{13}V}{a_{33}}}{(D_1+D_2)(D_5+D_6) - 4D_3^2} \qquad (4.91)$$

$$w(M+1, N+1) = w(M+1, N-1) + w(M, N+1) - w(M, N-1) \qquad (4.92)$$

$$w(M+1, N) = 2w(M, N) - w(M-1, N) + \Delta x^2 \frac{(D_5+D_6)\frac{f_{13}V}{a_{33}} + 2D_3\frac{d_{31}V}{a_{33}}}{4D_3^2 - (D_1+D_2)(D_5+D_6)} \qquad (4.93)$$

$$w(M,N+1)=2w(M,N)-w(M,N-1)+\Delta x^2\frac{(D_5+D_6)\frac{f_{13}V}{a_{33}}+2D_3\frac{d_{31}V}{a_{33}}}{4D_3^2-(D_1+D_2)(D_5+D_6)} \quad (4.94)$$

$$\begin{aligned}w(M+2,N)=&-2w(M+1,N)+2w(M-1,N)-w(M-2,N)-\\&\{-w(M+1,N-1)+2w(M+1,N)-w(M+1,N+1)+\\&w(M-1,N-1)-2w(M-1,N)+w(M-1,N+1)\}\frac{D_4}{D_1}-\\&\{u(M+1,N)-2u(M,N)+u(M-1,N)\}\frac{2\Delta xD_{12}}{D_1}-\{v(M+1,N-1)-\\&v(M-1,N-1)-v(M+1,N+1)+v(M-1,N+1)\}\frac{\Delta xD_{12}}{2D_1}\end{aligned} \quad (4.95)$$

$$\begin{aligned}w(M,N+2)=&w(M,N-2)-2w(M,N-1)+2w(M,N+1)+\\&\{w(M+1,N-1)-2w(M,N-1)+w(M-1,N-1)-w(M+\\&1,N+1)+2w(M,N+1)-w(M-1,N+1)\}\frac{D_4}{D_1}+\{-v(M,N-1)+\\&2v(M,N)-v(M,N+1)\}\frac{2\Delta xD_{12}}{D_1}+\{-u(M+1,N-1)+u(M,N-\\&1)+u(M+1,N+1)-u(M,N+1)\}\frac{\Delta xD_{12}}{2D_1}\end{aligned} \quad (4.96)$$

(5.4) Other out-of-the-plate points that are not related to the boundary conditions

From Figure 4-2, it can be seen that for out-of-the-plate mesh points (i.e. $(-2,j)$, $(0\le j\le N)$, $(M+2,j)$, $(0\le j\le N)$ and $(i,N+2)$, $(0\le i\le M)$), the displacements in both x and y directions ($u(i,j)$, $v(i,j)$) are not solved. In order to express them with the internal points, the finite difference scheme is applied.

For points $(-1,j)$, $(0\le j<N)$, and $(i,N+1)$, $(0<i<M)$, $u(-1,j)$ and $v(i,N+1)$ can be written using the central-difference method as,

$$u(-1,j)=\frac{u(0,j)+u(-2,j)+u(-1,j+1)+u(-1,j-1)}{4} \quad (4.97)$$

$$v(i,N+1)=\frac{v(i+1,N+1)+v(i-1,N+1)+v(i,N+2)+v(i,N)}{4} \quad (4.98)$$

Accordingly, the displacements of $u(-2,j)$, $u(M+2,j)$ and $v(i,N+2)$ can be expressed as,

$$u(-2,j) = 4u(-1,j) - u(0,j) - u(-1,j+1) - u(-1,j-1) \quad (4.99)$$

$$u(M+2,j) = 4u(M+1,j) - u(M,j) - u(M+1,j+1) - u(M+1,j-1) \quad (4.100)$$

$$v(i,N+2) = 4v(i,N+1) - v(i+1,N+1) - v(i-1,N+1) - v(i,N) \quad (4.101)$$

The finite difference schemes for the points $(0,N+1)$ and $(-1,N)$ that are next to the corner point $(0,N)$ are expressed as,

$$u(0,N+1) = \frac{u(1,N+1) + u(-1,N+1)}{2} \quad (4.102)$$

$$u(-1,N) = \frac{u(-1,N-1) + u(-1,N+1)}{2} = \frac{u(-2,N) + u(0,N)}{2} \quad (4.103)$$

$$v(0,N+1) = \frac{v(1,N+1) + v(-1,N+1)}{2} \quad (4.104)$$

$$v(-1,N) = \frac{v(-1,N-1) + v(-1,N+1)}{2} = \frac{v(0,N+2) + v(0,N)}{2} \quad (4.105)$$

Accordingly, the expressions of $u(-1,N+1)$, $u(-2,N)$, $v(-1,N+1)$ and $v(0,N+2)$ can thus be determined as,

$$u(-1,N+1) = \frac{2u(0,N+1) + 2u(-1,N) - u(1,N+1) - u(-1,N-1)}{2} \quad (4.106)$$

$$u(-2,N) = 2u(-1,N) - u(0,N) \quad (4.107)$$

$$v(-1,N+1) = \frac{2v(0,N+1) + 2v(-1,N) - v(1,N+1) - v(-1,N-1)}{2} \quad (4.108)$$

$$v(0,N+2) = 2v(0,N+1) - v(0,N) \quad (4.109)$$

Similarly, based on the finite difference schemes for points $(M, N+1)$ and $(M+1, N)$ which are outside the corner point (M, N), $u(M+1, N+1)$, $u(M+2, N)$, $v(M+1, N+1)$ and $v(M, N+2)$ are derived as,

$$u(M+1,N+1) = \frac{2u(M,N+1)+2u(M+1,N)-u(M-1,N+1)-u(M+1,N-1)}{2} \quad (4.110)$$

$$u(M+2,N) = 2u(M+1,N)-u(M,N) \quad (4.111)$$

$$v(M+1,N+1) = \frac{2v(M,N+1)+2v(M+1,N)-v(M-1,N+1)-v(M+1,N-1)}{2} \quad (4.112)$$

$$v(M,N+2) = 2v(M,N+1)-v(M,N) \quad (4.113)$$

So far, all the out-of-the-plate mesh points involved in the finite difference scheme of the governing equations are described by the internal points. Thus, the governing equations (4.26)-(4.28) can be rewritten for each point. Since the displacements for points along the clamped edge ($y = 0$) are known as 0 as shown by Eq (4.34), there are $3 \times (M+1) \times N$ equations for $(M+1) \times N$ internal mesh points, whose displacements are to be determined. These $3 \times (M+1) \times N$ equations can be expressed in the matrix form as,

$$\begin{bmatrix} A^1 & B^1 & C^1 \\ A^2 & B^2 & C^2 \\ A^3 & B^3 & C^3 \end{bmatrix} \begin{Bmatrix} w \\ u \\ v \end{Bmatrix} = \begin{Bmatrix} Q^1 \\ Q^2 \\ Q^3 \end{Bmatrix} \quad (4.114)$$

where $\{w\} = [w_{0,1};\ w_{0,2}; \cdots w_{M-1,N};\ w_{M,N}]$, $\{u\} = [u_{0,1};\ u_{0,2}; \cdots u_{M-1,N};\ u_{M,N}]$, $\{v\} = [v_{0,1};\ v_{0,2}; \cdots v_{M-1,N};\ v_{M,N}]$ and $[Q_{i_{0,1}};\ Q_{i_{0,2}}; \cdots Q_{i_{M-1,N}};\ Q_{i_{M,N}}]$ $(i = 1, 2 \text{ and } 3)$ denote the vectors of nodal displacements and external electrical and mechanical loads, respectively. Matrices $A^i\big((M+1) \times N, (M+1) \times N\big)$, $B^i\big((M+1) \times N, (M+1) \times N\big)$ and $C^i\big((M+1) \times N, (M+1) \times N\big), (i = 1, 2 \text{ and } 3)$ stand for coefficients of displacements $\{w\}, \{u\} \text{ and } \{v\}$ for the three governing equations (4.26)-(4.28),

respectively. The specific value of A^i, B^i and C^i is provided in Appendix A while their expressions can be written as,

$$[A^i] = \begin{bmatrix} A^i{}_{(0,1),(0,1)} & A^i{}_{(0,1),(0,2)} & \cdots & A^i{}_{(0,1),(M-1,N)} & A^i{}_{(0,1),(M,N)} \\ A^i{}_{(0,2),(0,1)} & A^i{}_{(0,2),(0,2)} & \cdots & A^i{}_{(0,2),(M-1,N)} & A^i{}_{(0,2),(M,N)} \\ \vdots & \vdots & \ddots & \vdots & \vdots \\ A^i{}_{(M-1,N),(0,1)} & A^i{}_{(M-1,N),(0,2)} & \cdots & A^i{}_{(M-1,N),(M-1,N)} & A^i{}_{(M-1,N),(M,N)} \\ A^i{}_{(M,N),(0,1)} & A^i{}_{(M,N),(0,2)} & & A^i{}_{(M,N),(M-1,N)} & A^i{}_{(M,N),(M,N)} \end{bmatrix} \quad (4.115)$$

$$[B^i] = \begin{bmatrix} B^i{}_{(0,1),(0,1)} & B^i{}_{(0,1),(0,2)} & \cdots & B^i{}_{(0,1),(M-1,N)} & B^i{}_{(0,1),(M,N)} \\ B^i{}_{(0,2),(0,1)} & B^i{}_{(0,2),(0,2)} & \cdots & B^i{}_{(0,2),(M-1,N)} & B^i{}_{(0,2),(M,N)} \\ \vdots & \vdots & \ddots & \vdots & \vdots \\ B^i{}_{(M-1,N),(0,1)} & B^i{}_{(M-1,N),(0,2)} & \cdots & B^i{}_{(M-1,N),(M-1,N)} & B^i{}_{(M-1,N),(M,N)} \\ B^i{}_{(M,N),(0,1)} & B^i{}_{(M,N),(0,2)} & & B^i{}_{(M,N),(M-1,N)} & B^i{}_{(M,N),(M,N)} \end{bmatrix} \quad (4.116)$$

$$[C^i] = \begin{bmatrix} C^i{}_{(0,1),(0,1)} & C^i{}_{(0,1),(0,2)} & \cdots & C^i{}_{(0,1),(M-1,N)} & C^i{}_{(0,1),(M,N)} \\ C^i{}_{(0,2),(0,1)} & C^i{}_{(0,2),(0,2)} & \cdots & C^i{}_{(0,2),(M-1,N)} & C^i{}_{(0,2),(M,N)} \\ \vdots & \vdots & \ddots & \vdots & \vdots \\ C^i{}_{(M-1,N),(0,1)} & C^i{}_{(M-1,N),(0,2)} & \cdots & C^i{}_{(M-1,N),(M-1,N)} & C^i{}_{(M-1,N),(M,N)} \\ C^i{}_{(M,N),(0,1)} & C^i{}_{(M,N),(0,2)} & & C^i{}_{(M,N),(M-1,N)} & C^i{}_{(M,N),(M,N)} \end{bmatrix} \quad (4.117)$$

By solving the governing equation matrix (4.114) numerically via MATLAB, the deflection of the cantilevered PNP under applied mechanical and electrical loads can be determined. Accordingly, the complete electroelastic fields of the plate can be derived, which will be used to interpret the flexoelectric effects upon the bending behaviors of the cantilevered PNP. The MATLAB routine written for predicting the static deflection of the plate is provided in Appendix A.

Chapter 5

5 The flexoelectric effect on the bending behavior of a cantilevered piezoelectric nanoplate (PNP)

In this section, the electroelastic fields of a cantilevered PNP with various geometries in response to a uniformly distributed load q and an electric voltage V are investigated to study the flexoelectric effect. $BaTiO_3$ is taken as the example material with its material properties given by Giannakopoulos and Suresh (1999). Based on this information, the material's elastic, piezoelectric, and dielectric constants are calculated as $c_{11} = 167.55\ GPa$, $c_{12} = 78.15\ GPa$, $c_{66} = 44.7\ GPa$, $a_{33} = 0.79 \times 10^8\ V.m/C$, $d_{31} = 3.5 \times 10^8\ V/m$ for a plane strain condition. Meanwhile, $b_{33} = 1 \times 10^{-9}\ Jm^3/C^2$ was given in References (Maranganti *et al.*, 2006; Eliseev *et al.*, 2009). According to References (Tagantsev, 1986; Ponomareva *et al.*, 2012; Zubko *et al.*, 2013), the flexocoupling constant f_{13} is within the range of $1 - 10\ V$.

5.1 Validation of the finite difference method (FDM) for the numerical simulation

The accuracy of the FDM is first validated by comparing the numerical results with existing results in the literature for special cases. For an elastic Kirchhoff plate under a uniformly distributed load q, the deflection function w was derived by Lin and Yuan (1985) using the method of two-direction trigonometric series as,

$$w = \frac{qb^4}{24D}\left(6\frac{y^2}{b^2} - 4\frac{y^3}{b^3} + \frac{y^4}{b^4}\right) + \sum_{m=2,4,\ldots}^{18}\left(A_m \operatorname{sh}\frac{m\pi y}{a} + B_m \operatorname{ch}\frac{m\pi y}{a} + C_m \frac{m\pi y}{a}\operatorname{sh}\frac{m\pi y}{a} + D_m \frac{m\pi y}{a}\operatorname{ch}\frac{m\pi y}{a}\right)\cos\frac{m\pi x}{a} + \sum_{i=1}^{9}\left(F_i \operatorname{ch}\frac{i\pi x}{b} + G_i \frac{i\pi x}{b}\operatorname{sh}\frac{i\pi x}{b}\right)\cos\frac{i\pi y}{b} + K_o + K_3 x^2 + K_4 y^2 = \frac{\alpha q b^4}{D} \quad (5.1)$$

where D is the flexural rigidity of the plate. For a plate made of $BaTiO_3$ with the size of $a = b = 10h$ ($h = 50\ nm$), the flexural rigidity is calculated as $D = 1.6697 \times 10^{-12}$. The coefficients A_m, B_m, C_m, D_m, F_i, G_i, K_o, K_3 and K_4 were provided by Lin and Yuan (1985). The deflection factors α for different positions along the free edges ($y = b, x = 0$ and $x = a$) of the plate were also provided by Lin *et al*. (1985) and are shown in Table 5-1 & Table

5-2, respectively. Based on the value of the deflection factors, the corresponding deflections can be calculated, and they are listed in these two tables, too. Without considering the flexoelectricity, our FDM simulation results under the same loading condition ($q = 0.1\ pN/nm^2$) are also presented here for comparison. It is found that the FDM results are in good agreement with the results in Reference (Lin *et al*., 1985).

Table 5-1 The deflection of points along the free edge $y = b$

x/a	α	w (*reference value for Lin et al., 1985*) (nm)	w (*FDM*) (nm)	$\frac{w(re)-w(FDM)}{w(re)}$ (%)
0.5	0.12912	0.48332	0.48789	-0.95
0.25 or 0.75	0.12861	0.48141	0.48617	-0.99
0 or 1	0.12728	0.47633	0.48143	-1.05

Table 5-2 The deflection of points along the free edge $x = 0$ and $x = a$

y/b	α	w (*reference value for Lin et al., 1985*) (nm)	w (*FDEM*) (nm)	$\frac{w(re)-w(FDM)}{w(re)}$ (%)
0.25	0.011824	0.044259	0.044156	0.23
0.5	0.043336	0.162215	0.163271	-0.65
0.75	0.084078	0.314720	0.317677	-0.94

When the plate becomes slender, i.e., one in-plane dimension is much larger than the other one, it can be simplified as a beam model. For example, a $BaTiO_3$ plate with dimensions of $a = h = 20\ nm$ and $b = 20h$ can be treated as a beam. For a piezoelectric nanobeam subjected to a concentrated load $F = 0.1\ nN$ at the free end, the transverse deflection for the points along the longitudinal direction y was analytically solved by Yan and Jiang (2013) as,

$$w = \frac{Fy^2}{6(EI)}(y - 3b) - \frac{c_{11}f_{13}Vay^2}{2(a_{33}C_{11} - d_{31}^2)(EI)} \quad (5.2)$$

where $EI = \left(c_{11} - \frac{\epsilon_0 d_{31}^2}{\epsilon_0 a_{33}+1}\right)\frac{bh^3}{12} - \frac{f_{13}^2}{a_{33}}bh$ is the effective bending rigidity of the beam with the consideration of the flexoelectricity. In Reference (Yan and Jiang, 2013), the material constants were taken as $c_{11} = 131\ GPa$, $d_{31} = 1.87 \times 10^8\ V/m$, $a_{33} = 0.79 \times 10^8 V.m/$

C, and $f_{13} = 5\ V$. The corresponding deflection profile of the beam calculated by Eq. (5.2) is plotted in Figure 5-1. Our FDM simulation result for this slender plate is also provided in this figure for comparison. It is observed that our numerical results agree very well with the existing results for a piezoelectric nanobeam in Reference (Yan and Jiang, 2013).

For those two special cases, the FDM scheme developed for the cantilevered PNP with the consideration of the flexoelectric effect is validated. Thus, it will be further employed to study the bending behavior of the cantilevered PNP.

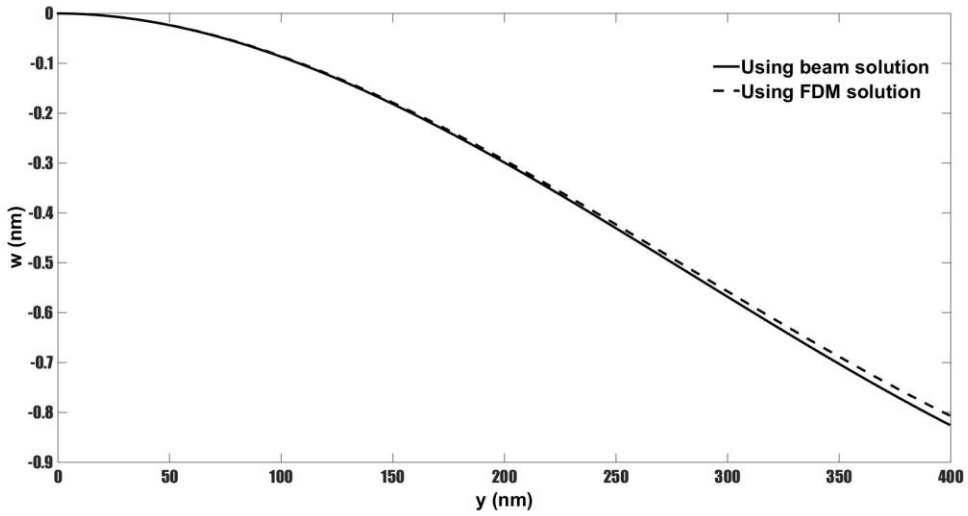

Figure 5-1 Comparison of the deflection of the plate using FDM and the deflection of the beam

5.2 The flexoelectric effect on the static deflection of the cantilevered PNP

Since there is no exact value for the flexocoupling constant provided in the literature for $BaTiO_3$, for the illustration purpose of demonstrating the flexoelectric effects, $f_{13} = 10V$ is taken in the current work hereafter as in the other literature (Zhang, Yan and Jiang, 2014). Meanwhile, we must ensure that the applied distributed load q will only induce small deformation in accordance with the theories stated in the previous section.

First, the flexoelectric effect on the overall bending profile of the plate is examined. For a cantilevered PNP with a size of $b = 2.5a, a = 12h$ and $h = 30nm$, under a mechanical distributed load $q = -0.01\, pN/nm^2$and an electrical load $V = 0.002\, V$, the bending profiles of the plate without and with considering the flexoelectricity are sketched in Figure 5-2, respectively. From this figure, it can be seen that under the current loading condition, the bending profile of the plate under the flexoelectric effect is significantly different from that without considering the flexoelectricity. Thus, we can conclude that the flexoelectricity plays an important role in the plate deformation. The plate still keeps a symmetric profile with the plane of $x = \frac{a}{2}$, while the flexoelectricity influences the local deflection of the individual position points. For points with the same y position, there is little difference among their bending deflections as shown in the figure below. Therefore, in the following analysis, we will take the points along the middle plane of the plate ($x = \frac{a}{2}$) as examples for simplification.

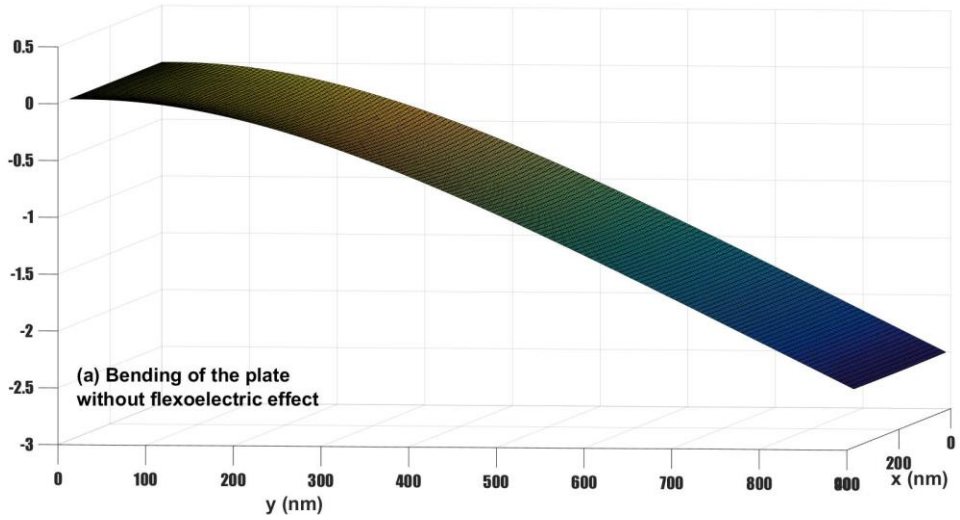

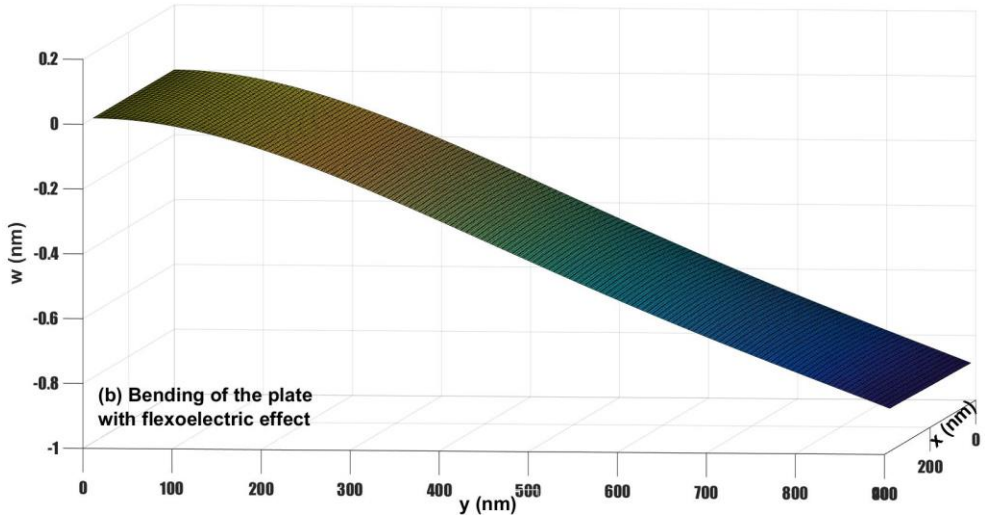

Figure 5-2 Bending profile of the cantilevered PNP (a) without flexoelectric effect and (b) with flexoelectric effect

5.2.1 The effect of plate thickness on the flexoelectricity

As illustrated in the Introduction section, the flexoelectricity is closely linked to the feature scale of the nanostructures. Particularly for the nanoplate, since only the strain gradients along the thickness direction are considered, we will first investigate how the flexoelectric effect varies with the plate thickness.

For a nanoplate with constant aspect ratios ($b = 2.5a, a = 12h$, for example) under a mechanical distributed load $q = -0.01pN/nm^2$ and various electrical voltages, Figure 5-3 plots the normalized maximum deflection (w/w_0^V) against the plate thickness h for the middle point of the free edge ($x = 0.5a, y = b$). w_0^V stands for the maximum deflection of the same point under the same loading conditions without the flexoelectric effect. Without any applied electric voltage, the cantilevered PNP exhibits a stiffer elastic behavior than the conventional one, as evidenced by a smaller deflection induced in the plate when considering the flexoelectric effect. A similar behavior was also observed for a cantilevered nanobeam (Yan and Jiang, 2013), which can be attributed to the fact that the flexoelectricity decreases the effective bending rigidity of the plate. It should also be noted that such flexoelectric effect could also be modified by the applied voltage as shown in boundary condition Eqs. (3.70), (3.72), (3.74) and (3.76). For example, when the applied voltage

is negative, the applied electrical load magnifies the soft bending behavior, i.e., with the increase of the voltage magnitude, the plate becomes softer. However, with the voltage applied in the opposite direction, the increase of the voltage magnitude could even stiffen the bending of the plate. It is also observed in this figure that the flexoelectric effect depends on the size of the plate and is more noticeable for plates with smaller thickness. As the plate thickness h increases, the flexoelectric effects will diminish as expected and all the curves approach unity.

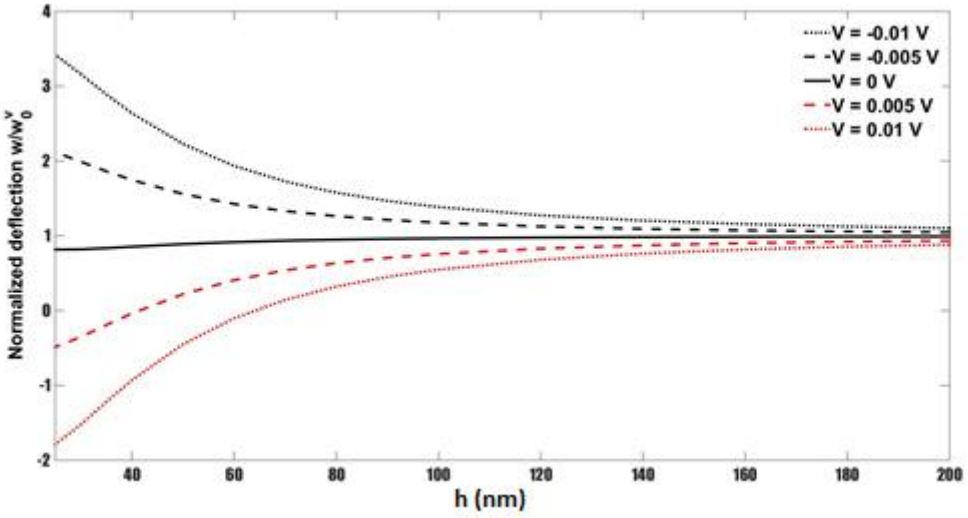

Figure 5-3 Normalized deflection versus plate thickness under different voltages

It is also interesting to notice that the direction and the magnitude of the applied voltage will influence how the plate deforms when the plate thickness is small enough, $h = 30\ nm$, for example. Figure 5-4 shows the lateral view of the bending profile of a cantilevered PNP under different applied voltages while the mechanical load is fixed as $q = -0.01\ pN/nm^2$. It is concluded from the figure that when the thickness is small, the flexoelectricity has such a significant impact on the bending behavior of the plate that the deformation direction can even be altered when a voltage is applied. However, as the thickness increases, such flexoelectric effect decreases and the deformation direction will not be changed by the applied voltage.

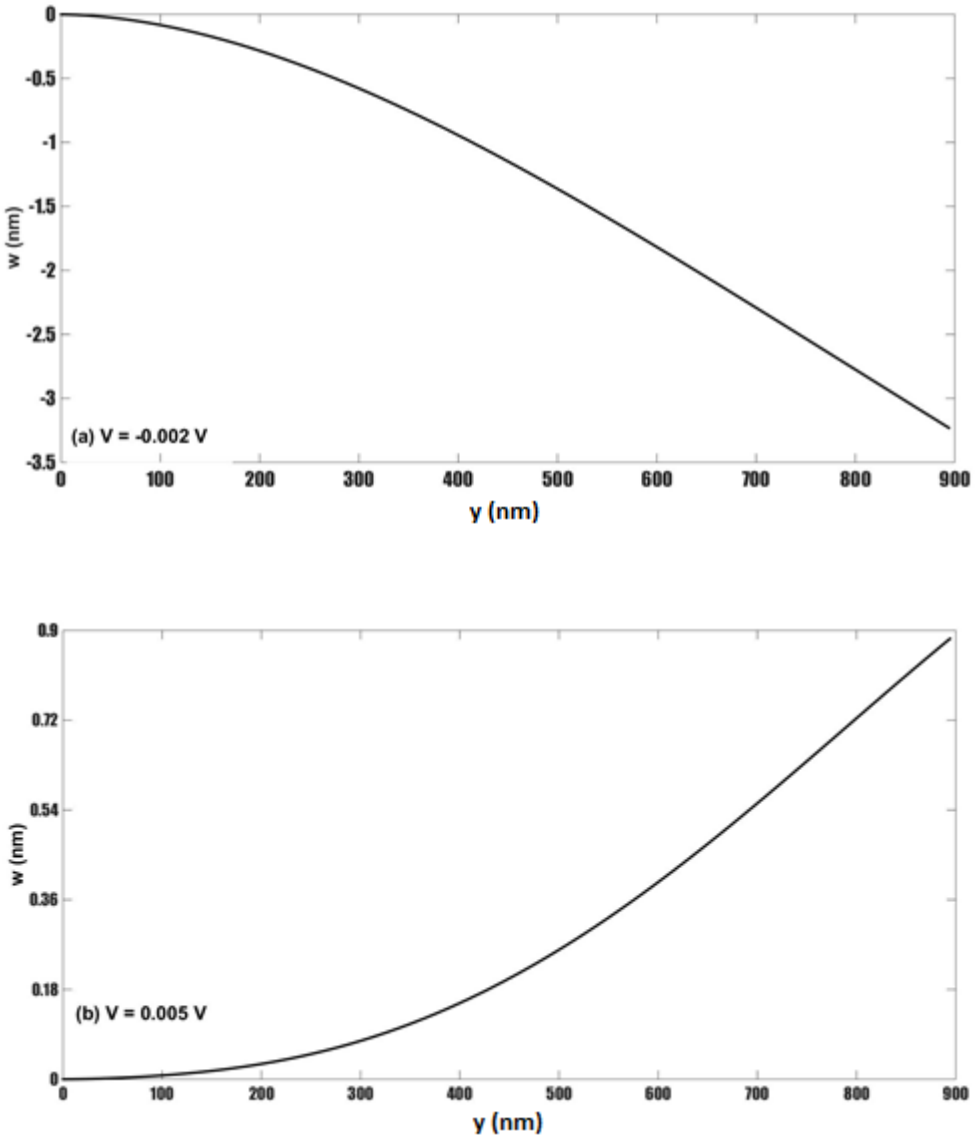

Figure 5-4 Lateral bending profile view of a cantilevered PNP under different voltages (a) $V = -0.002V$, and (b) $V = 0.005V$

5.2.2 The effect of the plate ratio on the flexoelectricity

As discussed in the Reference (Zhang, Yan and Jiang, 2014), it was found that the flexoelectric effect might depend on the plate aspect ratio. For a rectangular plate with fixed in-plane aspect ratio and thickness ($b = 2.5a, h = 30\ nm$), Figure 5-5 plots the normalized maximum deflection (w/w_0^V) against the plate aspect ratio (b/h) for the middle point of the free edge ($x = 0.5a, y = b$) under different voltages while the mechanical

distributed load is fixed as $q = -0.01 pN/nm^2$. From this figure, it is indicated that the aspect ratio a/h, along with the applied voltage, also has an impact on the flexoelectric effect upon the bending of the plate. For example, the flexoelectric effect is not affected by the aspect ratio without the applied voltage, as demonstrated by the straight line for the case of $V = 0\,V$. This phenomenon was also observed for a clamped PNP in Reference (Zhang, Yan and Jiang, 2014). However, when a voltage is applied, the effect of the flexoelectricity is more pronounced for the plates with smaller aspect ratios. With the increase of the plate aspect ratio, the applied voltage has negligible effects upon the flexoelectricity.

It should be mentioned that for a clamped PNP in Reference (Zhang, Yan and Jiang, 2014), the variation of the flexoelectricity with the combined effects of aspect ratios and applied voltages is quite different from the current cantilevered PNP. Such discrepancy is mainly attributed to the boundary conditions. For a clamped nanoplate, the flexoelectricity will change the effective bending rigidity as well as the strain gradients. For the cantilevered nanoplate, the flexoelectricity will also modify the traditional boundary conditions as shown by Eqs. (3.70)-(3.77), which were defined as non-homogeneous boundary conditions for a cantilevered piezoelectric nanobeam in Reference (Yan and Jiang, 2013). Thus, it is concluded that the flexoelectric effect on the bending of the plate is also sensitive to the boundary conditions of the plate.

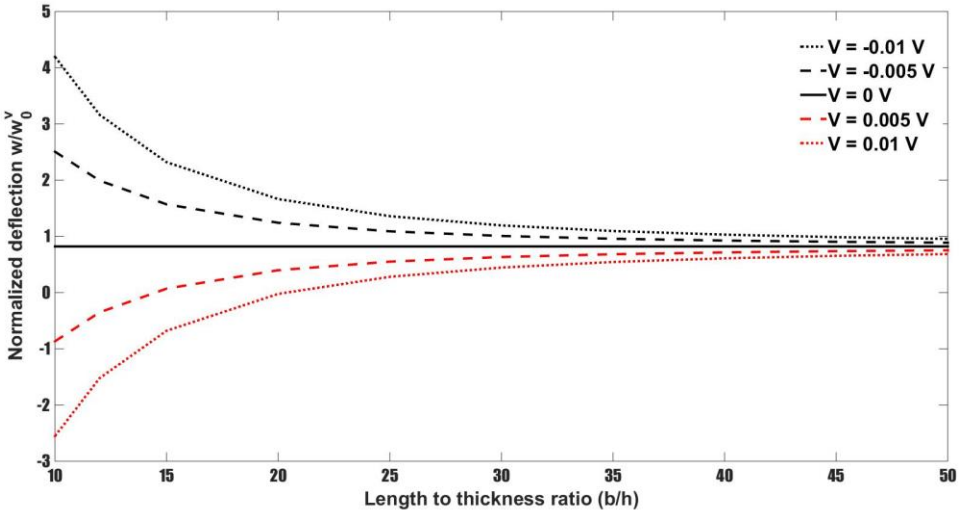

Figure 5-5 Normalized deflection with length to thickness ratio under different voltages

The results shown in Figure 5-3 and Figure 5-5 clearly demonstrate that the flexoelectric effect upon the static bending behavior of a cantilevered PNP depends on the plate thickness, the aspect ratio and the applied electrical load.

5.3 The flexoelectric effect on the relaxation strain of the cantilevered PNP

As discussed in Chapter 2, for a cantilevered PNP under free axial loading conditions at the free ends, there exist relaxation strains along the axial x and y directions, which are induced by the applied voltage due to the intrinsic electromechanical coupling effect. From Equation (3.42), it can be seen that the relaxation strain is also affected by the flexoelectricity but not reliant on the z position of the point. Figure 5-6 plots the in-plane distribution of the relaxation strain for a plate ($b = 2.5a, a = 12h, h = 40nm$) under a negative applied voltage ($V = -0.005\,V$). In the absence of the flexoelectricity, the relaxation strain ($\varepsilon_0 = \frac{d_{31}V}{a_{33}h(C_{11}+C_{12})-2d_{31}^2h}$) is independent of the point positions and caused solely by the applied voltage, which is indicated by the flat plane in this figure. However, under the effect of the flexoelectricity, the relaxation strain varies with the point positions through the whole plate due to the change of the strain gradients. Particularly, the

flexoelectric effect on the relaxation strain is more prominent for the clamped edge due to the high strain gradient near the edge.

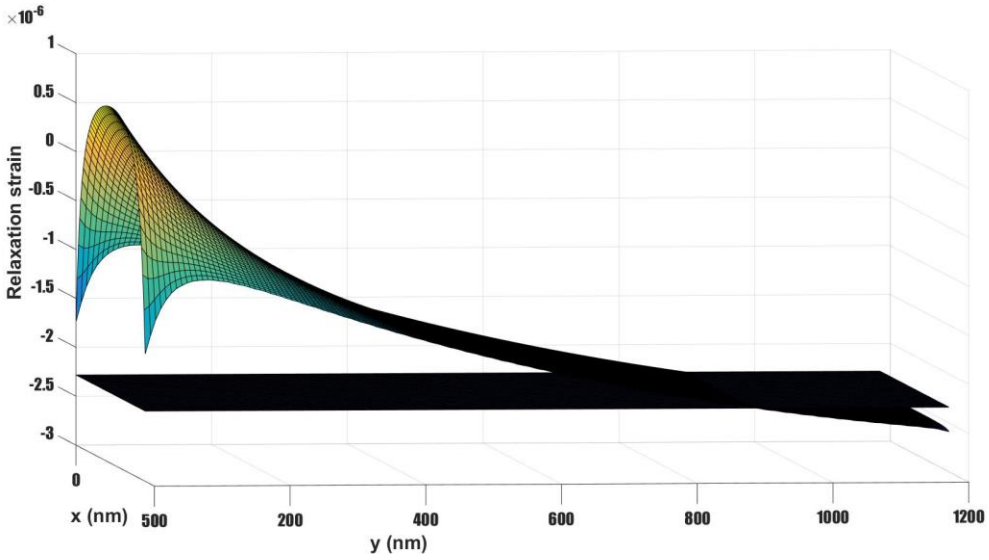

Figure 5-6 In-plane distribution of relaxation strain under $V = -0.005V$

5.3.1 The effect of plate thickness and applied voltages on the relaxation strain

In order to see how the flexoelectric effect upon the relaxation strain varies with the plate thickness, Figure 5-7 plots the variation of the relaxation strain with the plate thickness h for the middle point of the free edge ($x = 0.5a, y = b$). This plate is set with constant dimension ratios ($b = 2.5a, a = 12h$) and is subject to a mechanical load $q = -0.01\, pN/nm^2$ and different applied voltages. Without the consideration of the flexoelectricity, the relaxation strain due to the inherent electromechanical coupling is also provided in these figures for comparison, which is constant for all the points throughout the plate.

It is obvious from these figures that both the plate thickness and the applied voltage have impacts on the relaxation strain. It is also found that the effect of the flexoelectricity is more pronounced when the plate thickness h is small, and such an effect becomes weaker with the increase of the plate thickness h. When the plate thickness is sufficiently large,

the relaxation strain approaches the one without the consideration of the flexoelectricity as expected.

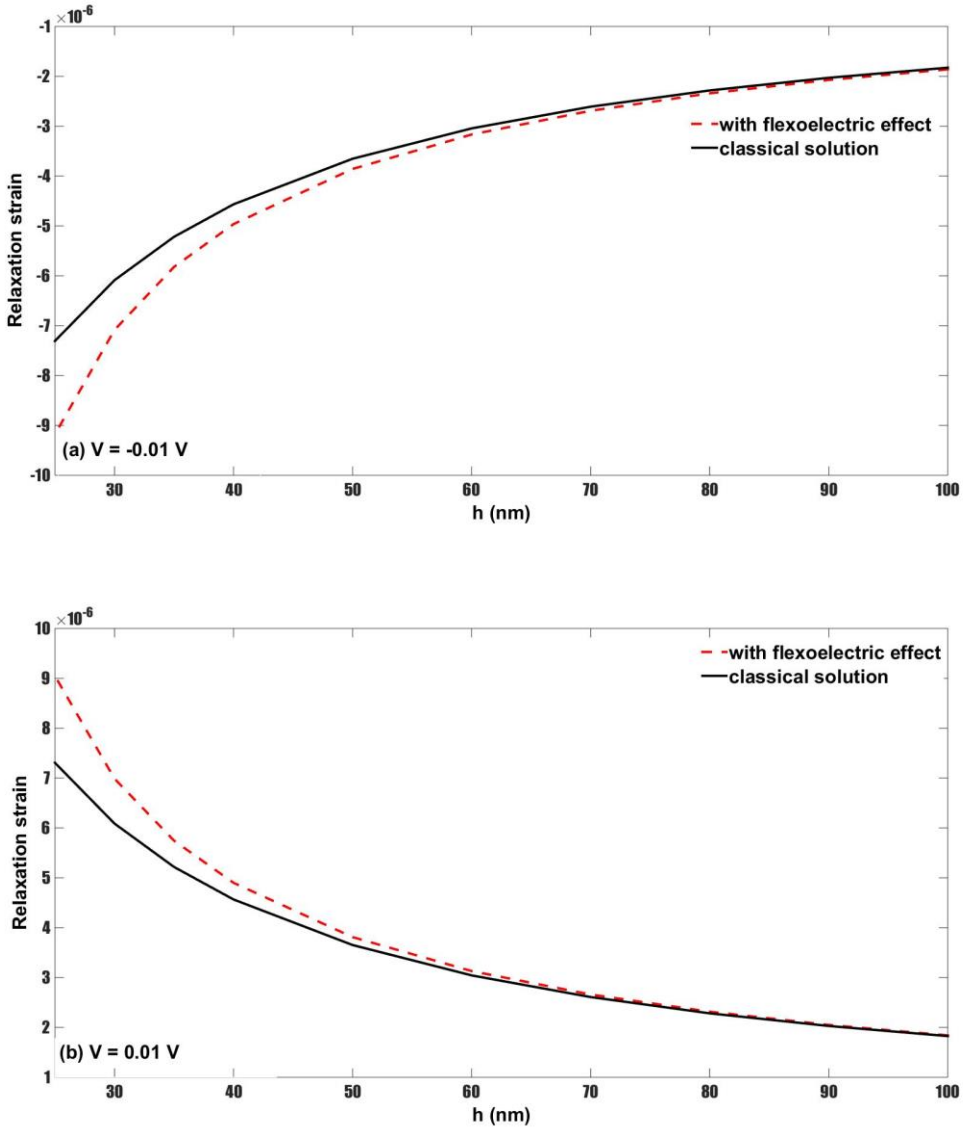

Figure 5-7 Relaxation strain with beam thickness under different voltages (a) $V = -0.01V$ and (b) $V = 0.01V$

5.3.2 The effect of applied mechanical loads on the relaxation strain

As discussed in the previous section that the flexoelectricity is induced by the non-uniform strain, it is reasonable to assume that the transverse mechanical load applied to the plate

will have an influence upon the flexoelectric effect. For a plate whose geometry is set as $b = 2.5a, a = 12h$, Figure 5-8 plots the variation of the relaxation strain with the plate thickness for the middle point at the free edge ($x = 0.5a, y = b$) when the plate is under an applied voltage $V = -0.002V$ and different applied mechanical loads. The relaxation strain without the flexoelectricity is also provided in this figure for comparison.

Under such a negative applied voltage ($V = -0.002V$), the relaxation strain is negative. The magnitude of the relaxation strain with the flexoelectric effect is larger compared with the one without considering the flexoelectricity. Furthermore, the magnitude of the relaxation strain is enhanced by increasing the magnitude of the applied load q. With the increase of the plate thickness, the flexoelectric effect diminishes and the relaxation strain approaches that of the classical piezoelectric nanoplate.

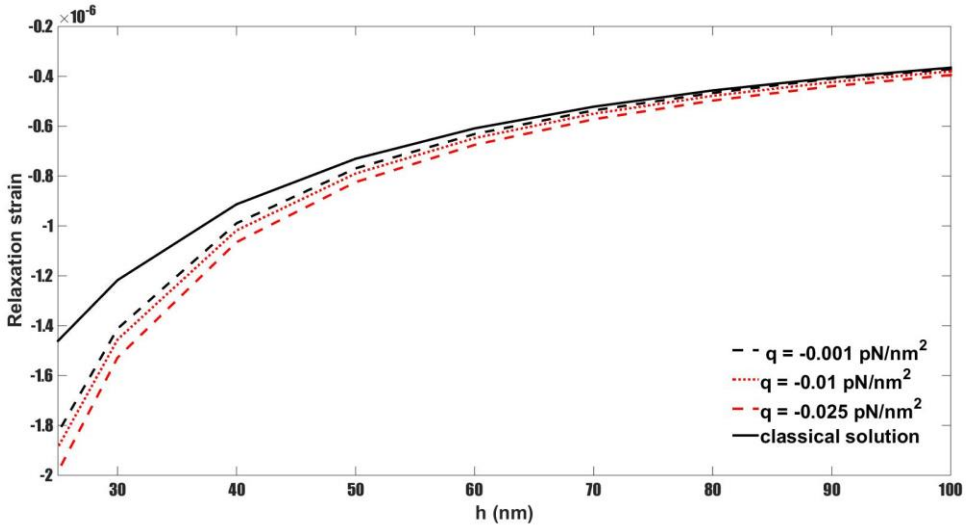

Figure 5-8 Relaxation strain with different applied loads

5.4 The flexoelectric effect on the electric field of the cantilevered PNP

As indicated by the electric filed Eq.(3.26), the strain gradients will have an effect on the electric field distribution. Thus, in this section, efforts will be made to investigate the influence of different factors, such as the plate dimensions, the applied voltage, and the applied mechanical loads on the electric field distribution.

5.4.1 The effect of plate thickness on the electric field distribution

To study how the plate thickness influences the electric field distribution, two plates with the same aspect ratios ($b = 2.5a, a = 12h$) but different thicknesses ($h = 50\,nm$ and $h = 300\,nm$) are used as samples here. Figure 5-9 plots the electric field distribution E along the plate thickness direction for points at the middle of the free edge ($x = 0.5a, y = b$) for these two plates when the applied loads $q = -0.01\,pN/nm^2$ and the applied voltage $V = -0.002\,V$.

It can be seen that the flexoelectricity has a more noticeable impact upon the electric field for plates with smaller thickness, as the discrepancy between the plot considering the flexoelectricity and that of the classical solution is larger when $h = 50\,nm$. There are jumps of the electric field for points near the boundary surfaces for both cases. This kind of discrepancy near the surface when considering the flexoelectricity is a typical boundary behavior for a gradient theory, which was also seen in the polarization gradient result of a plate (Mindlin, 1969), the electric field result of a clamped PNP (Zhang, Yan and Jiang, 2014) and the electric field of a circular cylindrical shell (Yang *et al.*, 2004).

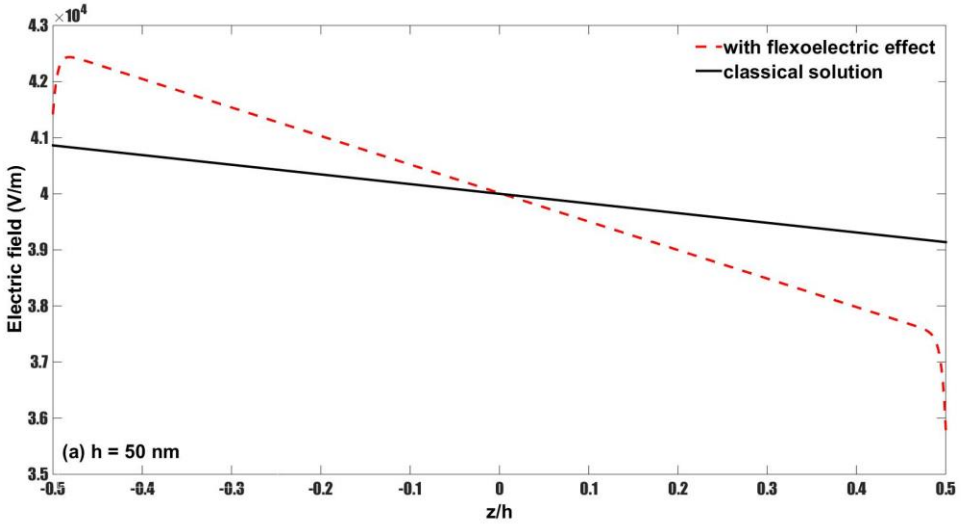

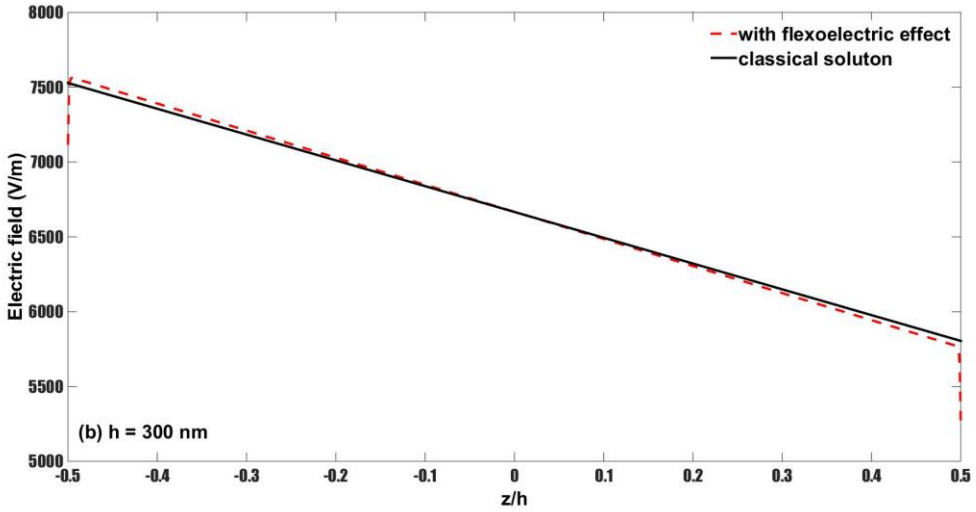

Figure 5-9 Electric field distribution along thickness direction at the middle of the free edge with different thickness (a) $h = 50\ nm$ and (b) $h = 300\ nm$

5.4.2 The effect of applied voltages on the electric field distribution

In order to see how the electric field changes with the applied voltages, for a PNP with dimension set as $b = 2.5a, a = 12h$ and $h = 30\ nm$, Figure 5-10 depicts the normalized electric field (E/E^0) along the thickness direction at the middle of the free edge ($x = 0.5a, y = b$) under a fixed mechanical load $q = -0.05pN/nm^2$ and different applied voltages, where E^0 stands for the electric field of the plate without considering the flexoelectric effect.

From this figure, it can be seen that when the applied mechanical load is fixed ($q = -0.01pN/nm^2$, for example) and the applied voltage is negative, the flexoelectric effect decreases with the increase of the magnitude of the applied load; however, an opposite trend is observed when the applied voltage is positive.

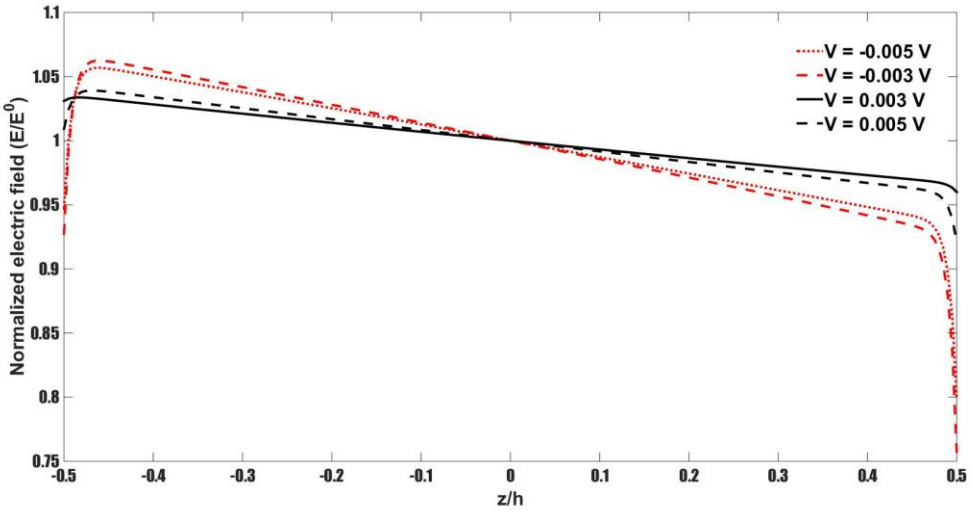

Figure 5-10 Electric field distribution along thickness direction at the middle of the free edge with different applied voltages

5.4.3 The effect of applied mechanical loads on the electric field distribution

For a PNP with constant aspect ratios and thickness ($b = 2.5a, a = 12h$ and $h = 20\ nm$) under an electrical load $V = -0.002\ V$ and various mechanical loads, Figure 5-11 plots the normalized electric field (E/E_0) along the thickness direction for the points at the middle of the free edge ($x = 0.5a, y = b$). As seen from Figure 5-11, it is concluded that the applied loads also modify the effect of the flexoelectricity on the electric field distribution. For example, the flexoelectric effect is enhanced by increasing the magnitude of the applied load, as the slope of the normalized electric field gets larger with the increase of the magnitude of the applied load.

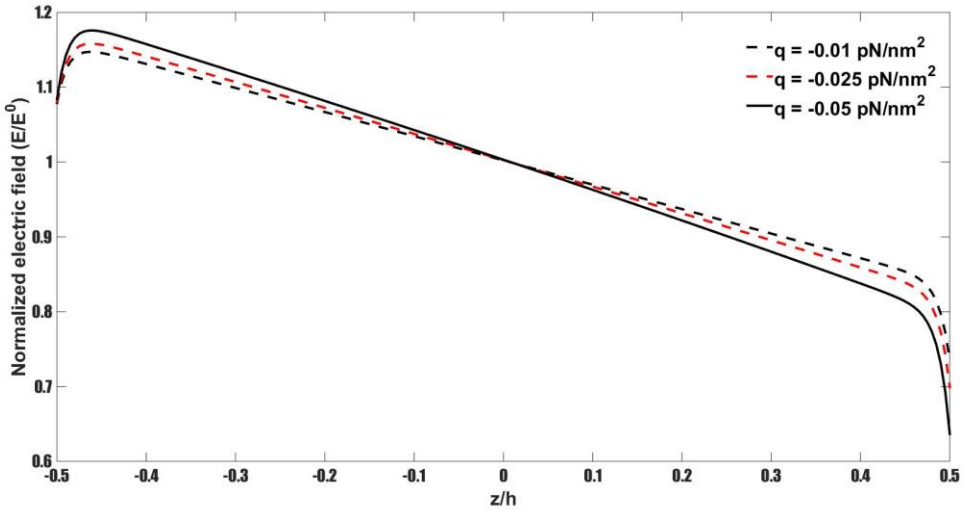

Figure 5-11 Normalized electric field distribution along thickness direction at the middle of the free edge with different applied loads

5.5 The flexoelectric effect on the polarization of the cantilevered PNP

Due to the strain gradient, there will be a spontaneous electric polarization along the thickness direction, whose expression is shown as,

$$
\begin{aligned}
P_z = {} & \frac{e_{13}h\left(\frac{\partial^2 w}{\partial x^2}+\frac{\partial^2 w}{\partial y^2}\right)-2e_{13}\left(\frac{\partial u^0}{\partial x}+\frac{\partial v^0}{\partial y}\right)}{2b_{33}\lambda\left(e^{\frac{\lambda h}{2}}-e^{\frac{-\lambda h}{2}}\right)}e^{\lambda z} \\
& + \frac{e_{13}h\left(\frac{\partial^2 w}{\partial x^2}+\frac{\partial^2 w}{\partial y^2}\right)+2e_{13}\left(\frac{\partial u^0}{\partial x}+\frac{\partial v^0}{\partial y}\right)}{2b_{33}\lambda\left(e^{\frac{\lambda h}{2}}-e^{\frac{-\lambda h}{2}}\right)}e^{-\lambda z} \\
& + \frac{kd_{31}}{1+ka_{33}}\left(\frac{\partial^2 w}{\partial x^2}+\frac{\partial^2 w}{\partial y^2}\right)z \\
& + \left(\frac{f_{13}}{a_{33}}+\frac{f_{13}}{b_{33}\lambda^2}\right)\left(\frac{\partial^2 w}{\partial x^2}+\frac{\partial^2 w}{\partial y^2}\right)-\frac{d_{31}}{a_{33}}\left(\frac{\partial u^0}{\partial x}+\frac{\partial v^0}{\partial y}\right) \\
& - \frac{V}{a_{33}h}
\end{aligned}
\tag{5.3}
$$

Within the range of the thickness considered in this work, the varying terms in relation to the point position along the thickness direction are relatively negligible in comparison with the fixed terms. Thus, we can neglect those terms and assume that the electric polarization of the bending PNP distributes uniformly along the plate thickness. Therefore, the expression for the polarization is simplified as,

$$P_z = \left(\frac{f_{13}}{a_{33}} + \frac{f_{13}}{b_{33}\lambda^2}\right)\left(\frac{\partial^2 w}{\partial x^2} + \frac{\partial^2 w}{\partial y^2}\right) - \frac{d_{31}}{a_{33}}\left(\frac{\partial u^0}{\partial x} + \frac{\partial v^0}{\partial y}\right) - \frac{V}{a_{33}h} \qquad (5.4)$$

Figure 5-12 plots the in-plane distribution of the polarization for a plate ($b = 2.5a, a = 12h, h = 50nm$) under an applied mechanical load ($q = -0.01pN/nm^2$) and a negative applied voltage ($V = -0.002\ V$). Without the effect caused by the flexoelectricity, the polarization ($P_z = -\frac{V}{a_{33}h}$) remains constant throughout the plate as shown by the flat plane in this figure, which is purely intrigued by the applied electric voltage. However, since the strain gradient effect associated with the flexoelectricity is substantial and depends on the position (x, y) of the point, the in-plane distribution of the polarization is influenced significantly by the flexoelectricity as shown by the non-uniform profile. For example, the polarization drops near the side of the clamped edge, and it increases gradually when approaching the end of the free edge ($y = b$). Except for the points near the clamped edge, it can be seen from the figure that the polarization various little along the x direction for the points with the same y position, as the strain gradients along the x direction is smaller compared with that along the y direction.

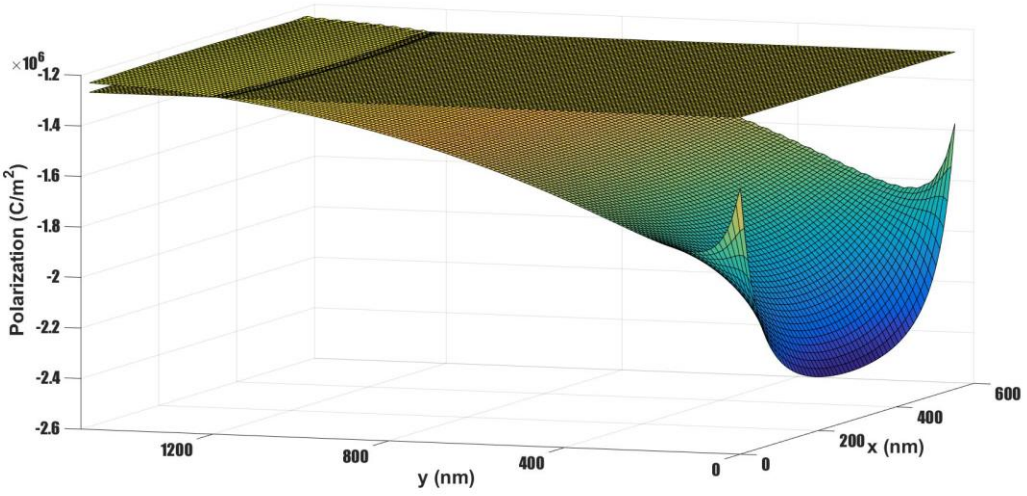

Figure 5-12 In-plane distribution of polarization under $V = -0.002V$

5.5.1 The effect of plate thickness and applied voltages on the polarization

In order to study the relationship between the flexoelectricity and the plate thickness, for a particular plate ($b = 2.5a, a = 12h$), Figure 5-13 plots the polarization against the plate thickness under different electrical loads for the middle point of the free edge ($x = 0.5a, y = b$). From Figure 5-13, positive polarization is induced for this point without any applied voltage or with a negative voltage i.e., $V = -0.01V$, while negative polarization is induced with a positive voltage, i.e., $V = 0.01V$. Meanwhile, the magnitude of polarization is larger than that of the conventional plate for all of the three cases. It can also be seen that the flexoelectricity has a greater impact on the polarization for the plate with smaller thicknesses, and such impact decays with the increase of the plate thickness and eventually the polarization results approach those of the conventional plate.

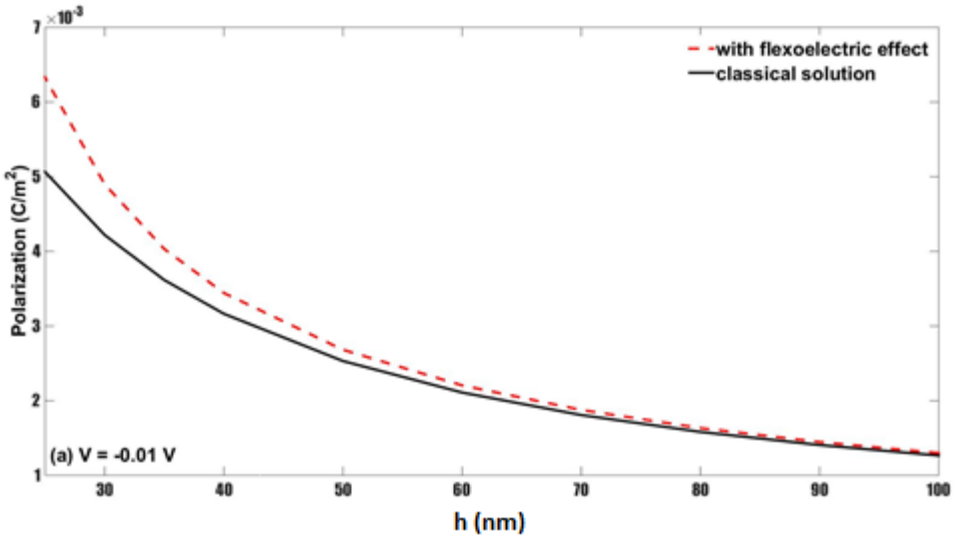
×10^-3
7
6
5
4
3
2
1
Polarization (C/m^2)
with flexoelectric effect
classical solution
(a) V = -0.01 V
30
40
50
60
70
80
90
100
h (nm)

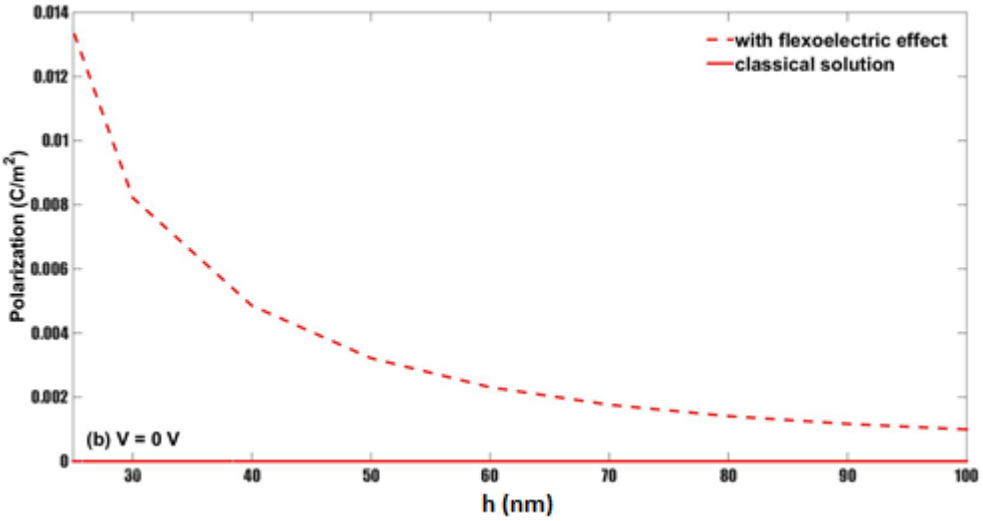
0.014
0.012
0.01
0.008
0.006
0.004
0.002
0
Polarization (C/m^2)
with flexoelectric effect
classical solution
(b) V = 0 V
30
40
50
60
70
80
90
100
h (nm)

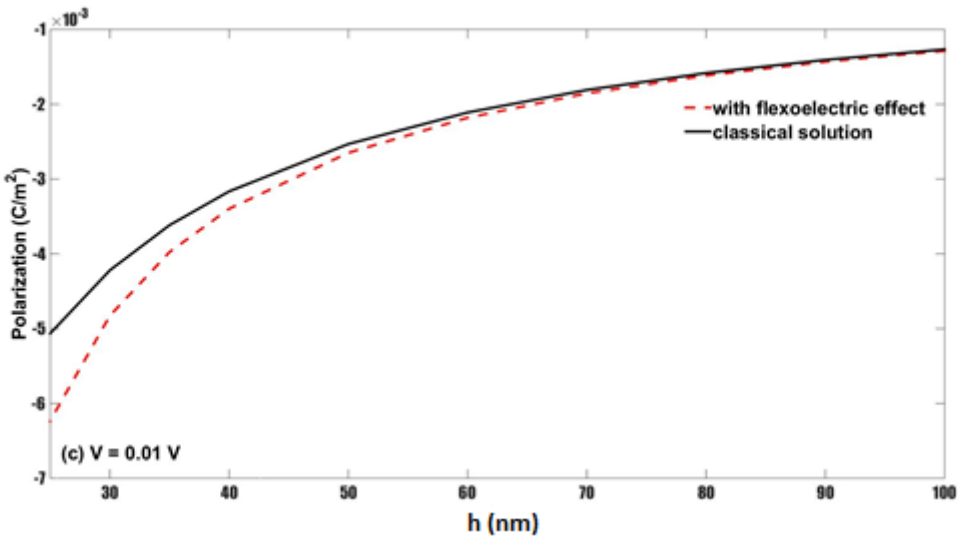

Figure 5-13 Variation of polarization with plate thickness under different voltage (a) $V = -0.01\ V$, (b) $V = 0\ V$ and (c) $V = 0.01\ V$

5.5.2 The effect of applied mechanical loads on the polarization

To study the relationship between the flexoelectricity and the applied loads, for PNPs with the same aspect ratios ($b = 2.5a, a = 12h$) under an electrical load $V = -0.002\ V$ and various mechanical loads, Figure 5-14 plots the polarization against the plate thickness h for the middle point of the free edge ($x = 0.5a, y = b$).

As revealed in Figure 5-14, the effect of the flexoelectricity is proportional to the magnitude of the applied loads. For example, for an arbitrary plate thickness, the effect of the flexoelectricity is boosted by increasing the magnitude of the applied mechanical load. As the plate thickness increases, although such reliance of the flexoelectric effect on the applied load still exists, the flexoelectric effect diminishes as indicated by the fact that all of the polarization lines approach the one without considering the flexoelectric effect. Thus, it is concluded that the plate thickness has a greater influence on the flexoelectric effect compared with the applied mechanical load.

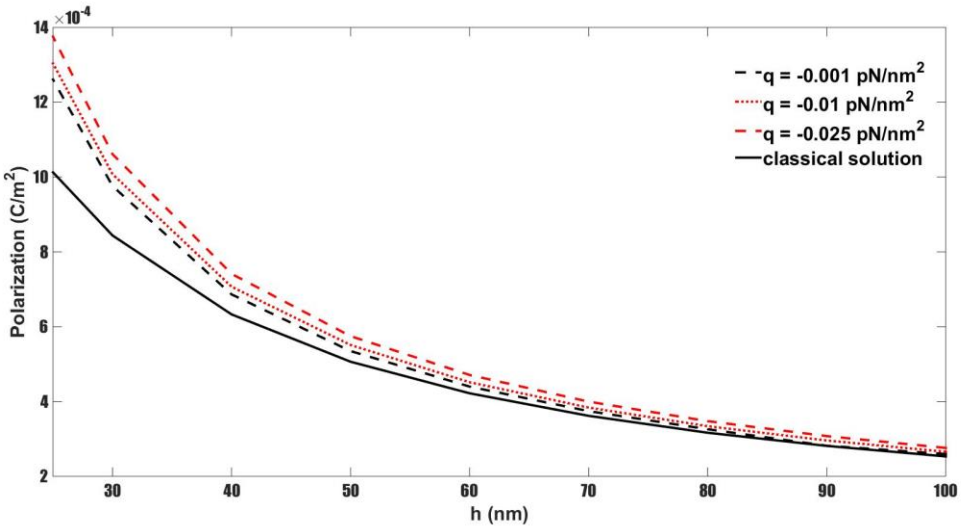

Figure 5-14 Variation of polarization under different applied loads

5.6 The flexoelectric effect on the electric potential of the cantilevered PNP

As shown by the electric potential equation Eq.(3.25), the electric potential is dependent on the strain gradients, applied voltages and so on. Therefore, in the following section, we will pay our attention to studying the relationship between the electric potential and some factors, such as the plate dimensions, applied voltages and so on.

5.6.1 The effect of plate thickness on the electric potential

In order to study the correlation between the plate thickness and the electric potential, two plates with different thickness ($h = 20nm$ and $h = 100nm$) are taken as the study cases, while they share the same aspect ratios ($b = 2.5a,\ a = 12h$). Figure 5-15 depicts the electric potential distribution along the thickness direction for points at the middle of the free edge ($x = 0.5, y = b$) when the distributed load $q = -0.01pN/nm^2$and the applied voltage $V = -0.01V$.

From the figures below, it implies that the electric potential relies more heavily on the flexoelectricity when the thickness is small, while such reliance reduces with the increase of the thickness. As shown in Figure 5-15 (a), when the thickness is small (for example, $h = 20nm$), the electric potential changes suddenly at points near the boundary layers,

while it decrease gradually at other points. As discussed in 5.4.1, this kind of discrepancy is a typical boundary behavior for a gradient theory as observed in the literature.

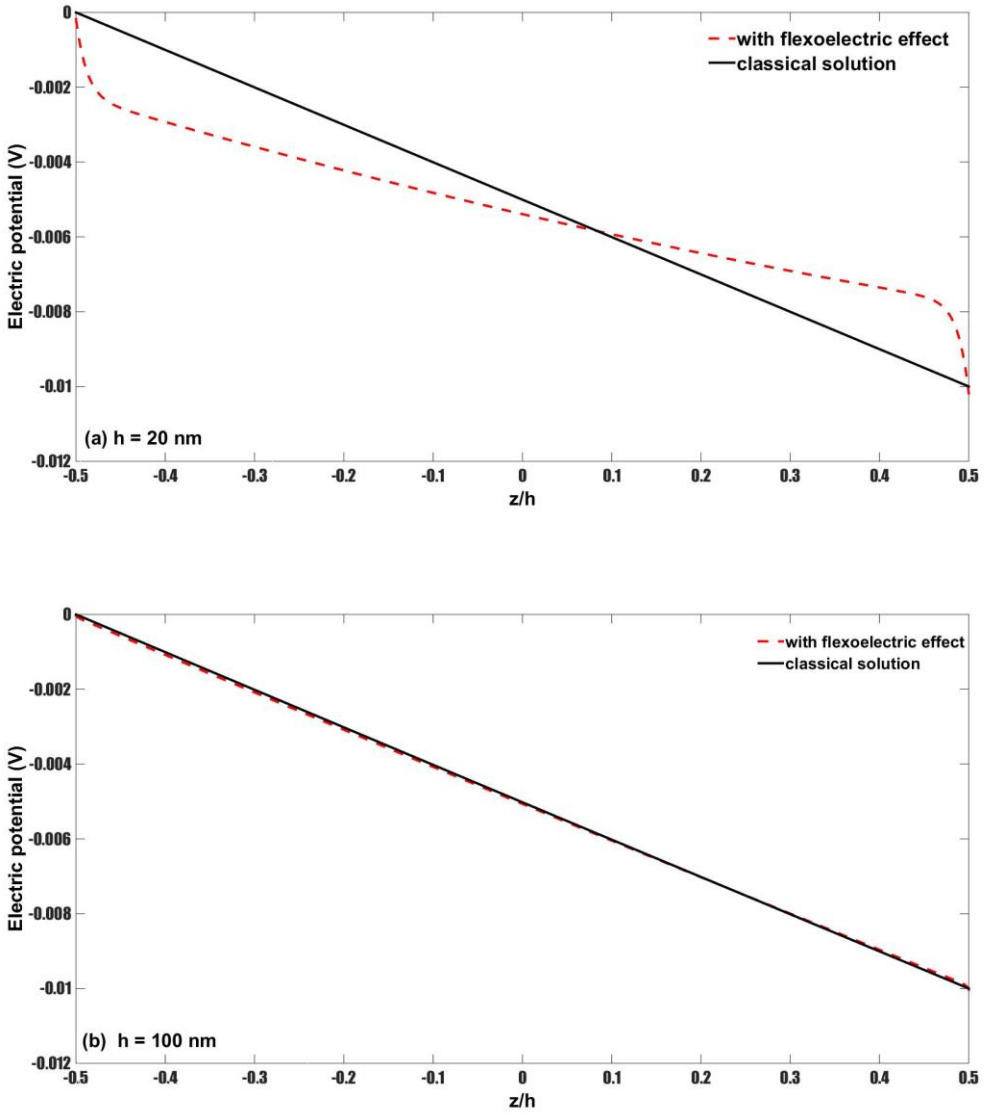

Figure 5-15 Electric potential with difference thickness (a) $h = 20nm$ and (b) $h = 100nm$

5.6.2 The effect of applied voltages on the electric potential

For a PNP with fixed properties ($b = 2.5a, a = 12h, h = 20nm$) under a distributed load $q = -0.01pN/nm^2$, Figure 5-16 shows the electric potential with different applied

voltages along the thickness direction for points at the middle of the free edge ($x = 0.5a, y = b$).

As shown in Figure 5-16, the flexoelectricity disturbs the electrical potential distribution and such an effect is influenced by the applied voltage. Even when the applied voltage is zero ($V = 0V$), the strain gradient induced flexoelectricity alters the distribution of the electric potential significantly. When the applied voltage is negative, such as $V = -0.01V$, the electric potential for the points near the bottom layer of the plate is smaller than that of the conventional plate, while for the points near the top layer, the electric potential surpasses that of the conventional plate. However, if the applied voltage is positive, an opposite trend is observed. Thus, we can concluded that the direction and magnitude of the applied electrical loads have a great influence on the distribution of the electric potential of the plate with the consideration of the flexoelectric effect.

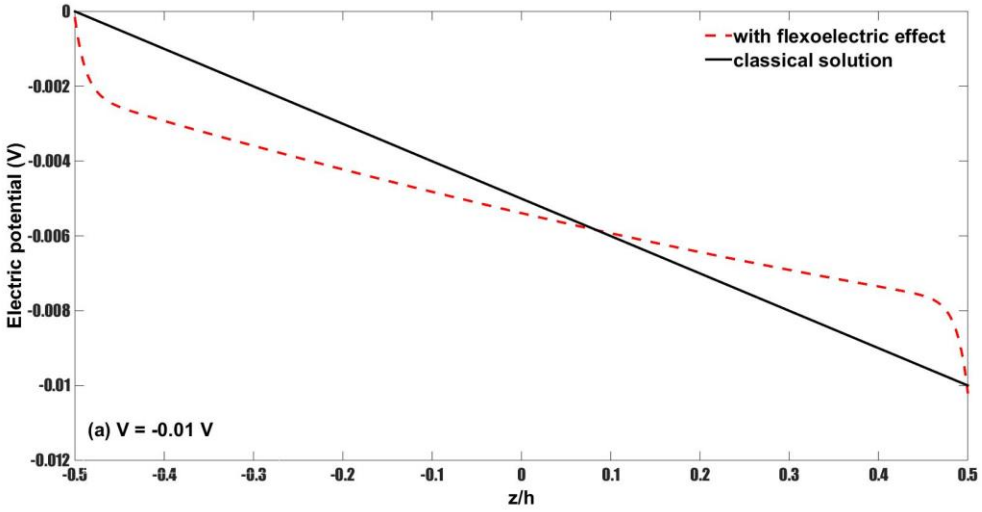

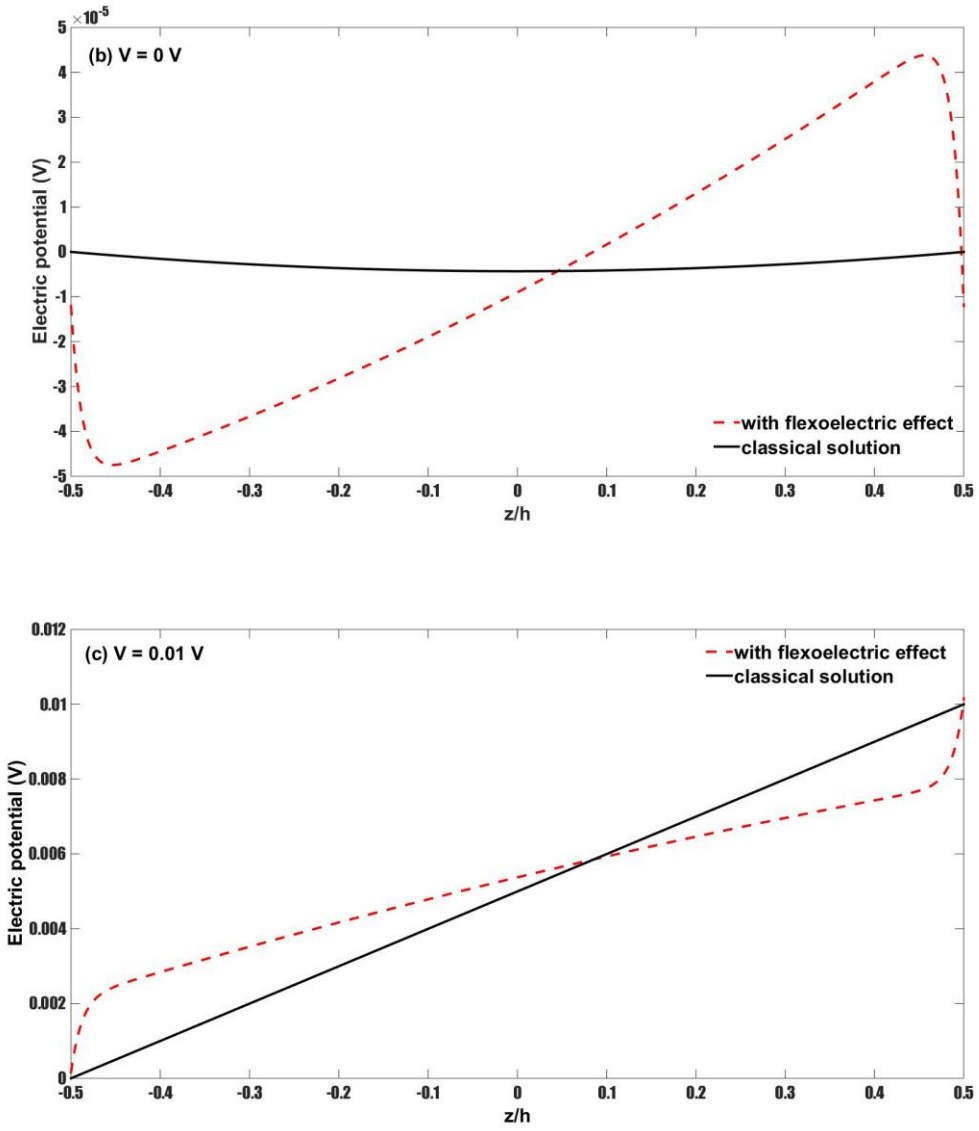

Figure 5-16 Electric potential with different applied voltages (a) $V = -0.01V$, (b) $V = 0V$ and (c) $V = 0.01\ V$

5.6.3 The effect of applied mechanical loads on the electric potential

To study how the applied mechanical load affects the electric potential, the electric potential of a plate ($b = 2.5a, a = 12h, h = 20\ nm$) under a constant electrical load ($V = -0.002V$) and various applied loads is depicted in Figure 5-17. It can be seen that the flexoelectric effect on the electric potential is more significant for applied loads with a larger magnitude, as the difference between the electric potential considering the

flexoelectric effect and that of a conventional plate keeps increasing with the increase of the magnitude of applied loads.

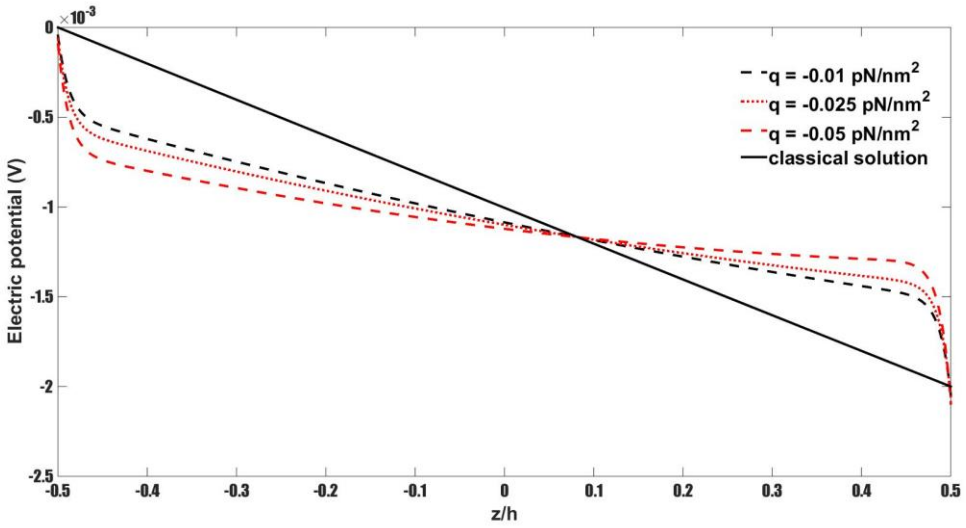

Figure 5-17 Electric potential with different applied loads

From the results, it can be inferred that the impact of the flexoelectricity on the bending behavior of the cantilevered PNP is influenced by both the geometric properties of the plate and the applied electromechanical loads, i.e., the plate thickness, the plate in-plane dimensions, the applied electrical load and the applied mechanical load.

Chapter 6

6 Conclusions and recommendations

6.1 Conclusions

There is a growing interest in developing piezoelectric nanostructures due to their distinct electromechanical coupling features, which have extensive applications in nanoelectromechanical systems (NEMS). Different from macroscale piezoelectric materials, nanoscale piezoelectric materials exhibit size-dependent mechanical and electrical properties. Thus, to make the best use of the piezoelectric nanomaterials, it is essential to have a better understanding of such size-dependent properties. In this thesis, based on the modified Kirchhoff plate continuum model, the size-dependent electromechanical behaviors of a cantilevered piezoelectric nanoplate have been investigated. The major findings and contributions are summarized as:

1) Developed a mathematical model for a cantilevered piezoelectric nanoplates (PNP) accounting for the flexoelectricity, from which the non-conventional governing equations and boundary conditions can be directly derived from the variational principle. This model can be used to quantitatively predict the size-dependent mechanical and electrical properties of the cantilevered PNP. It should be mentioned that such a methodology is universal, which could be applied for any kind of piezoelectric nanostructures.
2) Applied finite difference method (FDM) to obtain the approximate numerical solutions to the governing equations accompanied by the boundary conditions, resulting from the incorporation of the flexoelectric effect in the modified continuum mechanics model.
3) Carried out a comprehensive investigation of the flexoelectric effect on the size-dependent properties of the cantilevered PNP. From the numerical results calculated via FDM, it is found that the flexoelectricity has a significant influence on the electromechanical behaviors of the cantilevered PNP. Such effects are more evident with the decrease of the plate thickness, and it also depends on some other factors, such as the boundary constraints, the plate geometric ratio, and the applied mechanical and electrical loads.

6.2 Recommendations for future work

This thesis developed a mathematical model to study the size-dependent properties of a cantilevered PNP under different mechanical and electrical loading conditions. Although the model is able to predict how the flexoelectricity influences the electromechanical coupling behaviors of the plate, there are still some limitations for the current work that need to be addressed and some other aspects that need to be further explored:

1) The current work only investigated the flexoelectric effect upon the static bending behaviors of a cantilevered PNP. To fulfill the potential applications of the piezoelectric nanostructures for dynamics applications, the flexoelectric effect upon the dynamic performance of PNPs, such as the vibrational behaviors, needs further investigation. In this case, the dynamic bulk flexoelectricity should be considered in the formulation.
2) When using the extended linear piezoelectric theory to derive the governing equations and the boundary conditions of the PNP, some factors are ignored to simplify the mathematical formulation process, such as the higher-order couplings between the strain and strain gradients, the strain gradient and the strain gradient and the strain gradient and the polarization gradient. Nevertheless, those factors might have a significant impact on the size effects of nanoscale piezoelectric materials.
3) The present model only incorporated the flexoelectricity in the model. However, as discussed in the Introduction Section, surface effects such as surface piezoelectricity, surface elasticity and surface stress also contribute to the size-dependent properties of the nanoscale piezoelectric materials. Thus, to predict the size-dependent behaviors of PNP more accurately, it is of importance to develop a more comprehensive model with the combined effects.
4) The current study focused on a single-layer nanoplate. In fact, such nanoplates are often used as building blocks for complex structures, multi-layer nanocomposites for example. To meet the application demands, it is necessary to investigate the size effects of these complex nanostructures.

References

Agrawal, R. and Espinosa, H.D., 2011. Giant piezoelectric size effects in zinc oxide and gallium nitride nanowires. A first principles investigation. *Nano letters*, *11*(2), pp.786-790.

Agrawal, R., Peng, B., Gdoutos, E.E. and Espinosa, H.D., 2008. Elasticity size effects in ZnO nanowires− a combined experimental-computational approach. *Nano Letters*, *8*(11), pp.3668-3674.

Alivisatos, A.P., 1996. Semiconductor clusters, nanocrystals, and quantum dots. *Science*, *271*(5251), p.933.

Ang, W.T., Khosla, P.K. and Riviere, C.N., 2007. Feedforward controller with inverse rate-dependent model for piezoelectric actuators in trajectory-tracking applications. *IEEE/ASME transactions on mechatronics*, *12*(2), pp.134-142.

Arnau, A. ed., 2004. *Piezoelectric transducers and applications* (Vol. 2004). Heidelberg: Springer.

Asemi, S.R., Farajpour, A. and Mohammadi, M., 2014. Nonlinear vibration analysis of piezoelectric nanoelectromechanical resonators based on nonlocal elasticity theory. *Composite Structures*, *116*, pp.703-712.

Ashley, S., 2003. Artificial muscles. *Scientific American*, *289*(4), pp.52-59.

Askar, A., Lee, P.C.Y. and Cakmak, A.S., 1970. Lattice-dynamics approach to the theory of elastic dielectrics with polarization gradient. *Physical Review B*, *1*(8), p.3525.

Assadi, A., Farshi, B. and Alinia-Ziazi, A., 2010. Size dependent dynamic analysis of nanoplates. *Journal of Applied Physics*, *107*(12), p.124310.

Assadi, A. and Farshi, B., 2011. Size dependent vibration of curved nanobeams and rings including surface energies. *Physica E: Low-dimensional Systems and Nanostructures*, *43*(4), pp.975-978.

Assadi, A. and Farshi, B., 2011. Size dependent stability analysis of circular ultrathin films in elastic medium with consideration of surface energies.*Physica E: Low-dimensional Systems and Nanostructures*, *43*(5), pp.1111-1117.

Aydogdu, M., 2009. Axial vibration of the nanorods with the nonlocal continuum rod model. *Physica E: Low-dimensional Systems and Nanostructures*, *41*(5), pp.861-864.

Borisevich, A.Y., Eliseev, E.A., Morozovska, A.N., Cheng, C.J., Lin, J.Y., Chu, Y.H., Kan, D., Takeuchi, I., Nagarajan, V. and Kalinin, S.V., 2012. Atomic-scale evolution of modulated phases at the ferroelectric–antiferroelectric morphotropic phase boundary controlled by flexoelectric interaction. *Nature communications*, *3*, p.775.

Bühlmann, S., Dwir, B., Baborowski, J. and Muralt, P., 2002. Size effect in mesoscopic epitaxial ferroelectric structures: Increase of piezoelectric response with decreasing feature size. *Applied Physics Letters*, *80*(17), pp.3195-3197.

Buzea, C., Pacheco, I.I. and Robbie, K., 2007. Nanomaterials and nanoparticles: sources and toxicity. *Biointerphases*, *2*(4), pp.MR17-MR71.

Cammarata, R.C., 1997. Surface and interface stress effects on the growth of thin films. *Journal of Electronic Materials*, *26*(9), pp.966-968.

Catalan, G., Sinnamon, L.J. and Gregg, J.M., 2004. The effect of flexoelectricity on the dielectric properties of inhomogeneously strained ferroelectric thin films. *Journal of Physics: Condensed Matter*, *16*(13), p.2253.

Catalan, G., Noheda, B., McAneney, J., Sinnamon, L.J. and Gregg, J.M., 2005. Strain gradients in epitaxial ferroelectrics. *Physical Review B*, *72*(2), p.020102.

Catalan, G., Lubk, A., Vlooswijk, A.H.G., Snoeck, E., Magen, C., Janssens, A., Rispens, G., Rijnders, G., Blank, D.H.A. and Noheda, B., 2011. Flexoelectric rotation of polarization in ferroelectric thin films. *Nature materials*, *10*(12), pp.963-967.

Chang, C., Tran, V.H., Wang, J., Fuh, Y.K. and Lin, L., 2010. Direct-write piezoelectric polymeric nanogenerator with high energy conversion efficiency. *Nano letters*, *10*(2), pp.726-731.

Chen, C.Q., Shi, Y., Zhang, Y.S., Zhu, J. and Yan, Y.J., 2006. Size dependence of Young's modulus in ZnO nanowires. *Physical review letters*, *96*(7), p.075505.

Chee, C.Y., Tong, L. and Steven, G.P., 1998. A review on the modelling of piezoelectric sensors and actuators incorporated in intelligent structures. *Journal of Intelligent Material Systems and Structures*, *9*(1), pp.3-19.

Chen, H.T. and Soh, A.K., 2012. Influence of flexoelectric effects on multiferroic nanocomposite thin bilayer films. *Journal of Applied Physics*, *112*(7), p.074104.

Chen, Y.Y., Chen, C.L., Ou, M.N. and Lee, P.C., 2011. *Fabrication, characterization and thermal properties of nanowires*. INTECH Open Access Publisher.

Christman, J.A., Maiwa, H., Kim, S.H., Kingon, A.I. and Nemanich, R.J., 1998. Piezoelectric measurements with atomic force microscopy. In *MRS Proceedings* (Vol. 541, p. 617). Cambridge University Press.

Crawley, E.F. and De Luis, J., 1987. Use of piezoelectric actuators as elements of intelligent structures. *AIAA journal*, *25*(10), pp.1373-1385.

Croft, D., Shed, G. and Devasia, S., 2001. Creep, hysteresis, and vibration compensation for piezoactuators: atomic force microscopy application. *Journal of Dynamic Systems, Measurement, and Control*, *123*(1), pp.35-43.

Cross, L.E., 2006. Flexoelectric effects: Charge separation in insulating solids subjected to elastic strain gradients. *Journal of Materials Science*, *41*(1), pp.53-63.

Curie, J. and Curie, P., 1880. Development par compression de l'eletricite polaire dans les cristaux hemiedres a faces inclines. Comptes Rendus Acad. Sci. 91, 294-295.

Dai, L., Cheong, W.C.D., Sow, C.H., Lim, C.T. and Tan, V.B.C., 2009. Molecular dynamics simulation of ZnO nanowires: size effects, defects, and super ductility. *Langmuir*, *26*(2), pp.1165-1171.

Dahlstrom, D.K., Fife, M.E. and Judy, C.R., Allied Corporation, 1988.*Underwater transducer*. U.S. Patent 4,764,907.

Demishev, S.V., Pronin, A.A., Sluchanko, N.E., Samarin, N.A., Glushkov, V.V., Lyapin, A.G., Kondrin, M.V., Brazhkin, V.V., Varfolomeeva, T.D., Popova, S.V. and Ohta, H., 2002. A new nanocluster carbyne-based material synthesized under high pressure. *Physics of the Solid State*, *44*(4), pp.607-611.

Desai, A.V. and Haque, M.A., 2007. Mechanical properties of ZnO nanowires. *Sensors and Actuators A: Physical*, *134*(1), pp.169-176.

Dingreville, R., Qu, J. and Cherkaoui, M., 2005. Surface free energy and its effect on the elastic behavior of nano-sized particles, wires and films.*Journal of the Mechanics and Physics of Solids*, *53*(8), pp.1827-1854.

Dodds, J.S., Meyers, F.N. and Loh, K.J., 2012. Piezoelectric characterization of PVDF-TrFE thin films enhanced with ZnO nanoparticles. *IEEE Sensors Journal*, *12*(6), pp.1889-1890.

Dubois, M.A. and Muralt, P., 1999. Properties of aluminum nitride thin films for piezoelectric transducers and microwave filter applications. *Applied Physics Letters*, *74*(20), pp.3032-3034.

Eliseev, E.A., Morozovska, A.N., Glinchuk, M.D. and Blinc, R., 2009. Spontaneous flexoelectric/flexomagnetic effect in nanoferroics. *Physical Review B*, *79*(16), p.165433.

Eringen, A.C., 2002. *Nonlocal continuum field theories*. Springer Science & Business Media.

Fang, X.Q., Liu, J.X. and Gupta, V., 2013. Fundamental formulations and recent achievements in piezoelectric nano-structures: a review. *Nanoscale*,*5*(5), pp.1716-1726.

Flynn, A.M. and Sanders, S.R., 2002. Fundamental limits on energy transfer and circuit considerations for piezoelectric transformers. *IEEE transactions on power electronics*, *17*(1), pp.8-14.

Fousek, J., Cross, L.E. and Litvin, D.B., 1999. Possible piezoelectric composites based on the flexoelectric effect. *Materials Letters*, *39*(5), pp.287-291.

Fo-van, C., 1980. Bending of uniformly cantilever rectangular plates. *Applied Mathematics and Mechanics*, *1*(3), pp.371-383.

Gao, Y. and Wang, Z.L., 2007. Electrostatic potential in a bent piezoelectric nanowire. The fundamental theory of nanogenerator and nanopiezotronics. *Nano letters*, *7*(8), pp.2499-2505.

Gautschi, D.I.E.G., 2002. Piezoelectric sensors. In *Piezoelectric Sensorics* (pp. 73-91). Springer Berlin Heidelberg.

Gharbi, M., Sun, Z.H., Sharma, P., White, K. and El-Borgi, S., 2011. Flexoelectric properties of ferroelectrics and the nanoindentation size-effect. *International Journal of Solids and Structures*, *48*(2), pp.249-256.

Giannakopoulos, A.E. and Suresh, S., 1999. Theory of indentation of piezoelectric materials. *Acta materialia*, *47*(7), pp.2153-2164.

Green, M.J., 2010. Analysis and measurement of carbon nanotube dispersions: nanodispersion versus macrodispersion. *Polymer International*, *59*(10), pp.1319-1322.

Gurtin, M.E. and Murdoch, A.I., 1975. A continuum theory of elastic material surfaces. *Archive for Rational Mechanics and Analysis*, *57*(4), pp.291-323.

Hankel, W.G, 1881. Uber die aktinound piezoelektrischen eigen schaften des bergkrystalles und ihre beziehung zi den thermoelektrischen. Abh Sachs 12:457.

He, J. and Lilley, C.M., 2008. Surface stress effect on bending resonance of nanowires with different boundary conditions. *Applied physics letters*, *93*(26), p.263108.

He, L.H., Lim, C.W. and Wu, B.S., 2004. A continuum model for size-dependent deformation of elastic films of nano-scale thickness. *International Journal of Solids and Structures*, *41*(3), pp.847-857.

Hlinka, J. and Marton, P., 2006. Phenomenological model of a 90° domain wall in Ba Ti O 3-type ferroelectrics. *Physical Review B*, *74*(10), p.104104.

Hong, J., Catalan, G., Scott, J.F. and Artacho, E., 2010. The flexoelectricity of barium and strontium titanates from first principles. *Journal of Physics: Condensed Matter*, *22*(11), p.112201.

Hong, J. and Vanderbilt, D., 2013. First-principles theory and calculation of flexoelectricity. *Physical Review B*, *88*(17), p.174107.

Horsley, E.L., Foster, M.P. and Stone, D.A., 2007, September. State-of-the-art piezoelectric transformer technology. In *Power Electronics and Applications, 2007 European Conference on* (pp. 1-10). IEEE.

Hu, S. and Shen, S., 2010. Variational principles and governing equations in nano-dielectrics with the flexoelectric effect. *Science China Physics, Mechanics and Astronomy*, *53*(8), pp.1497-1504.

Huang, G.Y. and Yu, S.W., 2006. Effect of surface piezoelectricity on the electromechanical behaviour of a piezoelectric ring. *physica status solidi (b)*,*243*(4), pp.R22-R24.

Ivensky, G., Zafrany, I. and Ben-Yaakov, S., 2002. Generic operational characteristics of piezoelectric transformers. *IEEE Transactions on Power Electronics*, *17*(6), pp.1049-1057.

Jordan, T.L. and Ounaies, Z., 2001. Piezoelectric ceramics characterization (No. ICASE-2001-28). *Institute for Computer Applications in Science and Engineering Hampton Va.*

Kityk, A.V., Schranz, W., Sondergeld, P., Havlik, D., Salje, E.K.H. and Scott, J.F., 2000. Nonlinear elastic behaviour of SrTiO3 crystals in the quantum paraelectric regime. *EPL (Europhysics Letters)*, *50*(1), p.41.

Kogan, S.M., 1964. Piezoelectric effect during inhomogeneous deformation and acoustic scattering of carriers in crystals. *Soviet Physics-Solid State*,*5*(10), pp.2069-2070.

Komanduri, R., Chandrasekaran, N. and Raff, L.M., 2003. Molecular dynamic simulations of uniaxial tension at nanoscale of semiconductor materials for micro-electro-mechanical systems (MEMS) applications. *Materials Science and Engineering: A*, *340*(1), pp.58-67.

Krimholtz, R., Leedom, D.A. and Matthaei, G.L., 1970a. New equivalent circuits for elementary piezoelectric transducers. *Electronics Letters*, *13*(6), pp.398-399.

Krimholtz, R., Leedom, D.A. and Matthaei, G.L., 1970b. Erratum: New equivalent circuits for elementary piezoelectric transducers. *Electronics Letters*, *6*(17), p.560.

Kulkarni, A.J., Zhou, M. and Ke, F.J., 2005. Orientation and size dependence of the elastic properties of zinc oxide nanobelts. *Nanotechnology*, *16*(12), p.2749.

Kvasov, A. and Tagantsev, A.K., 2015. Dynamic flexoelectric effect in perovskites from first-principles calculations. *Physical Review B*, *92*(5), p.054104.

Landi, B.J., Castro, S.L., Ruf, H.J., Evans, C.M., Bailey, S.G. and Raffaelle, R.P., 2005. CdSe quantum dot-single wall carbon nanotube complexes for polymeric solar cells. *Solar Energy Materials and Solar Cells*, *87*(1), pp.733-746.

Lao, C.S., Kuang, Q., Wang, Z.L., Park, M.C. and Deng, Y., 2007. Polymer functionalized piezoelectric-FET as humidity/chemical nanosensors. *Applied physics letters*, *90*(26), p.262107.

Le Quang, H. and He, Q.C., 2011, March. The number and types of all possible rotational symmetries for flexoelectric tensors. In *Proceedings of the Royal Society of London A: Mathematical, Physical and Engineering Sciences* (p. rspa20100521). The Royal Society.

Leach, W.M., 1994. Controlled-source analogous circuits and SPICE models for piezoelectric transducers. *IEEE Transactions on ultrasonics, ferroelectrics, and frequency control*, *41*(1), pp.60-66.

Lee, D., Yang, S.M., Yoon, J.G. and Noh, T.W., 2012. Flexoelectric rectification of charge transport in strain-graded dielectrics. *Nano letters*, *12*(12), pp.6436-6440.

Lee, D., Yoon, A., Jang, S.Y., Yoon, J.G., Chung, J.S., Kim, M., Scott, J.F. and Noh, T.W., 2011. Giant flexoelectric effect in ferroelectric epitaxial thin films. *Physical Review Letters*, *107*(5), p.057602.

Li, X., Wang, X., Zhang, L., Lee, S. and Dai, H., 2008. Chemically derived, ultrasmooth graphene nanoribbon semiconductors. *Science*, *319*(5867), pp.1229-1232.

Li, Y., Fang, B., Zhang, J. and Song, J., 2011. Surface effects on the wrinkling of piezoelectric films on compliant substrates. *Journal of Applied Physics*, *110*(11), p.114303.

Liang, W. and Zhou, M., 2003. Size and strain rate effects in tensile deformation of Cu nanowires. *Nanotechnology*, *2*, pp.452-455.

Liang, X., Yang, W., Hu, S. and Shen, S., 2016. Buckling and vibration of flexoelectric nanofilms subjected to mechanical loads. *Journal of Physics D: Applied Physics*, *49*(11), p.115307.

Lin, X.S. and Yuan, W.B., 1985. Solution of bending of cantilever rectangular plates under uniform surface-load by the method of two-direction trigonometric series. *Applied Mathematics and Mechanics*, *6*(8), pp.789-799.

Lippmann, G. 1881. "Principe de la conservation de l'électricité" [Principle of the conservation of electricity]. Annales de chimie et de physique *(in French)* 24: 145.

Liu, C., Hu, S. and Shen, S., 2012. Effect of flexoelectricity on electrostatic potential in a bent piezoelectric nanowire. *Smart Materials and Structures*, *21*(11), p.115024.

Lü, C.F., Chen, W.Q. and Lim, C.W., 2009. Elastic mechanical behavior of nano-scaled FGM films incorporating surface energies. *Composites Science and Technology*, *69*(7), pp.1124-1130.

Lu, H., Bark, C.W., De Los Ojos, D.E., Alcala, J., Eom, C.B., Catalan, G. and Gruverman, A., 2012. Mechanical writing of ferroelectric polarization. *Science*, *336*(6077), pp.59-61.

Ma, W. and Cross, L.E., 2002. Flexoelectric polarization of barium strontium titanate in the paraelectric state. *Applied Physics Letters*, *81*, pp.3440-3442.

Ma, W. and Cross, L.E., 2005. Flexoelectric effect in ceramic lead zirconate titanate. *Applied Physics Letters*, *86*(7), p.072905.

Ma, W. and Cross, L.E., 2006. Flexoelectricity of barium titanate. *Applied Physics Letters*, *88*(23), p.2902.

Majdoub, M.S., Sharma, P. and Çağin, T., 2008a. Dramatic enhancement in energy harvesting for a narrow range of dimensions in piezoelectric nanostructures. *Physical Review B*, *78*(12), p.121407.

Majdoub, M.S., Sharma, P. and Cagin, T., 2008b. Enhanced size-dependent piezoelectricity and elasticity in nanostructures due to the flexoelectric effect. *Physical Review B*, *77*(12), p.125424.

Majdoub, M.S., Maranganti, R. and Sharma, P., 2009. Understanding the origins of the intrinsic dead layer effect in nanocapacitors. *Physical Review B*, *79*(11), p.115412.

Maranganti, R., Sharma, N.D. and Sharma, P., 2006. Electromechanical coupling in nonpiezoelectric materials due to nanoscale nonlocal size effects: Green's function solutions and embedded inclusions. *Physical Review B*, *74*(1), p.014110.

Maranganti, R. and Sharma, P., 2009. Atomistic determination of flexoelectric properties of crystalline dielectrics. *Physical Review B*, *80*(5), p.054109.

Mashkevich, V.S. and Tolpygo, K.B., 1957. Electrical, optical and elastic properties of diamond type crystals. 1. *Soviet Physics* JETP-USSR, *5*(3), pp.435-439.

Miller, R.E. and Shenoy, V.B., 2000. Size-dependent elastic properties of nanosized structural elements. *Nanotechnology*, *11*(3), p.139.

Minary-Jolandan, M., Bernal, R.A., Kuljanishvili, I., Parpoil, V. and Espinosa, H.D., 2012. Individual GaN nanowires exhibit strong piezoelectricity in 3D.*Nano letters*, *12*(2), pp.970-976.

Mindlin, R.D., 1968. Polarization gradient in elastic dielectrics. *International Journal of Solids and Structures*, *4*(6), pp.637-642.

Mindlin, R.D., 1969. Continuum and lattice theories of influence of electromechanical coupling on capacitance of thin dielectric films.*International Journal of Solids and Structures*, *5*(11), pp.1197-1208.

Momeni, K., Odegard, G.M. and Yassar, R.S., 2012. Finite size effect on the piezoelectric properties of ZnO nanobelts: a molecular dynamics approach. *Acta materialia*, *60*(13), pp.5117-5124.

Morgan Matroc, Inc., http://www.morgantechnicalceramics.com/, Guide to Piezoelectric and Dielectric Ceramic, Chapter 2.

Mishra, S. and Sethy, B. K., 2013. *Nano-Indentation of Copper–Nickel thin films-A Molecular Dynamics Simulation Study* (Doctoral dissertation, National Institute of Technology Rourkela).

Murmu, T. and Pradhan, S.C., 2009. Vibration analysis of nano-single-layered graphene sheets embedded in elastic medium based on nonlocal elasticity theory. *Journal of Applied Physics*, *105*(6), p.064319.

Ottman, G.K., Hofmann, H.F., Bhatt, A.C. and Lesieutre, G.A., 2002. Adaptive piezoelectric energy harvesting circuit for wireless remote power supply. *IEEE Transactions on power electronics*, *17*(5), pp.669-676.

Park, K.I., Xu, S., Liu, Y., Hwang, G.T., Kang, S.J.L., Wang, Z.L. and Lee, K.J., 2010. Piezoelectric BaTiO3 thin film nanogenerator on plastic substrates. *Nano letters*, *10*(12), pp.4939-4943.

Ponomareva, I., Tagantsev, A.K. and Bellaiche, L., 2012. Finite-temperature flexoelectricity in ferroelectric thin films from first principles. *Physical Review B*, *85*(10), p.104101.

Qi, Y., Jafferis, N.T., Lyons Jr, K., Lee, C.M., Ahmad, H. and McAlpine, M.C., 2010. Piezoelectric ribbons printed onto rubber for flexible energy conversion. *Nano letters*, *10*(2), pp.524-528.

Rakotondrabe, M., 2011. Bouc-Wen modeling and inverse multiplicative structure to compensate hysteresis nonlinearity in piezoelectric actuators. *IEEE Transactions on Automation Science and Engineering*, *8*(2), pp.428-431.

Reddy, J.N., 2006. *Theory and analysis of elastic plates and shells*. CRC press.

Ritter, T.A., Shrout, T.R., Tutwiler, R. and Shung, K.K., 2002. A 30-MHz piezo-composite ultrasound array for medical imaging applications. *IEEE transactions on ultrasonics, ferroelectrics, and frequency control*, *49*(2), pp.217-230.

Shah, A.A., 2011. A FEM-BEM interactive coupling for modeling the piezoelectric health monitoring systems. *Latin American Journal of Solids and Structures*, *8*(3), pp.305-334.

Sharma, N.D., Maranganti, R. and Sharma, P., 2007. On the possibility of piezoelectric nanocomposites without using piezoelectric materials. *Journal of the Mechanics and Physics of Solids*, *55*(11), pp.2328-2350.

Sharma, N.D., Landis, C.M. and Sharma, P., 2010. Piezoelectric thin-film superlattices without using piezoelectric materials. *Journal of Applied Physics*, *108*(2), p.024304.

Shen, S. and Hu, S., 2010. A theory of flexoelectricity with surface effect for elastic dielectrics. *Journal of the Mechanics and Physics of Solids*, *58*(5), pp.665-677.

Shenoy, V.B., 2002. Size-dependent rigidities of nanosized torsional elements. *International Journal of Solids and Structures*, *39*(15), pp.4039-4052.

Shimpi, R.P. and Sivakumar S., 1994. On the suitability of finite difference methods to plate bending problems involving corner singularities - a study. *Computational Structural Mechanics*, pp. 46-62.

Shu, L., Wei, X., Pang, T., Yao, X. and Wang, C., 2011. Symmetry of flexoelectric coefficients in crystalline medium. *Journal of Applied Physics*, *110*(10), p.104106.

Shu, Y.C., Lien, I.C. and Wu, W.J., 2007. An improved analysis of the SSHI interface in piezoelectric energy harvesting. *Smart Materials and Structures*, *16*(6), p.2253.

Shung, K.K., Cannata, J.M. and Zhou, Q.F., 2007. Piezoelectric materials for high frequency medical imaging applications: A review. *Journal of Electroceramics*, *19*(1), pp.141-147.

Sirohi, J. and Chopra, I., 2000. Fundamental understanding of piezoelectric strain sensors. *Journal of Intelligent Material Systems and Structures*, *11*(4), pp.246-257.

Smith, G.D., 1985. *Numerical solution of partial differential equations: finite difference methods*. Oxford university press.

Sodano, H.A., Park, G. and Inman, D.J., 2004. Estimation of electric charge output for piezoelectric energy harvesting. *Strain*, *40*(2), pp.49-58.

Stan, G., Ciobanu, C.V., Parthangal, P.M. and Cook, R.F., 2007. Diameter-dependent radial and tangential elastic moduli of ZnO nanowires. *Nano Letters*, *7*(12), pp.3691-3697.

Streitz, F.H., Cammarata, R.C. and Sieradzki, K., 1994. Surface-stress effects on elastic properties. I. Thin metal films. *Physical Review B*, *49*(15), p.10699.

Tagantsev, A.K., 1985. A theory of the flexoelectric effect in crystals.*Zhurnal Eksperimentalnoi i Teoreticheskoi Fiziki*, *88*, pp.2108-2122.

Tagantsev, A.K., 1986. Piezoelectricity and flexoelectricity in crystalline dielectrics. *Physical Review B*, *34*(8), p.5883.

Tagantsev, A.K. and Gerra, G., 2006. Interface-induced phenomena in polarization response of ferroelectric thin films. *Journal of applied physics*, *100*(5), p.051607.

Tagantsev, A.K. and Yurkov, A.S., 2012. Flexoelectric effect in finite samples. *Journal of Applied Physics*, *112*(4), p.044103.

Ting, R.Y., 1992. A review on the development of piezoelectric composites for underwater acoustic transducer applications. *IEEE transactions on instrumentation and measurement*, *41*(1), pp.64-67.

Timoshenko, S.P. and Woinowsky-Krieger, S., 1959. *Theory of plates and shells*. McGraw-Hill.

Toupin, R., 1956. The elastic dielectric. *Journal of Rational Mechanics and Analysis*, *5*(6), pp.849-915.

Tressler, J.F., 2008. Piezoelectric transducer designs for sonar applications. In *Piezoelectric and Acoustic Materials for Transducer Applications* (pp. 217-239). Springer US.

Walters, D.A., Cleveland, J.P., Thomson, N.H., Hansma, P.K., Wendman, M.A., Gurley, G. and Elings, V., 1996. Short cantilevers for atomic force microscopy. *Review of Scientific Instruments*, *67*(10), pp.3583-3590.

Wang, C.M. and Duan, W.H., 2008. Free vibration of nanorings/arches based on nonlocal elasticity. *Journal of Applied Physics*, *104*(1), p.014303.

Wang, G.F. and Feng, X.Q., 2009. Timoshenko beam model for buckling and vibration of nanowires with surface effects. *Journal of physics D: applied physics*, *42*(15), p.155411.

Wang, G.F. and Feng, X.Q., 2010. Effect of surface stresses on the vibration and buckling of piezoelectric nanowires. *EPL (Europhysics Letters)*, *91*(5), p.56007.

Wang, J.S., Feng, X.Q., Wang, G.F. and Yu, S.W., 2008. Twisting of nanowires induced by anisotropic surface stresses. *Applied Physics Letters*, *92*(19), p.191901.

Wang, Z., Hu, J., Suryavanshi, A.P., Yum, K. and Yu, M.F., 2007. Voltage generation from individual BaTiO3 nanowires under periodic tensile mechanical load. *Nano letters*, *7*(10), pp.2966-2969.

Wang, Z. and Zhao, Y., 2009. Self-instability and bending behaviors of nano plates. *Acta Mechanica Solida Sinica*, *22*(6), pp.630-643.

Wang, Z.L. and Song, J., 2006. Piezoelectric nanogenerators based on zinc oxide nanowire arrays. *Science*, *312*(5771), pp.242-246.

Wen, B., Sader, J.E. and Boland, J.J., 2008. Mechanical properties of ZnO nanowires. *Physical review letters*, *101*(17), p.175502.

Xu, T., Wang, J., Shimada, T. and Kitamura, T., 2013. Direct approach for flexoelectricity from first-principles calculations: cases for SrTiO3 and BaTiO3. *Journal of Physics: Condensed Matter*, *25*(41), p.415901.

Yan, Z., 2013. Continuum Modeling on Size-dependent Properties of Piezoelectric Nanostructures.

Yan, Z. and Jiang, L.Y., 2011a. The vibrational and buckling behaviors of piezoelectric nanobeams with surface effects. *Nanotechnology*, *22*(24), p.245703.

Yan, Z. and Jiang, L.Y, 2011b. Surface effects on the electromechanical coupling and bending behaviours of piezoelectric nanowires. *Journal of Physics D: Applied Physics*, *44*(7), p.075404.

Yan, Z. and Jiang, L.Y, 2011c. Electromechanical response of a curved piezoelectric nanobeam with the consideration of surface effects. *Journal of Physics D: Applied Physics*, *44*(36), p.365301.

Yan, Z. and Jiang, L.Y, 2012a. Surface effects on the electroelastic responses of a thin piezoelectric plate with nanoscale thickness. *Journal of Physics D: Applied Physics*, *45*(25), p.255401.

Yan, Z. and Jiang, L.Y., 2012b. Vibration and buckling analysis of a piezoelectric nanoplate considering surface effects and in-plane constraints. In *Proc. R. Soc. A* (p. rspa20120214). The Royal Society.

Yan, Z. and Jiang, L.Y., 2012c. Surface effects on the vibration and buckling of piezoelectric nanoplates. *EPL (Europhysics Letters)*, *99*(2), p.27007.

Yan, Z. and Jiang, L.Y., 2013. Flexoelectric effect on the electroelastic responses of bending piezoelectric nanobeams. *Journal of Applied Physics*, *113*(19), p.194102.

Yang, X.M., Hu, Y.T. and Yang, J.S., 2004. Electric field gradient effects in anti-plane problems of polarized ceramics. *International journal of solids and structures*, *41*(24), pp.6801-6811.

Yang, Y., Qi, J., Liao, Q., Li, H., Wang, Y., Tang, L. and Zhang, Y., 2009. High-performance piezoelectric gate diode of a single polar-surface dominated ZnO nanobelt. *Nanotechnology*, *20*(12), p.125201.

Yin, B. and Qu, S., 2014. An ab initio investigation of flexoelectric effect in ultrathin BaTiO3 nanotubes. *Journal of Applied Physics*, *115*(7), p.074102.

Yudin, P.V. and Tagantsev, A.K., 2013. Fundamentals of flexoelectricity in solids. *Nanotechnology*, *24*(43), p.432001.

Yudin, P.V., Tagantsev, A.K., Eliseev, E.A., Morozovska, A.N. and Setter, N., 2012. Bichiral structure of ferroelectric domain walls driven by flexoelectricity. *Physical Review B*, *86*(13), p.134102.

Zhang, C., Chen, W. and Zhang, C., 2013. Two-dimensional theory of piezoelectric plates considering surface effect. *European Journal of Mechanics-A/Solids*, *41*, pp.50-57.

Zhang, C., Zhu, J., Chen, W. and Zhang, C., 2014. Two-dimensional theory of piezoelectric shells considering surface effect. *European Journal of Mechanics-A/Solids*, *43*, pp.109-117.

Zhang, J. and Wang, C., 2012. Vibrating piezoelectric nanofilms as sandwich nanoplates. *Journal of Applied Physics*, *111*(9), p.094303.

Zhang, J., Wang, C. and Adhikari, S., 2012. Surface effect on the buckling of piezoelectric nanofilms. *Journal of Physics D: Applied Physics*, *45*(28), p.285301.

Zhang, Y., Hong, J., Liu, B. and Fang, D., 2009. Strain effect on ferroelectric behaviors of BaTiO3 nanowires: a molecular dynamics study. *Nanotechnology*, *21*(1), p.015701.

Zhang, Y., Liu, B. and Fang, D., 2011. Stress-induced phase transition and deformation behavior of BaTiO3 nanowires. *Journal of Applied Physics*, *110*(5), p.054109.

Zhang, Z. and Jiang, L.Y, 2014. Size effects on electromechanical coupling fields of a bending piezoelectric nanoplate due to surface effects and flexoelectricity. *Journal of Applied Physics*, *116*(13), p.134308.

Zhang, Z., Yan, Z. and Jiang, L.Y, 2014. Flexoelectric effect on the electroelastic responses and vibrational behaviors of a piezoelectric nanoplate. *Journal of Applied Physics*, *116*(1), p.014307.

Zhao, M., Qian, C., Lee, S.W.R., Tong, P., Suemasu, H. and Zhang, T.Y., 2007. Electro-elastic analysis of piezoelectric laminated plates. *Advanced Composite Materials*, *16*(1), pp.63-81.

Zhao, M.H., Wang, Z.L. and Mao, S.X., 2004. Piezoelectric characterization of individual zinc oxide nanobelt probed by piezoresponse force microscope. *Nano Letters*, *4*(4), pp.587-590.

Zhigilei, L.V., Volkov, A.N. and Dongare, A.M., 2012. Computational study of nanomaterials: From large-scale atomistic simulations to mesoscopic modeling. In *Encyclopedia of Nanotechnology* (pp. 470-480). Springer Netherlands.

Zhou, H., Hong, J., Zhang, Y., Li, F., Pei, Y. and Fang, D., 2012a. External uniform electric field removing the flexoelectric effect in epitaxial ferroelectric thin films. *EPL (Europhysics Letters)*, *99*(4), p.47003.

Zhou, H., Hong, J., Zhang, Y., Li, F., Pei, Y. and Fang, D., 2012b. Flexoelectricity induced increase of critical thickness in epitaxial ferroelectric thin films. *Physica B: Condensed Matter*, *407*(17), pp.3377-3381.

Zhu, R., Wang, D., Xiang, S., Zhou, Z. and Ye, X., 2008. Piezoelectric characterization of a single zinc oxide nanowire using a nanoelectromechanical oscillator. *Nanotechnology*, *19*(28), p.285712.

Zhu, W., Fu, J.Y., Li, N. and Cross, L., 2006. Piezoelectric composite based on the enhanced flexoelectric effects. *Applied physics letters*, *89*(19), p.2904.

Zong, X., Kim, K., Fang, D., Ran, S., Hsiao, B.S. and Chu, B., 2002. Structure and process relationship of electrospun bioabsorbable nanofiber membranes. *Polymer*, *43*(16), pp.4403-4412.

Zubko, P., Catalan, G., Buckley, A., Welche, P.R.L. and Scott, J.F., 2007. Strain-gradient-induced polarization in SrTiO 3 single crystals. *Physical Review Letters*, *99*(16), p.167601.

Zubko, P., Catalan, G., Buckley, A., Welche, P.R.L. and Scott, J.F., 2008. Erratum: Strain-Gradient-Induced Polarization in SrTiO 3 Single Crystals [Phys. Rev. Lett. 99, 167601 (2007)]. *Physical Review Letters*, *100*(19), p.199906.

Zubko, P., Catalan, G. and Tagantsev, A.K., 2013. Flexoelectric effect in solids. *Annual Review of Materials Research*, *43*, pp.387-421.

Appendices

Appendix A: MATLAB routine for predicting the static deflection of a cantilevered PNP

```
clc;
clear all;
format long;
% Program is built for calculation of the flexoelectric effect on the
% vibrational behaviors of a cantilevered piezoelectric nanoplate
% Xining Wang

% Matrix of displacement (N+1,M+1)
%*****************************************%
% System parameters                       %
%*****************************************%
% Material properties
C11=167.55*10^9; % Pa - elastic constant
C12=78.15*10^9;  % Pa - elastic constant
C66=44.7*10^9;   % Pa - elastic constant
a33=0.79*10^8;   % V.m/C - reciprocal dielectric susceptibility
d31=3.5*10^8;    % V/m - piezoelectric constant tensor
b33=10^(-9);     % Jm^3/C^2 - tensor used for the interaction of
polarization
% polarization gradient
q=-0.1*10^5;       % pN/nm^2 - pressure
V=0;           % V - voltage
% Gradient and polarization gradient
f13=0;          % V - tensor used for the interaction of the strain
gradient

% Plate physical properties
th=50*10^-9;    % m - plate thickness
wp=20*th;        % m - plate width
lp=wp;        % m - plate length
M=81; % Number of nodal elements on x
N=81; % Number of nodal elements on y

k0=8.85*10^-12;  % C.V^-1.m^-1 - permittivity of the vacuum of the air
kb=6.62;         % C.V^-1.m^-1 - background permittivity of BaTiO3
k1=k0*kb;        % C.V^-1.m^-1
lamda=sqrt((1+k1*a33)/(k1*b33));
%*****************************************%
% Analysis*********************************%
%*****************************************%
% Mesh the plate and initialize some variables
h=wp/(M-1);          % Step size in x
k=lp/(N1);          % Step size in y

% Coefficients of the equation
D111=-(f13^2*th^2)/(4*b33*lamda)*(exp(lamda*th/2)+exp(-
lamda*th/2))/(exp(lamda*th/2)-exp(-lamda*th/2));
D112=-k1*d31^2*th^3/(24*(1+k1*a33));
```

```
D113=b33*th*k1^2*d31^2/(2*(1+k1*a33)^2);
D114=-f13^2*th/(2*a33*(1+k1*a33));
D11=D111+D112+D113+D114;

D12=2*f13*d31/(b33*lamda^3)+th*d31*f13/a33-k1*d31*f13*th/(1+k1*a33);

D221=f13^2/(b33*lamda)*(exp(lamda*th/2)+exp(-
lamda*th/2))/(exp(lamda*th/2)-exp(-lamda*th/2));
D222=-2*f13^2/(b33*lamda)-0.5*th*d31^2/a33;
D22=D221+D222;

% Coefficients of the governing equations
A=C11*th^3/12+2*D11;
B=2*(C12*th^3/12+2*D11+C66*th^3/6);
D=th*C12+2*D22+th*C66;
E=th*C11+2*D22;
F=th*C11+2*D22;
G=th*C66;

% Coefficients of boundary conditions
D1=C11*th^3/12+2*D11;
D2=C12*th^3/12+2*D11;
D3=D12;
D4=C12*th^3/12+2*D11+2*C66*th^3/6;
D5=th*C12+2*D22;
D6=th*C11+2*D22;

% Matrix of Governing equation
G00=D3^2-D1*D5;
G01=D3*f13*V*h^2/a33+D1*d31*V*h^2/a33;
G02=D5*f13*V*h^2/a33+D3*d31*V*h^2/a33;
G03=4*D3^2-(D1+D2)*(D5+D6);
G05=(C11*h^3/12+2*D11)*d31*V*h^2/a33+D12*f13*V*h^2/a33;
G06=(D5+D6)*f13*V*h^2/a33+2*D3*d31*V*h^2/a33;
G07=(D1+D2)*2*d31*V*h^2/a33+D3*4*f13*V*h^2/a33;
G08=C11*h^3/12+C12*h^3/12+4*D11+2*C66*h^3/6;
G09=4*D3^2-2*D1*D5-2*D2*D5;

% For x=1,(1,j)
% For equation 1
G11=(0.5*D12*(D3^2-D2*D5)+0.5*D*(D2*D3-D1*D3))/G00-0.5*D12;
G12=(D12*(D1*D5+D2*D5-2*D3^2)+D*(D1*D3-D2*D3))/G00+2*D12;
G13=(0.5*D12*(D3*D5*h*0.5-D3*D6*h*0.5)+0.5*D*(D1*D6*h*0.5-
D3^2*h*0.5))/G00;
G14=-2*G13-2*F*h-2*G*h;
% For equation 2
G21=(D12*D4/(2*D1)-D12/2)*(D2*D5-D3^2)/G00;

G221=(D12*D4/(2*D1)-D12/2)*G09;
G222=(D12-D12*D4/D1)*(D2*D5-D3^2);
G223=(2*E-2*D12*D3/D1)*(D2*D3-D1*D3);
G22=(G221+G222+G223)/G00;

G231=(D12*D4/D1-D12)*(D2*D5-D3^2);
G232=(D12-D12*D4/D1)*G09;
```

```
G233=(2*E-2*D12*D3/D1)*(2*D1*D3-2*D2*D3);
G23=(G231+G232+G233)/G00;

G24=D12-D12*D4/D1;
G25=(D12*D4/(2*D1)-D12/2)*(D3*D6*h/2-D3*D5*h/2)/G00;
G26=((D12-D12*D4/D1)*(D3*D6*h/2-D3*D5*h/2)+(E-D12*D3/D1)*(D1*D6*h-
D3^2*h))/G00;
G27=D12*D3*h/(4*D1)-D*h/4;
G28=3*D12*D3*h/(2*D1)-2*G*h-2*E*h+D*h/2;
G29=2*E*h-2*D12*D3*h/D1;
G210=(2*E-2*D12*D3/D1)*G01/G00;

% For equation 3
G31=(B-A*D4/D1)*(D2*D5-D3^2)/G00+A;

G321=(B-A*D4/D1)*G09;
G322=(2*A*D4/D1-2*A-2*B)*(D2*D5-D3^2);
G323=4*A*D3/D1*(D2*D3-D1*D3);
G32=(G321+G322+G323)/G00-4*A-2*B;

G331=(2*A*D4/D1-2*A-2*B)*G09;
G332=2*(B-A*D4/D1)*(D2*D5-D3^2);
G333=4*A*D3/D1*(2*D1*D3-2*D2*D3);
G33=(G331+G332+G333)/G00+12*A+4*B;

G34=2*A*D4/D1;
G35=-4*A-4*A*D4/D1;
G36=(B-A*D4/D1)*(D3*D6*h/2-D3*D5*h/2)/G00-D12*h/2;
G37=((A*D4/D1-A-B)*(D3*D6*h-D3*D5*h)+2*A*D3/D1*(D1*D6*h-
D3^2*h))/G00+2*D12*h;
G38=D12*h/2-A*D3*h/(2*D1);
G39=-D12*h/2-3*A*D3*h/D1;
G310=-2*D12*h+4*A*D3*h/D1;
G311=(-2*A*G02+4*A*D3/D1*G01)/G00-q*h^4;

% For x=2,(2,j)
% For equation 1
G41=(A*(D2*D5-D3^2)-D12*(D2*D3-D1*D3))/G00+B;
G42=(A*G09-D12*(2*D1*D3-2*D2*D3))/G00-4*A-2*B;
G43=(A*(D3*D6*h/2-D3*D5*h/2)-D12*(D1*D6*h-D3^2*h)/2)/G00-D12*h/2;
G44=(A*G02-D12*G01)/G00-q*h^4;
% For equation 2
G51=D12/2*(D3^2-D2*D5)/G00-D12/2;
G52=D12*(D1*D5+D2*D5-2*D3^2)/G00+2*D12;
G53=0.5*D12*(D3*D5*h/2-D3*D6*h/2)/G00+D*h/4;
G54=-0.5*D12*G02/G00;

% For x=1,(1,1)
% For equation 1
G61=(0.5*G231+G232+G233)/G00+D12-D12*D4/D1;
G62=D*h/4+7*D12*D3*h/(4*D1)-2*E*h-2*G*h;
G63=((D12/2-D12*D4/(2*D1))*G02+(2*E-2*D12*D3/D1)*G01)/G00;
G64=G25+D12*D3*h/(2*D1)-D*h/2;
% For equation 2
G71=(G331+0.5*G332+G333)/G00+13*A+2*B+2*A*D4/D1;
```

```
G72=7*A*D3*h/(2*D1);
G73=((A*D4/D1-2*A-B)*G02+4*A*D3/D1*G01)/G00-q*h^4;
G74=G36+D12*h-A*D3*h/D1;
% For equation 3
G82=-G13-2*F*h-2*G*h;
G83=(D12*0.5*G02-D*0.5*G01)/G00;

% For x=1,(1,N-1)
% For equation 1
G91=(G331+0.5*G332+G333)/G00+11*A+4*B;
G92=(G322+G323)/G00-2*A-2*A*D4/D1;
G93=-G36-D12*h+A*D3*h/D1;
G94=-G37+2*D12*h-2*A*D3*h/D1;
G95=-7*A*D3*h/(2*D1);
G96=((A+B-A*D4/D1)*G06-A*D3/(2*D1)*G07)/G03+((A*D4/D1-2*A-
B)*G02+4*A*D3/D1*G01)/G00-q*h^4;
% For equation 2
G101=(G231*0.5+G232+G233)/G00;
G102=(G222+G223)/G00-D12+D12*D4/D1;
G103=-G25+D*h/2-D12*D3*h/(2*D1);
G104=-G26+D12*D3*h/D1-D*h;
G105=D*h/2-D12*D3*h/(2*D1);
G106=D*h/4+7*D12*D3*h/(4*D1)-2*G*h-2*E*h;
G108=((D12*D4/(2*D1)-D12/2)*G06+(D12*D3/4-D/4)*G07)/G03+((D12/2-
D12*D4/(2*D1))*G02+(2*E-2*D12*D3/D1)*G01)/G00;
% For equation 3
G111=(D12*G06-D/4*G07)/G03+(D/2*G01-D12/2*G02)/G00;

% For x=1,y=N,(1,N)
% For equation 1
G12101=2*(2*B-2*A*D4/D1)*(D2*D5-D3^2);
G12102=2*(-3*A*D12/(2*D1)-D12/2)*(D2*D3-D1*D3);
G121=(G12101+G12102)/G00+4*A-4*B+8*A*D4/D1;

G1221=(2*B-2*A*D4/D1)*(4*D3^2-2*D1*D5-2*D2*D5);
G1222=-2*(-3*A*D12/(2*D1)-D12/2)*(D2*D3-D1*D3);
G122=(G1221+G1222)/G00-4*A-4*A*D4/D1;

G123=0.5*(G12101+G12102)/G00+2*A;
G124=8*A*D4/D1-4*B;

G1251=(2*B-2*A*D4/D1)*(D3*D6*h/2-D3*D5*h/2);
G1252=(-3*A*D12/(2*D1)-D12/2)*(D1*D6*h/2-D3^2*h/2);
G125=(G1251+G1252)/G00-13*A*D12*h/(4*D1)-D12*h/4;

G126=-3*D12*h/2+9*A*D12*h/(2*D1);
G127=-(G1251+G1252)/G00+D12*h/2;
G128=(-4*(A+B-A*D4/D1)*G06+2*(D12/2+5*A*D12/(2*D1))*G07)/G03+(2*(2*B-
2*A*D4/D1)*G02+2*(-3*A*D12/(2*D1)-D12/2)*G01)/G00-q*h^4;
G129=A*D12*h/(2*D1)-D12*h/2;
G1210=D12*h-A*D12*h/D1;
G1211=3*D12*h/4-3*A*D12*h/(4*D1);
% For equation 2
G13101=(-D12+D12*D4/D1)*(D2*D5-D3^2);
G13102=-(-3*D/4+3*D12^2/(4*D1))*(D1*D3-D2*D3);
G131=2*D12-2*D12*D4/D1+(G13101+G13102)/G00;
```

```
G132=2*D12*D4/D1-2*D12-2*G13102/G00;
G133=(-D12+D12*D4/D1)*(4*D3^2-2*D1*D5-2*D2*D5)/G00;
G134=2*D12-2*D12*D4/D1;
G135=G13101/G00;

G1361=(-3*D/4+3*D12^2/(4*D1))*(D1*D6*h/2-D3^2*h/2);
G136=-2*E*h-D*h/8+17*D12^2*h/(8*D1)+G1361/G00;

G137=(-D12+D12*D4/D1)*(D3*D6*h/2-D3*D5*h/2)/G00;
G138=((D12-D12*D4/D1)*G06+(E+D/4-5*D12^2/(4*D1))*G07)/G03+((-
D12+D12*D4/D1)*G02+(-3*D/4+3*D12^2/(4*D1))*G01)/G00;
G139=G13102/G00;
G1310=2*E*h-2*D12^2*h/D1;
G1311=-G1361/G00;
G1312=D*h/2-D12^2*h/(2*D1);
G1313=-3*D*h/8+3*D12^2*h/(8*D1);
G1314=-D*h/4+D12^2*h/(4*D1);

% For x=2,y=N-1,(2, N-1)
% For equation 1
G141=2*G41-B;
G142=2*G44+q*h^4;

% Oher coefficients
G151=A*D3*h/D1;
% Mesh the beam and initialize some variables
% Matrix of the first governing equation
A1=zeros(M*N);
B1=A1;
C1=A1;
E1=zeros(M*N,1);
% Matrix of the second governing equation
A2=A1;
B2=A1;
C2=A1;
E2=E1;
% Matrix of the third governing equation
A3=A1;
B3=A1;
C3=A1;
E3=E1;

% Set up the matrix
% 16 points
% For (1,1)
A1(1,1)=G61;
A1(1,M+1)=G22;
A1(1,2*M+1)=G21;
A1(1,2)=-2*G24;
A1(1,M+2)=G24;
B1(1,1)=G62;
B1(1,M+1)=G*h;
B1(1,2*M+1)=G27;
B1(1,2)=G29;
C1(1,1)=G64;
```

```
C1(1,M+1)=-G26;
C1(1,2*M+1)=-G25;
E1(1,1)=G63;

A2(1,1)=G71;
A2(1,M+1)=G32;
A2(1,2*M+1)=G31;
A2(1,2)=G35;
A2(1,M+2)=G34;
A2(1,3)=2*A;
B2(1,1)=G72;
B2(1,2*M+1)=G38;
B2(1,2)=G310;
B2(1,M+2)=D12*h/2;
B2(1,3)=D12*h/2;
C2(1,1)=G74;
C2(1,M+1)=-G37;
C2(1,2*M+1)=-G36;
C2(1,M+2)=D12*h;
E2(1,1)=G73;

A3(1,1)=-G11;
A3(1,M+1)=-G12;
A3(1,2*M+1)=-G11;
B3(1,1)=-D*h/2;
B3(1,M+1)=G*h;
C3(1,1)=G82;
C3(1,M+1)=F*h;
C3(1,2*M+1)=G13;
C3(1,2)=2*G*h;
E3(1,1)=G83;

% For (M,1)
A1(M,M)=-G61;
A1(M,2*M)=-G22;
A1(M,3*M)=-G21;
A1(M,M-1)=2*G24;
A1(M,2*M-1)=-G24;
B1(M,M)=G62;
B1(M,2*M)=G*h;
B1(M,3*M)=G27;
B1(M,M-1)=G29;
C1(M,M)=-G64;
C1(M,2*M)=G26;
C1(M,3*M)=G25;
E1(M,1)=-G63;

A2(M,M)=G71;
A2(M,2*M)=G32;
A2(M,3*M)=G31;
A2(M,M-1)=G35;
A2(M,2*M-1)=G34;
A2(M,M-2)=2*A;
B2(M,M)=-G72;
B2(M,3*M)=-G38;
B2(M,M-1)=-G310;
```

```
B2(M,2*M-1)=-D12*h/2;
B2(M,M-2)=-D12*h/2;
C2(M,M)=G74;
C2(M,2*M)=-G37;
C2(M,3*M)=-G36;
C2(M,2*M-1)=D12*h;
E2(M,1)=G73;

A3(M,M)=-G11;
A3(M,2*M)=-G12;
A3(M,3*M)=-G11;
B3(M,M)=-D*h/2;
B3(M,2*M)=G*h;
C3(M,M)=G82;
C3(M,2*M)=F*h;
C3(M,3*M)=G13;
C3(M,M-1)=2*G*h;
E3(M,1)=G83;

% For (1,2)
A1(1+M,1)=G12;
A1(1+M,1+2*M)=-G12;
A1(1+M,1+3*M)=-G11;
B1(1+M,1)=-G*h;
B1(1+M,1+2*M)=G*h;
C1(1+M,1)=F*h;
C1(1+M,1+M)=G14;
C1(1+M,1+2*M)=F*h;
C1(1+M,1+3*M)=G13;
C1(1+M,2+M)=2*G*h;

A2(1+M,1)=G22;
A2(1+M,1+M)=G23;
A2(1+M,1+2*M)=G22;
A2(1+M,1+3*M)=G21;
A2(1+M,2)=G24;
A2(1+M,2+M)=-2*G24;
A2(1+M,2+2*M)=G24;
B2(1+M,1)=G*h;
B2(1+M,1+M)=G28;
B2(1+M,1+2*M)=G*h;
B2(1+M,1+3*M)=G27;
B2(1+M,2+M)=G29;
C2(1+M,1)=G26;
C2(1+M,1+2*M)=-G26;
C2(1+M,1+3*M)=-G25;
E2(1+M,1)=G210;

A3(1+M,1)=G32;
A3(1+M,1+M)=G33;
A3(1+M,1+2*M)=G32;
A3(1+M,1+3*M)=G31;
A3(1+M,2)=G34;
A3(1+M,2+M)=G35;
A3(1+M,2+2*M)=G34;
A3(1+M,3+M)=2*A;
```

```
B3(1+M,1+M)=G39;
B3(1+M,1+3*M)=G38;
B3(1+M,2)=D12*h/2;
B3(1+M,2+M)=G310;
B3(1+M,2+2*M)=D12*h/2;
B3(1+M,3+M)=D12*h/2;
C3(1+M,1)=G37;
C3(1+M,1+2*M)=-G37;
C3(1+M,1+3*M)=-G36;
C3(1+M,2)=-D12*h;
C3(1+M,2+2*M)=D12*h;
E3(1+M,1)=G311;

% For (M,2)
A1(2*M,M)=G12;
A1(2*M,3*M)=-G12;
A1(2*M,4*M)=-G11;
B1(2*M,M)=-G*h;
B1(2*M,3*M)=G*h;
C1(2*M,M)=F*h;
C1(2*M,2*M)=G14;
C1(2*M,3*M)=F*h;
C1(2*M,4*M)=G13;
C1(2*M,2*M-1)=2*G*h;

A2(2*M,M)=-G22;
A2(2*M,2*M)=-G23;
A2(2*M,3*M)=-G22;
A2(2*M,4*M)=-G21;
A2(2*M,M-1)=-G24;
A2(2*M,2*M-1)=2*G24;
A2(2*M,3*M-1)=-G24;
B2(2*M,M)=G*h;
B2(2*M,2*M)=G28;
B2(2*M,3*M)=G*h;
B2(2*M,4*M)=G27;
B2(2*M,2*M-1)=G29;
C2(2*M,M)=-G26;
C2(2*M,3*M)=G26;
C2(2*M,4*M)=G25;
E2(2*M,1)=-G210;

A3(2*M,M)=G32;
A3(2*M,2*M)=G33;
A3(2*M,3*M)=G32;
A3(2*M,4*M)=G31;
A3(2*M,M-1)=G34;
A3(2*M,2*M-1)=G35;
A3(2*M,3*M-1)=G34;
A3(2*M,2*M-2)=2*A;
B3(2*M,2*M)=-G39;
B3(2*M,4*M)=-G38;
B3(2*M,M-1)=-D12*h/2;
B3(2*M,2*M-1)=-G310;
B3(2*M,3*M-1)=-D12*h/2;
B3(2*M,2*M-2)=-D12*h/2;
```

```
C3(2*M,M)=G37;
C3(2*M,3*M)=-G37;
C3(2*M,4*M)=-G36;
C3(2*M,M-1)=-D12*h;
C3(2*M,3*M-1)=D12*h;
E3(2*M,1)=G311;

% For (1,N-1)
A1(1+M*(N-2),1+M*(N-4))=G31;
A1(1+M*(N-2),1+M*(N-3))=G32;
A1(1+M*(N-2),1+M*(N-2))=G91;
A1(1+M*(N-2),1+M*(N-1))=G92;
A1(1+M*(N-2),2+M*(N-3))=G34;
A1(1+M*(N-2),2+M*(N-2))=G35;
A1(1+M*(N-2),2+M*(N-1))=G34;
A1(1+M*(N-2),3+M*(N-2))=2*A;
B1(1+M*(N-2),1+M*(N-4))=G38;
B1(1+M*(N-2),1+M*(N-2))=G95;
B1(1+M*(N-2),2+M*(N-3))=D12*h/2;
B1(1+M*(N-2),2+M*(N-2))=G310;
B1(1+M*(N-2),2+M*(N-1))=D12*h/2;
B1(1+M*(N-2),3+M*(N-2))=D12*h/2;
C1(1+M*(N-2),1+M*(N-4))=G36;
C1(1+M*(N-2),1+M*(N-3))=G37;
C1(1+M*(N-2),1+M*(N-2))=G93;
C1(1+M*(N-2),1+M*(N-1))=G94;
C1(1+M*(N-2),2+M*(N-3))=-D12*h;
C1(1+M*(N-2),2+M*(N-1))=G151;
E1(1+M*(N-2),1)=G96;

A2(1+M*(N-2),1+M*(N-4))=G21;
A2(1+M*(N-2),1+M*(N-3))=G22;
A2(1+M*(N-2),1+M*(N-2))=G101;
A2(1+M*(N-2),1+M*(N-1))=G102;
A2(1+M*(N-2),2+M*(N-3))=G24;
A2(1+M*(N-2),2+M*(N-2))=-2*G24;
A2(1+M*(N-2),2+M*(N-1))=G24;
B2(1+M*(N-2),1+M*(N-4))=G27;
B2(1+M*(N-2),1+M*(N-3))=G*h;
B2(1+M*(N-2),1+M*(N-2))=G106;
B2(1+M*(N-2),1+M*(N-1))=G*h;
B2(1+M*(N-2),2+M*(N-2))=G29;
C2(1+M*(N-2),1+M*(N-4))=G25;
C2(1+M*(N-2),1+M*(N-3))=G26;
C2(1+M*(N-2),1+M*(N-2))=G103;
C2(1+M*(N-2),1+M*(N-1))=G104;
C2(1+M*(N-2),2+M*(N-1))=G105;
E2(1+M*(N-2),1)=G108;

A3(1+M*(N-2),1+M*(N-4))=G11;
A3(1+M*(N-2),1+M*(N-3))=G12;
A3(1+M*(N-2),1+M*(N-2))=G11;
B3(1+M*(N-2),1+M*(N-3))=-G*h;
B3(1+M*(N-2),1+M*(N-1))=G*h;
C3(1+M*(N-2),1+M*(N-4))=G13;
C3(1+M*(N-2),1+M*(N-3))=F*h;
```

```
C3(1+M*(N-2),1+M*(N-2))=-G13-2*F*h-2*G*h;
C3(1+M*(N-2),1+M*(N-1))=F*h;
C3(1+M*(N-2),2+M*(N-2))=2*G*h;
E3(1+M*(N-2),1)=G111;

% For (M,N-1)
A1(M*(N-1),M*(N-3))=G31;
A1(M*(N-1),M*(N-2))=G32;
A1(M*(N-1),M*(N-1))=G91;
A1(M*(N-1),M*N)=G92;
A1(M*(N-1),M*(N-2)-1)=G34;
A1(M*(N-1),M*(N-1)-1)=G35;
A1(M*(N-1),M*N-1)=G34;
A1(M*(N-1),M*(N-1)-2)=2*A;
B1(M*(N-1),M*(N-3))=-G38;
B1(M*(N-1),M*(N-1))=-G95;
B1(M*(N-1),M*(N-2)-1)=-D12*h/2;
B1(M*(N-1),M*(N-1)-1)=-G310;
B1(M*(N-1),M*N-1)=-D12*h/2;
B1(M*(N-1),M*(N-1)-2)=-D12*h/2;
C1(M*(N-1),M*(N-3))=G36;
C1(M*(N-1),M*(N-2))=G37;
C1(M*(N-1),M*(N-1))=G93;
C1(M*(N-1),M*N)=G94;
C1(M*(N-1),M*(N-2)-1)=-D12*h;
C1(M*(N-1),M*N-1)=G151;
E1(M*(N-1),1)=G96;

A2(M*(N-1),M*(N-3))=-G21;
A2(M*(N-1),M*(N-2))=-G22;
A2(M*(N-1),M*(N-1))=-G101;
A2(M*(N-1),M*N)=-G102;
A2(M*(N-1),M*(N-2)-1)=-G24;
A2(M*(N-1),M*(N-1)-1)=2*G24;
A2(M*(N-1),M*N-1)=-G24;
B2(M*(N-1),M*(N-3))=G27;
B2(M*(N-1),M*(N-2))=G*h;
B2(M*(N-1),M*(N-1))=G106;
B2(M*(N-1),M*N)=G*h;
B2(M*(N-1),M*(N-1)-1)=G29;
C2(M*(N-1),M*(N-3))=-G25;
C2(M*(N-1),M*(N-2))=-G26;
C2(M*(N-1),M*(N-1))=-G103;
C2(M*(N-1),M*N)=-G104;
C2(M*(N-1),M*N-1)=-G105;
E2(M*(N-1),1)=-G108;

A3(M*(N-1),M*(N-3))=G11;
A3(M*(N-1),M*(N-2))=G12;
A3(M*(N-1),M*(N-1))=G11;
B3(M*(N-1),M*(N-2))=-G*h;
B3(M*(N-1),M*N)=G*h;
C3(M*(N-1),M*(N-3))=G13;
C3(M*(N-1),M*(N-2))=F*h;
C3(M*(N-1),M*(N-1))=-G13-2*F*h-2*G*h;
C3(M*(N-1),M*N)=F*h;
```

```
C3(M*(N-1),M*(N-1)-1)=2*G*h;
E3(M*(N-1),1)=G111;

% For (1,N)
A1(1+M*(N-1),1+M*(N-1))=G121;
A1(1+M*(N-1),2+M*(N-1))=G122;
A1(1+M*(N-1),3+M*(N-1))=G123;
A1(1+M*(N-1),1+M*(N-2))=G122;
A1(1+M*(N-1),2+M*(N-2))=G124;
A1(1+M*(N-1),1+M*(N-3))=G123;
B1(1+M*(N-1),1+M*(N-1))=G125;
B1(1+M*(N-1),2+M*(N-1))=G126;
B1(1+M*(N-1),3+M*(N-1))=G127;
B1(1+M*(N-1),1+M*(N-2))=G129;
B1(1+M*(N-1),2+M*(N-2))=G1210;
B1(1+M*(N-1),1+M*(N-3))=G1211;
C1(1+M*(N-1),1+M*(N-1))=-G125;
C1(1+M*(N-1),2+M*(N-1))=-G129;
C1(1+M*(N-1),3+M*(N-1))=-G1211;
C1(1+M*(N-1),1+M*(N-2))=-G126;
C1(1+M*(N-1),2+M*(N-2))=-G1210;
C1(1+M*(N-1),1+M*(N-3))=-G127;
E1(1+M*(N-1),1)=G128;

A2(1+M*(N-1),1+M*(N-1))=G131;
A2(1+M*(N-1),2+M*(N-1))=G132;
A2(1+M*(N-1),3+M*(N-1))=G139;
A2(1+M*(N-1),1+M*(N-2))=G133;
A2(1+M*(N-1),2+M*(N-2))=G134;
A2(1+M*(N-1),1+M*(N-3))=G135;
B2(1+M*(N-1),1+M*(N-1))=G136;
B2(1+M*(N-1),2+M*(N-1))=G1310;
B2(1+M*(N-1),3+M*(N-1))=G1311;
B2(1+M*(N-1),1+M*(N-2))=G1312;
B2(1+M*(N-1),1+M*(N-3))=G1313;
C2(1+M*(N-1),1+M*(N-1))=-G137;
C2(1+M*(N-1),2+M*(N-1))=G1314;
C2(1+M*(N-1),1+M*(N-2))=G1314;
C2(1+M*(N-1),2+M*(N-2))=G1312;
C2(1+M*(N-1),1+M*(N-3))=G137;
E2(1+M*(N-1),1)=G138;

A3(1+M*(N-1),1+M*(N-1))=-G131;
A3(1+M*(N-1),2+M*(N-1))=-G133;
A3(1+M*(N-1),3+M*(N-1))=-G135;
A3(1+M*(N-1),1+M*(N-2))=-G132;
A3(1+M*(N-1),2+M*(N-2))=-G134;
A3(1+M*(N-1),1+M*(N-3))=-G139;
B3(1+M*(N-1),1+M*(N-1))=-G137;
B3(1+M*(N-1),2+M*(N-1))=G1314;
B3(1+M*(N-1),3+M*(N-1))=G137;
B3(1+M*(N-1),1+M*(N-2))=G1314;
B3(1+M*(N-1),2+M*(N-2))=G1312;
C3(1+M*(N-1),1+M*(N-1))=G136;
C3(1+M*(N-1),2+M*(N-1))=G1312;
C3(1+M*(N-1),3+M*(N-1))=G1313;
```

```
C3(1+M*(N-1),1+M*(N-2))=G1310;
C3(1+M*(N-1),1+M*(N-3))=G1311;
E3(1+M*(N-1),1)=-G138;

% For (M,N)
A1(M*N,M*N)=G121;
A1(M*N,M*N-1)=G122;
A1(M*N,M*N-2)=G123;
A1(M*N,M*(N-1))=G122;
A1(M*N,M*(N-1)-1)=G124;
A1(M*N,M*(N-2))=G123;
B1(M*N,M*N)=-G125;
B1(M*N,M*N-1)=-G126;
B1(M*N,M*N-2)=-G127;
B1(M*N,M*(N-1))=-G129;
B1(M*N,M*(N-1)-1)=-G1210;
B1(M*N,M*(N-2))=-G1211;
C1(M*N,M*N)=-G125;
C1(M*N,M*N-1)=-G129;
C1(M*N,M*N-2)=-G1211;
C1(M*N,M*(N-1))=-G126;
C1(M*N,M*(N-1)-1)=-G1210;
C1(M*N,M*(N-2))=-G127;
E1(M*N,1)=G128;

A2(M*N,M*N)=-G131;
A2(M*N,M*N-1)=-G132;
A2(M*N,M*N-2)=-G139;
A2(M*N,M*(N-1))=-G133;
A2(M*N,M*(N-1)-1)=-G134;
A2(M*N,M*(N-2))=-G135;
B2(M*N,M*N)=G136;
B2(M*N,M*N-1)=G1310;
B2(M*N,M*N-2)=G1311;
B2(M*N,M*(N-1))=G1312;
B2(M*N,M*(N-2))=G1313;
C2(M*N,M*N)=G137;
C2(M*N,M*N-1)=-G1314;
C2(M*N,M*(N-1))=-G1314;
C2(M*N,M*(N-1)-1)=-G1312;
C2(M*N,M*(N-2))=-G137;
E2(M*N,1)=-G138;

A3(M*N,M*N)=-G131;
A3(M*N,M*N-1)=-G133;
A3(M*N,M*N-2)=-G135;
A3(M*N,M*(N-1))=-G132;
A3(M*N,M*(N-1)-1)=-G134;
A3(M*N,M*(N-2))=-G139;
B3(M*N,M*N)=-G137;
B3(M*N,M*N-1)=G1314;
B3(M*N,M*N-2)=G137;
B3(M*N,M*(N-1))=G1314;
B3(M*N,M*(N-1)-1)=G1312;
C3(M*N,M*N)=G136;
C3(M*N,M*N-1)=G1312;
```

```
C3(M*N,M*N-2)=G1313;
C3(M*N,M*(N-1))=G1310;
C3(M*N,M*(N-2))=G1311;
E3(M*N,1)=-G138;

% For (2,1)
A1(2,1)=G42;
A1(2,2)=12*A+4*B;
A1(2,3)=-4*A-2*B;
A1(2,4)=A;
A1(2,1+M)=G41;
A1(2,2+M)=-4*A-2*B;
A1(2,3+M)=B;
A1(2,2+2*M)=A;
B1(2,1)=2*D12*h;
B1(2,2)=-D12*h/2;
B1(2,3)=-2*D12*h;
B1(2,4)=D12*h/2;
B1(2,1+M)=-D12*h/2;
B1(2,3+M)=D12*h/2;
C1(2,2)=-D12*h/2;
C1(2,1+M)=-G43;
C1(2,2+M)=-2*D12*h;
C1(2,3+M)=D12*h/2;
C1(2,2+2*M)=D12*h/2;
E1(2,1)=G44;

A2(2,1)=G52;
A2(2,2)=D12/2;
A2(2,3)=-2*D12;
A2(2,4)=D12/2;
A2(2,1+M)=G51;
A2(2,3+M)=D12/2;
B2(2,1)=E*h;
B2(2,2)=-2*E*h-2*G*h;
B2(2,3)=E*h;
B2(2,2+M)=G*h;
C2(2,1+M)=-G53;
C2(2,3+M)=D*h/4;
E2(2,1)=G54;

A3(2,1+M)=D12/2;
A3(2,2)=-D12/2;
A3(2,2+M)=-2*D12;
A3(2,3+M)=D12/2;
A3(2,2+2*M)=D12/2;
B3(2,1+M)=-D*h/4;
B3(2,3+M)=D*h/4;
C3(2,1)=G*h;
C3(2,2)=-2*F*h-2*G*h;
C3(2,3)=G*h;
C3(2,2+M)=F*h;

% For (M-1,1)
A1(M-1,M)=G42;
A1(M-1,M-1)=12*A+4*B;
```

```
A1(M-1,M-2)=-4*A-2*B;
A1(M-1,M-3)=A;
A1(M-1,2*M)=G41;
A1(M-1,2*M-1)=-4*A-2*B;
A1(M-1,2*M-2)=B;
A1(M-1,3*M-1)=A;
B1(M-1,M)=-2*D12*h;
B1(M-1,M-1)=D12*h/2;
B1(M-1,M-2)=2*D12*h;
B1(M-1,M-3)=-D12*h/2;
B1(M-1,2*M)=D12*h/2;
B1(M-1,2*M-2)=-D12*h/2;
C1(M-1,M-1)=-D12*h/2;
C1(M-1,2*M)=-G43;
C1(M-1,2*M-1)=-2*D12*h;
C1(M-1,2*M-2)=D12*h/2;
C1(M-1,3*M-1)=D12*h/2;
E1(M-1,1)=G44;

A2(M-1,M)=-G52;
A2(M-1,M-1)=-D12/2;
A2(M-1,M-2)=2*D12;
A2(M-1,M-3)=-D12/2;
A2(M-1,2*M)=-G51;
A2(M-1,2*M-2)=-D12/2;
B2(M-1,M)=E*h;
B2(M-1,M-1)=-2*E*h-2*G*h;
B2(M-1,M-2)=E*h;
B2(M-1,2*M-1)=G*h;
C2(M-1,2*M)=G53;
C2(M-1,2*M-2)=-D*h/4;
E2(M-1,1)=-G54;

A3(M-1,2*M)=D12/2;
A3(M-1,M-1)=-D12/2;
A3(M-1,2*M-1)=-2*D12;
A3(M-1,2*M-2)=D12/2;
A3(M-1,3*M-1)=D12/2;
B3(M-1,2*M)=-D*h/4;
B3(M-1,2*M-2)=D*h/4;
C3(M-1,M)=G*h;
C3(M-1,M-1)=-2*F*h-2*G*h;
C3(M-1,M-2)=G*h;
C3(M-1,2*M-1)=F*h;

% For x=2,(2,2)
A1(2+M,1)=G41;
A1(2+M,1+M)=G42;
A1(2+M,1+2*M)=G41;
A1(2+M,2)=-4*A-2*B;
A1(2+M,2+M)=11*A+4*B;
A1(2+M,2+2*M)=-4*A-2*B;
A1(2+M,2+3*M)=A;
A1(2+M,3)=B;
A1(2+M,3+M)=-4*A-2*B;
A1(2+M,3+2*M)=B;
```

```
A1(2+M,4+M)=A;
B1(2+M,1)=-D12*h/2;
B1(2+M,1+M)=2*D12*h;
B1(2+M,1+2*M)=-D12*h/2;
B1(2+M,2+M)=-D12*h/2;
B1(2+M,3)=D12*h/2;
B1(2+M,3+M)=-2*D12*h;
B1(2+M,3+2*M)=D12*h/2;
B1(2+M,4+M)=D12*h/2;
C1(2+M,1)=G43;
C1(2+M,1+M*2)=-G43;
C1(2+M,2)=2*D12*h;
C1(2+M,2+M*2)=-2*D12*h;
C1(2+M,2+M*3)=D12*h/2;
C1(2+M,3)=-D12*h/2;
C1(2+M,3+M*2)=D12*h/2;
E1(2+M,1)=G44;

A2(2+M,1)=G51;
A2(2+M,1+M)=G52;
A2(2+M,1+M*2)=G51;
A2(2+M,2+M)=D12/2;
A2(2+M,3)=D12/2;
A2(2+M,3+M)=-2*D12;
A2(2+M,3+M*2)=D12/2;
A2(2+M,4+M)=D12/2;
B2(2+M,1+M)=E*h;
B2(2+M,2)=G*h;
B2(2+M,2+M)=-2*G*h-2*E*h;
B2(2+M,2+M*2)=G*h;
B2(2+M,3+M)=E*h;
C2(2+M,1)=G53;
C2(2+M,1+M*2)=-G53;
C2(2+M,3)=-D*h/4;
C2(2+M,3+M*2)=D*h/4;
E2(2+M,1)=G54;

A3(2+M,1)=-D12/2;
A3(2+M,1+M*2)=D12/2;
A3(2+M,2)=2*D12;
A3(2+M,2+M*2)=-2*D12;
A3(2+M,2+M*3)=D12/2;
A3(2+M,3)=-D12/2;
A3(2+M,3+M*2)=D12/2;
B3(2+M,1)=D*h/4;
B3(2+M,1+M*2)=-D*h/4;
B3(2+M,3)=-D*h/4;
B3(2+M,3+M*2)=D*h/4;
C3(2+M,1+M)=G*h;
C3(2+M,2)=F*h;
C3(2+M,2+M)=-2*F*h-2*G*h;
C3(2+M,2+M*2)=F*h;
C3(2+M,3+M)=G*h;


% For (M-1,2)
```

```
A1(2*M-1,M)=G41;
A1(2*M-1,2*M)=G42;
A1(2*M-1,3*M)=G41;
A1(2*M-1,M-1)=-4*A-2*B;
A1(2*M-1,2*M-1)=11*A+4*B;
A1(2*M-1,3*M-1)=-4*A-2*B;
A1(2*M-1,4*M-1)=A;
A1(2*M-1,M-2)=B;
A1(2*M-1,2*M-2)=-4*A-2*B;
A1(2*M-1,3*M-2)=B;
A1(2*M-1,2*M-3)=A;
B1(2*M-1,M)=D12*h/2;
B1(2*M-1,2*M)=-2*D12*h;
B1(2*M-1,3*M)=D12*h/2;
B1(2*M-1,2*M-1)=D12*h/2;
B1(2*M-1,M-2)=-D12*h/2;
B1(2*M-1,2*M-2)=2*D12*h;
B1(2*M-1,3*M-2)=-D12*h/2;
B1(2*M-1,2*M-3)=-D12*h/2;
C1(2*M-1,M)=G43;
C1(2*M-1,3*M)=-G43;
C1(2*M-1,M-1)=2*D12*h;
C1(2*M-1,M*3-1)=-2*D12*h;
C1(2*M-1,M*4-1)=D12*h/2;
C1(2*M-1,M-2)=-D12*h/2;
C1(2*M-1,M*3-2)=D12*h/2;
E1(2*M-1,1)=G44;

A2(2*M-1,M)=-G51;
A2(2*M-1,2*M)=-G52;
A2(2*M-1,3*M)=-G51;
A2(2*M-1,2*M-1)=-D12/2;
A2(2*M-1,M-2)=-D12/2;
A2(2*M-1,2*M-2)=2*D12;
A2(2*M-1,3*M-2)=-D12/2;
A2(2*M-1,2*M-3)=-D12/2;
B2(2*M-1,2*M)=E*h;
B2(2*M-1,M-1)=G*h;
B2(2*M-1,2*M-1)=-2*G*h-2*E*h;
B2(2*M-1,3*M-1)=G*h;
B2(2*M-1,2*M-2)=E*h;
C2(2*M-1,M)=-G53;
C2(2*M-1,3*M)=G53;
C2(2*M-1,M-2)=D*h/4;
C2(2*M-1,3*M-2)=-D*h/4;
E2(2*M-1,1)=-G54;

A3(2*M-1,M)=-D12/2;
A3(2*M-1,3*M)=D12/2;
A3(2*M-1,M-1)=2*D12;
A3(2*M-1,3*M-1)=-2*D12;
A3(2*M-1,4*M-1)=D12/2;
A3(2*M-1,M-2)=-D12/2;
A3(2*M-1,3*M-2)=D12/2;
B3(2*M-1,M)=D*h/4;
B3(2*M-1,3*M)=-D*h/4;
```

```
B3(2*M-1,M-2)=-D*h/4;
B3(2*M-1,3*M-2)=D*h/4;
C3(2*M-1,2*M)=G*h;
C3(2*M-1,M-1)=F*h;
C3(2*M-1,2*M-1)=-2*F*h-2*G*h;
C3(2*M-1,3*M-1)=F*h;
C3(2*M-1,2*M-2)=G*h;

% For (2,N-1)
A1(2+M*(N-2),1+M*(N-1))=G141;
A1(2+M*(N-2),2+M*(N-1))=G42;
A1(2+M*(N-2),3+M*(N-1))=G41;
A1(2+M*(N-2),1+M*(N-2))=G42;
A1(2+M*(N-2),2+M*(N-2))=10*A+4*B;
A1(2+M*(N-2),3+M*(N-2))=-4*A-2*B;
A1(2+M*(N-2),4+M*(N-2))=A;
A1(2+M*(N-2),1+M*(N-3))=G41;
A1(2+M*(N-2),2+M*(N-3))=-4*A-2*B;
A1(2+M*(N-2),3+M*(N-3))=B;
A1(2+M*(N-2),2+M*(N-4))=A;
B1(2+M*(N-2),1+M*(N-1))=G43;
B1(2+M*(N-2),3+M*(N-1))=-G43;
B1(2+M*(N-2),1+M*(N-2))=2*D12*h;
B1(2+M*(N-2),2+M*(N-2))=-D12*h/2;
B1(2+M*(N-2),3+M*(N-2))=-2*D12*h;
B1(2+M*(N-2),4+M*(N-2))=D12*h/2;
B1(2+M*(N-2),1+M*(N-3))=-D12*h/2;
B1(2+M*(N-2),3+M*(N-3))=D12*h/2;
C1(2+M*(N-2),1+M*(N-1))=-G43;
C1(2+M*(N-2),2+M*(N-1))=-2*D12*h;
C1(2+M*(N-2),3+M*(N-1))=D12*h/2;
C1(2+M*(N-2),2+M*(N-2))=D12*h/2;
C1(2+M*(N-2),1+M*(N-3))=G43;
C1(2+M*(N-2),2+M*(N-3))=2*D12*h;
C1(2+M*(N-2),3+M*(N-3))=-D12*h/2;
C1(2+M*(N-2),2+M*(N-4))=-D12*h/2;
E1(2+M*(N-2),1)=G142;

A2(2+M*(N-2),1+M*(N-1))=-G51;
A2(2+M*(N-2),2+M*(N-1))=-G52;
A2(2+M*(N-2),3+M*(N-1))=-G51;
A2(2+M*(N-2),2+M*(N-2))=-D12/2;
A2(2+M*(N-2),1+M*(N-3))=-D12/2;
A2(2+M*(N-2),2+M*(N-3))=2*D12;
A2(2+M*(N-2),3+M*(N-3))=-D12/2;
A2(2+M*(N-2),2+M*(N-4))=-D12/2;
B2(2+M*(N-2),1+M*(N-1))=-G53;
B2(2+M*(N-2),3+M*(N-1))=G53;
B2(2+M*(N-2),1+M*(N-3))=D*h/4;
B2(2+M*(N-2),3+M*(N-3))=-D*h/4;
C2(2+M*(N-2),2+M*(N-1))=F*h;
C2(2+M*(N-2),1+M*(N-2))=G*h;
C2(2+M*(N-2),2+M*(N-2))=-2*F*h-2*G*h;
C2(2+M*(N-2),3+M*(N-2))=G*h;
C2(2+M*(N-2),2+M*(N-3))=F*h;
E2(2+M*(N-2),1)=-G54;
```

```
A3(2+M*(N-2),1+M*(N-1))=G51;
A3(2+M*(N-2),3+M*(N-1))=D12/2;
A3(2+M*(N-2),1+M*(N-2))=G52;
A3(2+M*(N-2),2+M*(N-2))=D12/2;
A3(2+M*(N-2),3+M*(N-2))=-2*D12;
A3(2+M*(N-2),4+M*(N-2))=D12/2;
A3(2+M*(N-2),1+M*(N-3))=G51;
A3(2+M*(N-2),3+M*(N-3))=D12/2;
B3(2+M*(N-2),2+M*(N-1))=G*h;
B3(2+M*(N-2),1+M*(N-2))=E*h;
B3(2+M*(N-2),2+M*(N-2))=-2*E*h-2*G*h;
B3(2+M*(N-2),3+M*(N-2))=E*h;
B3(2+M*(N-2),2+M*(N-3))=G*h;
C3(2+M*(N-2),1+M*(N-1))=-G53;
C3(2+M*(N-2),3+M*(N-1))=D*h/4;
C3(2+M*(N-2),1+M*(N-3))=G53;
C3(2+M*(N-2),3+M*(N-3))=-D*h/4;
E3(2+M*(N-2),1)=G54;

% For (M-1,N-1)
A1(M*(N-1)-1,M*N)=G141;
A1(M*(N-1)-1,M*N-1)=G42;
A1(M*(N-1)-1,M*N-2)=G41;
A1(M*(N-1)-1,M*(N-1))=G42;
A1(M*(N-1)-1,M*(N-1)-1)=10*A+4*B;
A1(M*(N-1)-1,M*(N-1)-2)=-4*A-2*B;
A1(M*(N-1)-1,M*(N-1)-3)=A;
A1(M*(N-1)-1,M*(N-2))=G41;
A1(M*(N-1)-1,M*(N-2)-1)=-4*A-2*B;
A1(M*(N-1)-1,M*(N-2)-2)=B;
A1(M*(N-1)-1,M*(N-3)-1)=A;
B1(M*(N-1)-1,M*N)=-G43;
B1(M*(N-1)-1,M*N-2)=G43;
B1(M*(N-1)-1,M*(N-1))=-2*D12*h;
B1(M*(N-1)-1,M*(N-1)-1)=D12*h/2;
B1(M*(N-1)-1,M*(N-1)-2)=2*D12*h;
B1(M*(N-1)-1,M*(N-1)-3)=-D12*h/2;
B1(M*(N-1)-1,M*(N-2))=D12*h/2;
B1(M*(N-1)-1,M*(N-2)-2)=-D12*h/2;
C1(M*(N-1)-1,M*N)=-G43;
C1(M*(N-1)-1,M*N-1)=-2*D12*h;
C1(M*(N-1)-1,M*N-2)=D12*h/2;
C1(M*(N-1)-1,M*(N-1)-1)=D12*h/2;
C1(M*(N-1)-1,M*(N-2))=G43;
C1(M*(N-1)-1,M*(N-2)-1)=2*D12*h;
C1(M*(N-1)-1,M*(N-2)-2)=-D12*h/2;
C1(M*(N-1)-1,M*(N-3)-1)=-D12*h/2;
E1(M*(N-1)-1,1)=G142;

A2(M*(N-1)-1,M*N)=-G51;
A2(M*(N-1)-1,M*N-1)=-G52;
A2(M*(N-1)-1,M*N-2)=-G51;
A2(M*(N-1)-1,M*(N-1)-1)=-D12/2;
A2(M*(N-1)-1,M*(N-2))=-D12/2;
A2(M*(N-1)-1,M*(N-2)-1)=2*D12;
```

```
A2(M*(N-1)-1,M*(N-2)-2)=-D12/2;
A2(M*(N-1)-1,M*(N-3)-1)=-D12/2;
B2(M*(N-1)-1,M*N)=-G53;
B2(M*(N-1)-1,M*N-2)=G53;
B2(M*(N-1)-1,M*(N-2))=D*h/4;
B2(M*(N-1)-1,M*(N-2)-2)=-D*h/4;
C2(M*(N-1)-1,M*N-1)=F*h;
C2(M*(N-1)-1,M*(N-1))=G*h;
C2(M*(N-1)-1,M*(N-1)-1)=-2*F*h-2*G*h;
C2(M*(N-1)-1,M*(N-1)-2)=G*h;
C2(M*(N-1)-1,M*(N-2)-1)=F*h;
E2(M*(N-1)-1,1)=-G54;

A3(M*(N-1)-1,M*N)=-G51;
A3(M*(N-1)-1,M*N-2)=-D12/2;
A3(M*(N-1)-1,M*(N-1))=-G52;
A3(M*(N-1)-1,M*(N-1)-1)=-D12/2;
A3(M*(N-1)-1,M*(N-1)-2)=2*D12;
A3(M*(N-1)-1,M*(N-1)-3)=-D12/2;
A3(M*(N-1)-1,M*(N-2))=-G51;
A3(M*(N-1)-1,M*(N-2)-2)=-D12/2;
B3(M*(N-1)-1,M*N-1)=G*h;
B3(M*(N-1)-1,M*(N-1))=E*h;
B3(M*(N-1)-1,M*(N-1)-1)=-2*E*h-2*G*h;
B3(M*(N-1)-1,M*(N-1)-2)=E*h;
B3(M*(N-1)-1,M*(N-2)-1)=G*h;
C3(M*(N-1)-1,M*N)=G53;
C3(M*(N-1)-1,M*N-2)=-D*h/4;
C3(M*(N-1)-1,M*(N-2))=-G53;
C3(M*(N-1)-1,M*(N-2)-2)=D*h/4;
E3(M*(N-1)-1,1)=-G54;

% For (2,N)
A1(2+M*(N-1),1+M*(N-1))=G92;
A1(2+M*(N-1),2+M*(N-1))=G91;
A1(2+M*(N-1),3+M*(N-1))=G32;
A1(2+M*(N-1),4+M*(N-1))=G31;
A1(2+M*(N-1),1+M*(N-2))=G34;
A1(2+M*(N-1),2+M*(N-2))=G35;
A1(2+M*(N-1),3+M*(N-2))=G34;
A1(2+M*(N-1),2+M*(N-3))=2*A;
B1(2+M*(N-1),1+M*(N-1))=-G94;
B1(2+M*(N-1),2+M*(N-1))=-G93;
B1(2+M*(N-1),3+M*(N-1))=-G37;
B1(2+M*(N-1),4+M*(N-1))=-G36;
B1(2+M*(N-1),1+M*(N-2))=-G151;
B1(2+M*(N-1),3+M*(N-2))=D12*h;
C1(2+M*(N-1),2+M*(N-1))=-G93;
C1(2+M*(N-1),4+M*(N-1))=-G38;
C1(2+M*(N-1),1+M*(N-2))=-D12*h/2;
C1(2+M*(N-1),2+M*(N-2))=-G310;
C1(2+M*(N-1),3+M*(N-2))=-D12*h/2;
C1(2+M*(N-1),2+M*(N-3))=-D12*h/2;
E1(2+M*(N-1),1)=G96;

A2(2+M*(N-1),2+M*(N-1))=-G11;
```

```
A2(2+M*(N-1),3+M*(N-1))=-G12;
A2(2+M*(N-1),4+M*(N-1))=-G11;
B2(2+M*(N-1),1+M*(N-1))=E*h;
B2(2+M*(N-1),2+M*(N-1))=-G13-2*E*h-2*G*h;
B2(2+M*(N-1),3+M*(N-1))=E*h;
B2(2+M*(N-1),4+M*(N-1))=G13;
B2(2+M*(N-1),2+M*(N-2))=2*G*h;
C2(2+M*(N-1),1+M*(N-1))=G*h;
C2(2+M*(N-1),3+M*(N-1))=-G*h;
E2(2+M*(N-1),1)=-G111;

A3(2+M*(N-1),1+M*(N-1))=-G102;
A3(2+M*(N-1),2+M*(N-1))=-G101;
A3(2+M*(N-1),3+M*(N-1))=-G22;
A3(2+M*(N-1),4+M*(N-1))=-G21;
A3(2+M*(N-1),1+M*(N-2))=-G24;
A3(2+M*(N-1),2+M*(N-2))=2*G24;
A3(2+M*(N-1),3+M*(N-2))=-G24;
B3(2+M*(N-1),1+M*(N-1))=G104;
B3(2+M*(N-1),2+M*(N-1))=G103;
B3(2+M*(N-1),3+M*(N-1))=G26;
B3(2+M*(N-1),4+M*(N-1))=G25;
B3(2+M*(N-1),1+M*(N-2))=G105;
C3(2+M*(N-1),1+M*(N-1))=G*h;
C3(2+M*(N-1),2+M*(N-1))=G106;
C3(2+M*(N-1),3+M*(N-1))=G*h;
C3(2+M*(N-1),4+M*(N-1))=G27;
C3(2+M*(N-1),2+M*(N-2))=G29;
E3(2+M*(N-1),1)=-G108;

% For (M-1,N)
A1(M*N-1,M*N)=G92;
A1(M*N-1,M*N-1)=G91;
A1(M*N-1,M*N-2)=G32;
A1(M*N-1,M*N-3)=G31;
A1(M*N-1,M*(N-1))=G34;
A1(M*N-1,M*(N-1)-1)=G35;
A1(M*N-1,M*(N-1)-2)=G34;
A1(M*N-1,M*(N-2)-1)=2*A;
B1(M*N-1,M*N)=G94;
B1(M*N-1,M*N-1)=G93;
B1(M*N-1,M*N-2)=G37;
B1(M*N-1,M*N-3)=G36;
B1(M*N-1,M*(N-1))=G151;
B1(M*N-1,M*(N-1)-2)=-D12*h;
C1(M*N-1,M*N-1)=-G93;
C1(M*N-1,M*N-3)=-G38;
C1(M*N-1,M*(N-1))=-D12*h/2;
C1(M*N-1,M*(N-1)-1)=-G310;
C1(M*N-1,M*(N-1)-2)=-D12*h/2;
C1(M*N-1,M*(N-2)-1)=-D12*h/2;
E1(M*N-1,1)=G96;

A2(M*N-1,M*N-1)=G11;
A2(M*N-1,M*N-2)=G12;
A2(M*N-1,M*N-3)=G11;
```

```
B2(M*N-1,M*N)=E*h;
B2(M*N-1,M*N-1)=-G13-2*E*h-2*G*h;
B2(M*N-1,M*N-2)=E*h;
B2(M*N-1,M*N-3)=G13;
B2(M*N-1,M*(N-1)-1)=2*G*h;
C2(M*N-1,M*N)=-G*h;
C2(M*N-1,M*N-2)=G*h;
E2(M*N-1,1)=G111;

A3(M*N-1,M*N)=-G102;
A3(M*N-1,M*N-1)=-G101;
A3(M*N-1,M*N-2)=-G22;
A3(M*N-1,M*N-3)=-G21;
A3(M*N-1,M*(N-1))=-G24;
A3(M*N-1,M*(N-1)-1)=2*G24;
A3(M*N-1,M*(N-1)-2)=-G24;
B3(M*N-1,M*N)=G104;
B3(M*N-1,M*N-1)=G103;
B3(M*N-1,M*N-2)=G26;
B3(M*N-1,M*N-3)=G25;
B3(M*N-1,M*(N-1))=G105;
C3(M*N-1,M*N)=G*h;
C3(M*N-1,M*N-1)=G106;
C3(M*N-1,M*N-2)=G*h;
C3(M*N-1,M*N-3)=G27;
C3(M*N-1,M*(N-1)-1)=G29;
E3(M*N-1,1)=-G108;

% 4 x rows
for j=3:1:(N-2)
    % For x=1,(1,j)
    A1(1+M*(j-1),1+M*(j-3))=G11;
    A1(1+M*(j-1),1+M*(j-2))=G12;
    A1(1+M*(j-1),1+M*j)=-G12;
    A1(1+M*(j-1),1+M*(j+1))=-G11;
    B1(1+M*(j-1),1+M*(j-2))=-G*h;
    B1(1+M*(j-1),1+M*j)=G*h;
    C1(1+M*(j-1),1+M*(j-3))=G13;
    C1(1+M*(j-1),1+M*(j-2))=F*h;
    C1(1+M*(j-1),1+M*(j-1))=G14;
    C1(1+M*(j-1),1+M*j)=F*h;
    C1(1+M*(j-1),1+M*(j+1))=G13;
    C1(1+M*(j-1),2+M*(j-1))=2*G*h;

    A2(1+M*(j-1),1+M*(j-3))=G21;
    A2(1+M*(j-1),1+M*(j-2))=G22;
    A2(1+M*(j-1),1+M*(j-1))=G23;
    A2(1+M*(j-1),1+M*j)=G22;
    A2(1+M*(j-1),1+M*(j+1))=G21;
    A2(1+M*(j-1),2+M*(j-2))=G24;
    A2(1+M*(j-1),2+M*(j-1))=-2*G24;
    A2(1+M*(j-1),2+M*j)=G24;
    B2(1+M*(j-1),1+M*(j-3))=G27;
    B2(1+M*(j-1),1+M*(j-2))=G*h;
    B2(1+M*(j-1),1+M*(j-1))=G28;
    B2(1+M*(j-1),1+M*j)=G*h;
```

```
B2(1+M*(j-1),1+M*(j+1))=G27;
B2(1+M*(j-1),2+M*(j-1))=G29;
C2(1+M*(j-1),1+M*(j-3))=G25;
C2(1+M*(j-1),1+M*(j-2))=G26;
C2(1+M*(j-1),1+M*j)=-G26;
C2(1+M*(j-1),1+M*(j+1))=-G25;
E2(1+M*(j-1),1)=G210;

A3(1+M*(j-1),1+M*(j-3))=G31;
A3(1+M*(j-1),1+M*(j-2))=G32;
A3(1+M*(j-1),1+M*(j-1))=G33;
A3(1+M*(j-1),1+M*j)=G32;
A3(1+M*(j-1),1+M*(j+1))=G31;
A3(1+M*(j-1),2+M*(j-2))=G34;
A3(1+M*(j-1),2+M*(j-1))=G35;
A3(1+M*(j-1),2+M*j)=G34;
A3(1+M*(j-1),3+M*(j-1))=2*A;
B3(1+M*(j-1),1+M*(j-3))=G38;
B3(1+M*(j-1),1+M*(j-1))=G39;
B3(1+M*(j-1),1+M*(j+1))=G38;
B3(1+M*(j-1),2+M*(j-2))=D12*h/2;
B3(1+M*(j-1),2+M*(j-1))=G310;
B3(1+M*(j-1),2+M*j)=D12*h/2;
B3(1+M*(j-1),3+M*(j-1))=D12*h/2;
C3(1+M*(j-1),1+M*(j-3))=G36;
C3(1+M*(j-1),1+M*(j-2))=G37;
C3(1+M*(j-1),1+M*j)=-G37;
C3(1+M*(j-1),1+M*(j+1))=-G36;
C3(1+M*(j-1),2+M*(j-2))=-D12*h;
C3(1+M*(j-1),2+M*j)=D12*h;
E3(1+M*(j-1),1)=G311;

% For x=M,(M,j)
A1(M*j,M*(j-2))=G11;
A1(M*j,M*(j-1))=G12;
A1(M*j,M*(j+1))=-G12;
A1(M*j,M*(j+2))=-G11;
B1(M*j,M*(j-1))=-G*h;
B1(M*j,M*(j+1))=G*h;
C1(M*j,M*(j-2))=G13;
C1(M*j,M*(j-1))=F*h;
C1(M*j,M*j)=G14;
C1(M*j,M*(j+1))=F*h;
C1(M*j,M*(j+2))=G13;
C1(M*j,M*j-1)=2*G*h;

A2(M*j,M*(j-2))=-G21;
A2(M*j,M*(j-1))=-G22;
A2(M*j,M*j)=-G23;
A2(M*j,M*(j+1))=-G22;
A2(M*j,M*(j+2))=-G21;
A2(M*j,M*(j-1)-1)=-G24;
A2(M*j,M*j-1)=2*G24;
A2(M*j,M*(j+1)-1)=-G24;
B2(M*j,M*(j-2))=G27;
B2(M*j,M*(j-1))=G*h;
```

```
B2(M*j,M*j)=G28;
B2(M*j,M*(j+1))=G*h;
B2(M*j,M*(j+2))=G27;
B2(M*j,M*j-1)=G29;
C2(M*j,M*(j-2))=-G25;
C2(M*j,M*(j-1))=-G26;
C2(M*j,M*(j+1))=G26;
C2(M*j,M*(j+2))=G25;
E2(M*j,1)=-G210;

A3(M*j,M*(j-2))=G31;
A3(M*j,M*(j-1))=G32;
A3(M*j,M*j)=G33;
A3(M*j,M*(j+1))=G32;
A3(M*j,M*(j+2))=G31;
A3(M*j,M*(j-1)-1)=G34;
A3(M*j,M*j-1)=G35;
A3(M*j,M*(j+1)-1)=G34;
A3(M*j,M*j-2)=2*A;
B3(M*j,M*(j-2))=-G38;
B3(M*j,M*j)=-G39;
B3(M*j,M*(j+2))=-G38;
B3(M*j,M*(j-1)-1)=-D12*h/2;
B3(M*j,M*j-1)=-G310;
B3(M*j,M*(j+1)-1)=-D12*h/2;
B3(M*j,M*j-2)=-D12*h/2;
C3(M*j,M*(j-2))=G36;
C3(M*j,M*(j-1))=G37;
C3(M*j,M*(j+1))=-G37;
C3(M*j,M*(j+2))=-G36;
C3(M*j,M*(j-1)-1)=-D12*h;
C3(M*j,M*(j+1)-1)=D12*h;
E3(M*j,1)=G311;

% For x=2,(2,j)
A1(2+M*(j-1),1+M*(j-2))=G41;
A1(2+M*(j-1),1+M*(j-1))=G42;
A1(2+M*(j-1),1+M*j)=G41;
A1(2+M*(j-1),2+M*(j-3))=A;
A1(2+M*(j-1),2+M*(j-2))=-4*A-2*B;
A1(2+M*(j-1),2+M*(j-1))=11*A+4*B;
A1(2+M*(j-1),2+M*j)=-4*A-2*B;
A1(2+M*(j-1),2+M*(j+1))=A;
A1(2+M*(j-1),3+M*(j-2))=B;
A1(2+M*(j-1),3+M*(j-1))=-4*A-2*B;
A1(2+M*(j-1),3+M*j)=B;
A1(2+M*(j-1),4+M*(j-1))=A;
B1(2+M*(j-1),1+M*(j-2))=-D12*h/2;
B1(2+M*(j-1),1+M*(j-1))=2*D12*h;
B1(2+M*(j-1),1+M*j)=-D12*h/2;
B1(2+M*(j-1),2+M*(j-1))=-D12*h/2;
B1(2+M*(j-1),3+M*(j-2))=D12*h/2;
B1(2+M*(j-1),3+M*(j-1))=-2*D12*h;
B1(2+M*(j-1),3+M*j)=D12*h/2;
B1(2+M*(j-1),4+M*(j-1))=D12*h/2;
C1(2+M*(j-1),1+M*(j-2))=G43;
```

```
C1(2+M*(j-1),1+M*j)=-G43;
C1(2+M*(j-1),2+M*(j-3))=-D12*h/2;
C1(2+M*(j-1),2+M*(j-2))=2*D12*h;
C1(2+M*(j-1),2+M*j)=-2*D12*h;
C1(2+M*(j-1),2+M*(j+1))=D12*h/2;
C1(2+M*(j-1),3+M*(j-2))=-D12*h/2;
C1(2+M*(j-1),3+M*j)=D12*h/2;
E1(2+M*(j-1),1)=G44;

A2(2+M*(j-1),1+M*(j-2))=G51;
A2(2+M*(j-1),1+M*(j-1))=G52;
A2(2+M*(j-1),1+M*j)=G51;
A2(2+M*(j-1),2+M*(j-1))=D12/2;
A2(2+M*(j-1),3+M*(j-2))=D12/2;
A2(2+M*(j-1),3+M*(j-1))=-2*D12;
A2(2+M*(j-1),3+M*j)=D12/2;
A2(2+M*(j-1),4+M*(j-1))=D12/2;
B2(2+M*(j-1),1+M*(j-1))=E*h;
B2(2+M*(j-1),2+M*(j-2))=G*h;
B2(2+M*(j-1),2+M*(j-1))=-2*G*h-2*E*h;
B2(2+M*(j-1),2+M*j)=G*h;
B2(2+M*(j-1),3+M*(j-1))=E*h;
C2(2+M*(j-1),1+M*(j-2))=G53;
C2(2+M*(j-1),1+M*j)=-G53;
C2(2+M*(j-1),3+M*(j-2))=-D*h/4;
C2(2+M*(j-1),3+M*j)=D*h/4;
E2(2+M*(j-1),1)=G54;

A3(2+M*(j-1),1+M*(j-2))=-D12/2;
A3(2+M*(j-1),1+M*j)=D12/2;
A3(2+M*(j-1),2+M*(j-3))=-D12/2;
A3(2+M*(j-1),2+M*(j-2))=2*D12;
A3(2+M*(j-1),2+M*j)=-2*D12;
A3(2+M*(j-1),2+M*(j+1))=D12/2;
A3(2+M*(j-1),3+M*(j-2))=-D12/2;
A3(2+M*(j-1),3+M*j)=D12/2;
B3(2+M*(j-1),1+M*(j-2))=D*h/4;
B3(2+M*(j-1),1+M*j)=-D*h/4;
B3(2+M*(j-1),3+M*(j-1))=-D*h/4;
B3(2+M*(j-1),3+M*j)=D*h/4;
C3(2+M*(j-1),1+M*(j-1))=G*h;
C3(2+M*(j-1),2+M*(j-2))=F*h;
C3(2+M*(j-1),2+M*(j-1))=-2*F*h-2*G*h;
C3(2+M*(j-1),2+M*j)=F*h;
C3(2+M*(j-1),3+M*(j-1))=G*h;

% For x=M-1,(M-1,j)
A1(M*j-1,M*(j-1))=G41;
A1(M*j-1,M*j)=G42;
A1(M*j-1,M*(j+1))=G41;
A1(M*j-1,M*(j-2)-1)=A;
A1(M*j-1,M*(j-1)-1)=-4*A-2*B;
A1(M*j-1,M*j-1)=11*A+4*B;
A1(M*j-1,M*(j+1)-1)=-4*A-2*B;
A1(M*j-1,M*(j+2)-1)=A;
A1(M*j-1,M*(j-1)-2)=B;
```

```
A1(M*j-1,M*j-2)=-4*A-2*B;
A1(M*j-1,M*(j+1)-2)=B;
A1(M*j-1,M*j-3)=A;
B1(M*j-1,M*(j-1))=D12*h/2;
B1(M*j-1,M*j)=-2*D12*h;
B1(M*j-1,M*(j+1))=D12*h/2;
B1(M*j-1,M*j-1)=D12*h/2;
B1(M*j-1,M*(j-1)-2)=-D12*h/2;
B1(M*j-1,M*j-2)=2*D12*h;
B1(M*j-1,M*(j+1)-2)=-D12*h/2;
B1(M*j-1,M*j-3)=-D12*h/2;
C1(M*j-1,M*(j-1))=G43;
C1(M*j-1,M*(j+1))=-G43;
C1(M*j-1,M*(j-2)-1)=-D12*h/2;
C1(M*j-1,M*(j-1)-1)=2*D12*h;
C1(M*j-1,M*(j+1)-1)=-2*D12*h;
C1(M*j-1,M*(j+2)-1)=D12*h/2;
C1(M*j-1,M*(j-1)-2)=-D12*h/2;
C1(M*j-1,M*(j+1)-2)=D12*h/2;
E1(M*j-1,1)=G44;

A2(M*j-1,M*(j-1))=-G51;
A2(M*j-1,M*j)=-G52;
A2(M*j-1,M*(j+1))=-G51;
A2(M*j-1,M*j-1)=-D12/2;
A2(M*j-1,M*(j-1)-2)=-D12/2;
A2(M*j-1,M*j-2)=2*D12;
A2(M*j-1,M*(j+1)-2)=-D12/2;
A2(M*j-1,M*j-3)=-D12/2;
B2(M*j-1,M*j)=E*h;
B2(M*j-1,M*(j-1)-1)=G*h;
B2(M*j-1,M*j-1)=-2*G*h-2*E*h;
B2(M*j-1,M*(j+1)-1)=G*h;
B2(M*j-1,M*j-2)=E*h;
C2(M*j-1,M*(j-1))=-G53;
C2(M*j-1,M*(j+1))=G53;
C2(M*j-1,M*(j-1)-2)=D*h/4;
C2(M*j-1,M*(j+1)-2)=-D*h/4;
E2(M*j-1,1)=-G54;

A3(M*j-1,M*(j-1))=-D12/2;
A3(M*j-1,M*(j+1))=D12/2;
A3(M*j-1,M*(j-2)-1)=-D12/2;
A3(M*j-1,M*(j-1)-1)=2*D12;
A3(M*j-1,M*(j+1)-1)=-2*D12;
A3(M*j-1,M*(j+2)-1)=D12/2;
A3(M*j-1,M*(j-1)-2)=-D12/2;
A3(M*j-1,M*(j+1)-2)=D12/2;
B3(M*j-1,M*(j-1))=D*h/4;
B3(M*j-1,M*(j+1))=-D*h/4;
B3(M*j-1,M*(j-1)-2)=-D*h/4;
B3(M*j-1,M*(j+1)-2)=D*h/4;
C3(M*j-1,M*j)=G*h;
C3(M*j-1,M*(j-1)-1)=F*h;
C3(M*j-1,M*j-1)=-2*F*h-2*G*h;
C3(M*j-1,M*(j+1)-1)=F*h;
```

```
    C3(M*j-1,M*j-2)=G*h;
end

for i=3:1:(M-2)
    % For y=N,(i,N)
    A1(i+M*(N-1),i-2+M*(N-1))=G31;
    A1(i+M*(N-1),i-1+M*(N-1))=G32;
    A1(i+M*(N-1),i+M*(N-1))=G33;
    A1(i+M*(N-1),i+1+M*(N-1))=G32;
    A1(i+M*(N-1),i+2+M*(N-1))=G31;
    A1(i+M*(N-1),i-1+M*(N-2))=G34;
    A1(i+M*(N-1),i+M*(N-2))=G35;
    A1(i+M*(N-1),i+1+M*(N-2))=G34;
    A1(i+M*(N-1),i+M*(N-3))=2*A;
    B1(i+M*(N-1),i-2+M*(N-1))=G36;
    B1(i+M*(N-1),i-1+M*(N-1))=G37;
    B1(i+M*(N-1),i+1+M*(N-1))=-G37;
    B1(i+M*(N-1),i+2+M*(N-1))=-G36;
    B1(i+M*(N-1),i-1+M*(N-2))=-D12*h;
    B1(i+M*(N-1),i+1+M*(N-2))=D12*h;
    C1(i+M*(N-1),i-2+M*(N-1))=-G38;
    C1(i+M*(N-1),i+M*(N-1))=-G39;
    C1(i+M*(N-1),i+2+M*(N-1))=-G38;
    C1(i+M*(N-1),i-1+M*(N-2))=-D12*h/2;
    C1(i+M*(N-1),i+M*(N-2))=-G310;
    C1(i+M*(N-1),i+1+M*(N-2))=-D12*h/2;
    C1(i+M*(N-1),i+M*(N-3))=-D12*h/2;
    E1(i+M*(N-1),1)=G311;

    A2(i+M*(N-1),i-2+M*(N-1))=G11;
    A2(i+M*(N-1),i-1+M*(N-1))=G12;
    A2(i+M*(N-1),i+1+M*(N-1))=-G12;
    A2(i+M*(N-1),i+2+M*(N-1))=-G11;
    B2(i+M*(N-1),i-2+M*(N-1))=G13;
    B2(i+M*(N-1),i-1+M*(N-1))=E*h;
    B2(i+M*(N-1),i+M*(N-1))=G14;
    B2(i+M*(N-1),i+1+M*(N-1))=E*h;
    B2(i+M*(N-1),i+2+M*(N-1))=G13;
    B2(i+M*(N-1),i+M*(N-2))=2*G*h;
    C2(i+M*(N-1),i-1+M*(N-1))=G*h;
    C2(i+M*(N-1),i+1+M*(N-1))=-G*h;

    A3(i+M*(N-1),i-2+M*(N-1))=-G21;
    A3(i+M*(N-1),i-1+M*(N-1))=-G22;
    A3(i+M*(N-1),i+M*(N-1))=-G23;
    A3(i+M*(N-1),i+1+M*(N-1))=-G22;
    A3(i+M*(N-1),i+2+M*(N-1))=-G21;
    A3(i+M*(N-1),i-1+M*(N-2))=-G24;
    A3(i+M*(N-1),i+M*(N-2))=2*G24;
    A3(i+M*(N-1),i+1+M*(N-2))=-G24;
    B3(i+M*(N-1),i-2+M*(N-1))=-G25;
    B3(i+M*(N-1),i-1+M*(N-1))=-G26;
    B3(i+M*(N-1),i+1+M*(N-1))=G26;
    B3(i+M*(N-1),i+2+M*(N-1))=G25;
    C3(i+M*(N-1),i-2+M*(N-1))=G27;
    C3(i+M*(N-1),i-1+M*(N-1))=G*h;
```

```
C3(i+M*(N-1),i+M*(N-1))=G28;
C3(i+M*(N-1),i+1+M*(N-1))=G*h;
C3(i+M*(N-1),i+2+M*(N-1))=G27;
C3(i+M*(N-1),i+M*(N-2))=G29;
E3(i+M*(N-1),1)=-G210;

% For y=N-1,(i,N-1)
A1(i+M*(N-2),i-1+M*(N-1))=G41;
A1(i+M*(N-2),i+M*(N-1))=G42;
A1(i+M*(N-2),i+1+M*(N-1))=G41;
A1(i+M*(N-2),i-2+M*(N-2))=A;
A1(i+M*(N-2),i-1+M*(N-2))=-4*A-2*B;
A1(i+M*(N-2),i+M*(N-2))=11*A+4*B;
A1(i+M*(N-2),i+1+M*(N-2))=-4*A-2*B;
A1(i+M*(N-2),i+2+M*(N-2))=A;
A1(i+M*(N-2),i-1+M*(N-3))=B;
A1(i+M*(N-2),i+M*(N-3))=-4*A-2*B;
A1(i+M*(N-2),i+1+M*(N-3))=B;
A1(i+M*(N-2),i+M*(N-4))=A;
B1(i+M*(N-2),i-1+M*(N-1))=G43;
B1(i+M*(N-2),i+1+M*(N-1))=-G43;
B1(i+M*(N-2),i-2+M*(N-2))=-D12*h/2;
B1(i+M*(N-2),i-1+M*(N-2))=2*D12*h;
B1(i+M*(N-2),i+1+M*(N-2))=-2*D12*h;
B1(i+M*(N-2),i+2+M*(N-2))=D12*h/2;
B1(i+M*(N-2),i-1+M*(N-3))=-D12*h/2;
B1(i+M*(N-2),i+1+M*(N-3))=D12*h/2;
C1(i+M*(N-2),i-1+M*(N-1))=D12*h/2;
C1(i+M*(N-2),i+M*(N-1))=-2*D12*h;
C1(i+M*(N-2),i+1+M*(N-1))=D12*h/2;
C1(i+M*(N-2),i+M*(N-2))=D12*h/2;
C1(i+M*(N-2),i-1+M*(N-3))=-D12*h/2;
C1(i+M*(N-2),i+M*(N-3))=2*D12*h;
C1(i+M*(N-2),i+1+M*(N-3))=-D12*h/2;
C1(i+M*(N-2),i+M*(N-4))=-D12*h/2;
E1(i+M*(N-2),1)=G44;

A2(i+M*(N-2),i-1+M*(N-1))=-G51;
A2(i+M*(N-2),i+M*(N-1))=-G52;
A2(i+M*(N-2),i+1+M*(N-1))=-G51;
A2(i+M*(N-2),i+M*(N-2))=-D12/2;
A2(i+M*(N-2),i-1+M*(N-3))=-D12/2;
A2(i+M*(N-2),i+M*(N-3))=2*D12;
A2(i+M*(N-2),i+1+M*(N-3))=-D12/2;
A2(i+M*(N-2),i+M*(N-4))=-D12/2;
B2(i+M*(N-2),i-1+M*(N-1))=-G53;
B2(i+M*(N-2),i+1+M*(N-1))=G53;
B2(i+M*(N-2),i-1+M*(N-3))=D*h/4;
B2(i+M*(N-2),i+1+M*(N-3))=-D*h/4;
C2(i+M*(N-2),i+M*(N-1))=F*h;
C2(i+M*(N-2),i-1+M*(N-2))=G*h;
C2(i+M*(N-2),i+M*(N-2))=-2*F*h-2*G*h;
C2(i+M*(N-2),i+1+M*(N-2))=G*h;
C2(i+M*(N-2),i+M*(N-3))=F*h;
E2(i+M*(N-2),1)=-G54;
```

```
A3(i+M*(N-2),i-1+M*(N-1))=-D12/2;
A3(i+M*(N-2),i+1+M*(N-1))=D12/2;
A3(i+M*(N-2),i-2+M*(N-2))=-D12/2;
A3(i+M*(N-2),i-1+M*(N-2))=2*D12;
A3(i+M*(N-2),i+1+M*(N-2))=-2*D12;
A3(i+M*(N-2),i+2+M*(N-2))=D12/2;
A3(i+M*(N-2),i-1+M*(N-3))=-D12/2;
A3(i+M*(N-2),i+1+M*(N-3))=D12/2;
B3(i+M*(N-2),i+M*(N-1))=G*h;
B3(i+M*(N-2),i-1+M*(N-2))=E*h;
B3(i+M*(N-2),i+M*(N-2))=-2*E*h-2*G*h;
B3(i+M*(N-2),i+1+M*(N-2))=E*h;
B3(i+M*(N-2),i+M*(N-3))=G*h;
C3(i+M*(N-2),i-1+M*(N-1))=-D*h/4;
C3(i+M*(N-2),i+1+M*(N-1))=D*h/4;
C3(i+M*(N-2),i-1+M*(N-3))=D*h/4;
C3(i+M*(N-2),i+1+M*(N-3))=-D*h/4;

% For y=2,(i,2)
A1(i+M,i-1)=B;
A1(i+M,i)=-4*A-2*B;
A1(i+M,i+1)=B;
A1(i+M,i-2+M)=A;
A1(i+M,i-1+M)=-4*A-2*B;
A1(i+M,i+M)=12*A+4*B;
A1(i+M,i+1+M)=-4*A-2*B;
A1(i+M,i+2+M)=A;
A1(i+M,i-1+2*M)=B;
A1(i+M,i+2*M)=-4*A-2*B;
A1(i+M,i+1+2*M)=B;
A1(i+M,i+3*M)=A;
B1(i+M,i-1)=-D12*h/2;
B1(i+M,i+1)=D12*h/2;
B1(i+M,i-2+M)=-D12*h/2;
B1(i+M,i-1+M)=2*D12*h;
B1(i+M,i+1+M)=-2*D12*h;
B1(i+M,i+2+M)=D12*h/2;
B1(i+M,i-1+2*M)=-D12*h/2;
B1(i+M,i+1+2*M)=D12*h/2;
C1(i+M,i-1)=-D12*h/2;
C1(i+M,i)=2*D12*h;
C1(i+M,i+1)=-D12*h/2;
C1(i+M,i-1+2*M)=D12*h/2;
C1(i+M,i+2*M)=-2*D12*h;
C1(i+M,i+1+2*M)=D12*h/2;
C1(i+M,i+3*M)=D12*h/2;
E1(i+M,1)=-q*h^4;

A2(i+M,i-1)=-D12/2;
A2(i+M,i+1)=D12/2;
A2(i+M,i-2+M)=-D12/2;
A2(i+M,i-1+M)=2*D12;
A2(i+M,i+1+M)=-2*D12;
A2(i+M,i+2+M)=D12/2;
A2(i+M,i-1+2*M)=-D12/2;
A2(i+M,i+1+2*M)=D12/2;
```

```
B2(i+M,i)=G*h;
B2(i+M,i-1+M)=E*h;
B2(i+M,i+M)=-2*E*h-2*G*h;
B2(i+M,i+1+M)=E*h;
B2(i+M,i+2*M)=G*h;
C2(i+M,i-1)=D*h/4;
C2(i+M,i+1)=-D*h/4;
C2(i+M,i-1+2*M)=-D*h/4;
C2(i+M,i+1+2*M)=D*h/4;

A3(i+M,i-1)=-D12/2;
A3(i+M,i)=2*D12;
A3(i+M,i+1)=-D12/2;
A3(i+M,i-1+2*M)=D12/2;
A3(i+M,i+2*M)=-2*D12;
A3(i+M,i+1+2*M)=D12/2;
A3(i+M,i+3*M)=D12/2;
B3(i+M,i-1)=D*h/4;
B3(i+M,i+1)=-D*h/4;
B3(i+M,i-1+2*M)=-D*h/4;
B3(i+M,i+1+2*M)=D*h/4;
C3(i+M,i)=F*h;
C3(i+M,i-1+M)=G*h;
C3(i+M,i+M)=-2*F*h-2*G*h;
C3(i+M,i+1+M)=G*h;
C3(i+M,i+2*M)=F*h;

% For y=1,(i,1)
A1(i,i-2)=A;
A1(i,i-1)=-4*A-2*B;
A1(i,i)=13*A+4*B;
A1(i,i+1)=-4*A-2*B;
A1(i,i+2)=A;
A1(i,i-1+M)=B;
A1(i,i+M)=-4*A-2*B;
A1(i,i+1+M)=B;
A1(i,i+2*M)=A;
B1(i,i-2)=-D12*h/2;
B1(i,i-1)=2*D12*h;
B1(i,i+1)=-2*D12*h;
B1(i,i+2)=D12*h/2;
B1(i,i-1+M)=-D12*h/2;
B1(i,i+1+M)=D12*h/2;
C1(i,i)=-D12*h/2;
C1(i,i-1+M)=D12*h/2;
C1(i,i+M)=-2*D12*h;
C1(i,i+1+M)=D12*h/2;
C1(i,i+2*M)=D12*h/2;
E1(i,1)=-q*h^4;

A2(i,i-2)=-D12/2;
A2(i,i-1)=2*D12;
A2(i,i+1)=-2*D12;
A2(i,i+2)=D12/2;
A2(i,i-1+M)=-D12/2;
A2(i,i+1+M)=D12/2;
```

```
    B2(i,i-1)=E*h;
    B2(i,i)=-2*E*h-2*G*h;
    B2(i,i+1)=E*h;
    B2(i,i+M)=G*h;
    C2(i,i-1+M)=-D*h/4;
    C2(i,i+1+M)=D*h/4;

    A3(i,i)=-D12/2;
    A3(i,i-1+M)=D12/2;
    A3(i,i+M)=-2*D12;
    A3(i,i+1+M)=D12/2;
    A3(i,i+2*M)=D12/2;
    B3(i,i-1+M)=-D*h/4;
    B3(i,i+1+M)=D*h/4;
    C3(i,i-1)=G*h;
    C3(i,i)=-2*F*h-2*G*h;
    C3(i,i+1)=G*h;
    C3(i,i+M)=F*h;
end

for i=3:1:(M-2) %(j,i)
    for j=3:1:(N-2)
        A1(i+M*(j-1),i+M*(j-3))=A;
        A1(i+M*(j-1),i-1+M*(j-2))=B;
        A1(i+M*(j-1),i+M*(j-2))=-4*A-2*B;
        A1(i+M*(j-1),i+1+M*(j-2))=B;
        A1(i+M*(j-1),i-2+M*(j-1))=A;
        A1(i+M*(j-1),i-1+M*(j-1))=-4*A-2*B;
        A1(i+M*(j-1),i+M*(j-1))=12*A+4*B;
        A1(i+M*(j-1),i+1+M*(j-1))=-4*A-2*B;
        A1(i+M*(j-1),i+2+M*(j-1))=A;
        A1(i+M*(j-1),i-1+M*j)=B;
        A1(i+M*(j-1),i+M*j)=-4*A-2*B;
        A1(i+M*(j-1),i+1+M*j)=B;
        A1(i+M*(j-1),i+M*(j+1))=A;
        B1(i+M*(j-1),i-1+M*(j-2))=-D12*h/2;
        B1(i+M*(j-1),i+1+M*(j-2))=D12*h/2;
        B1(i+M*(j-1),i-2+M*(j-1))=-D12*h/2;
        B1(i+M*(j-1),i-1+M*(j-1))=2*D12*h;
        B1(i+M*(j-1),i+1+M*(j-1))=-2*D12*h;
        B1(i+M*(j-1),i+2+M*(j-1))=D12*h/2;
        B1(i+M*(j-1),i-1+M*j)=-D12*h/2;
        B1(i+M*(j-1),i+1+M*j)=D12*h/2;
        C1(i+M*(j-1),i+M*(j-3))=-D12*h/2;
        C1(i+M*(j-1),i-1+M*(j-2))=-D12*h/2;
        C1(i+M*(j-1),i+M*(j-2))=2*D12*h;
        C1(i+M*(j-1),i+1+M*(j-2))=-D12*h/2;
        C1(i+M*(j-1),i-1+M*j)=D12*h/2;
        C1(i+M*(j-1),i+M*j)=-2*D12*h;
        C1(i+M*(j-1),i+1+M*j)=D12*h/2;
        C1(i+M*(j-1),i+M*(j+1))=D12*h/2;
        E1(i+M*(j-1),1)=-q*h^4;

        A2(i+M*(j-1),i-1+M*(j-2))=-D12/2;
        A2(i+M*(j-1),i+1+M*(j-2))=D12/2;
        A2(i+M*(j-1),i-2+M*(j-1))=-D12/2;
```

```
        A2(i+M*(j-1),i-1+M*(j-1))=2*D12;
        A2(i+M*(j-1),i+1+M*(j-1))=-2*D12;
        A2(i+M*(j-1),i+2+M*(j-1))=D12/2;
        A2(i+M*(j-1),i-1+M*j)=-D12/2;
        A2(i+M*(j-1),i+1+M*j)=D12/2;
        B2(i+M*(j-1),i+M*(j-2))=G*h;
        B2(i+M*(j-1),i-1+M*(j-1))=E*h;
        B2(i+M*(j-1),i+M*(j-1))=-2*E*h-2*G*h;
        B2(i+M*(j-1),i+1+M*(j-1))=E*h;
        B2(i+M*(j-1),i+M*j)=G*h;
        C2(i+M*(j-1),i-1+M*(j-2))=D*h/4;
        C2(i+M*(j-1),i+1+M*(j-2))=-D*h/4;
        C2(i+M*(j-1),i-1+M*j)=-D*h/4;
        C2(i+M*(j-1),i+1+M*j)=D*h/4;

        A3(i+M*(j-1),i+M*(j-3))=-D12/2;
        A3(i+M*(j-1),i-1+M*(j-2))=-D12/2;
        A3(i+M*(j-1),i+M*(j-2))=2*D12;
        A3(i+M*(j-1),i+1+M*(j-2))=-D12/2;
        A3(i+M*(j-1),i-1+M*j)=D12/2;
        A3(i+M*(j-1),i+M*j)=-2*D12;
        A3(i+M*(j-1),i+1+M*j)=D12/2;
        A3(i+M*(j-1),i+M*(j+1))=D12/2;
        B3(i+M*(j-1),i-1+M*(j-2))=D*h/4;
        B3(i+M*(j-1),i+1+M*(j-2))=-D*h/4;
        B3(i+M*(j-1),i-1+M*j)=-D*h/4;
        B3(i+M*(j-1),i+1+M*j)=D*h/4;
        C3(i+M*(j-1),i+M*(j-2))=F*h;
        C3(i+M*(j-1),i-1+M*(j-1))=G*h;
        C3(i+M*(j-1),i+M*(j-1))=-2*F*h-2*G*h;
        C3(i+M*(j-1),i+1+M*(j-1))=G*h;
        C3(i+M*(j-1),i+M*j)=F*h;
    end
end

% Integration matrix of the 3 governing equations
A11=[A1,B1,C1];
A12=[A2,B2,C2];
A13=[A3,B3,C3];
A144=[A11;A12;A13];
B=-1*[E1;E2;E3];
% Solving the displacement matrix
WUV=A144\B;
W=zeros(N,M);
U=W;
V=W;
for i=1:N
    for j=1:M
        W(i,j)=WUV(j+M*(i-1),1);
        U(i,j)=WUV(j+M*(i-1)+M*N,1);
        V(i,j)=WUV(j+M*(i-1)+2*M*N,1);
    end
end

x=[0:h:(wp-h)]*10^9;
y=[0:k:(lp-k)]*10^9;
```

```
[X,Y] = meshgrid(x,y);
WW=10^9*W;
surf(X,Y,WW);
```

Curriculum Vitae

Name:	Xining Wang
Post-secondary Education and Degrees:	Xi'an Jiaotong University Xi'an, Shaanxi, China 2010-1014 B.E. Western University London, Ontario, Canada 2014-2016 M.E.Sc
Related Work Experience	Teaching Assistant Western University 2014-2016 Research Assistant Western University 2014-2016